Analysis of the Influence of Pantographs in Railway Communications

Magali Mendes Correia

Thesis to obtain the Master of Science Degree in

Electrical and Computer Engineering

Supervisor: Prof. Luís Manuel de Jesus Sousa Correia

Examination Committee

Chairperson: Prof. José Eduardo Charters Ribeiro da Cunha Sanguino

Supervisor: Prof. Luís Manuel de Jesus Sousa Correia

Members of Committee: Prof. Custódio José de Oliveira Peixeiro

Eng. Fernando Manuel Lopes Santana

November 2019

I declare that this document is an original work of my own authorship and that it fulfils all the requirements of the Code of Conduct and Good Practices of the *Universidade de Lisboa*.

To my family and friends.

Acknowledgements

First and foremost, I would like to express my sincere gratitude to my thesis supervisor, Professor Luís M. Correia, for allowing me the opportunity to develop this thesis. I am grateful for all the weekly meetings, where I not only had the chance to clarify my doubts and received advice on how to develop and improve this work but also received feedback and guidance on my work methodology, which will be very important in my professional future. I am also very thankful for the opportunity to work with a prestigious multinational company that works in a broad scope of areas. Once again, thank you for your support and guidance in the development of this work.

I am grateful to Thales, in particular to Eng. Fernando Santana, Eng. Nuno Frigolet and Eng. Sérgio Rodrigues, who helped me to understand better the issue at hand, providing me with valuable insights into the railways environment, and giving me the necessary information to complete this work.

To all GROW members, for receiving me openly and for the support and advice throughout the thesis development, especially to my colleagues Sérgio Domingues and Tomás Duarte. Also, a special thank you to André Ribeiro, who, even after finishing his academic path, was always available to answer any questions.

To Professor Custódio Peixeiro and the IT manager, Eng. Nuno Silva, for providing access to the CST tool and being available for any problems that arose.

To my colleagues and friends that accompanied me throughout this journey, for their support and encouragement, in particular to Filipa Ribeiro, João Filipe, Francisco Pereira, and Luís Almeida.

Last but not least, I would like to thank my family, my mother, Máguida Pereira, my father, Abner Correia, and my sisters, Nair Correia and Denise Correia, for all their love and support. Thank you for investing in my education and for providing me with the fundamentals to thrive in this world.

Abstract

In high-speed railways, there are several interference sources. The interference caused by the pantograph, an element that collects the current from the power supply, and the catenary, the structure that transports the power, is one of them. Its importance is due to the effect that it has on railway communications and, consequently, the safety in high-speed railways. The main objective of this thesis was to analyse the performance of antennas for four different railway communication systems when influenced by the pantograph and the catenary. The communication technologies considered were TETRA at 380 MHz, GSM-R at 900 MHz, LTE-R at 2.6 GHz, and BBRS at 5.9 GHz. Two different approaches were taken to analyse the problem. The first one, regarding the antenna analysis, consisted of the development of a model based on the CST software, where one considered the antennas' parameters, as well as the pantograph/catenary structures. One identified four different scenarios regarding these structures: only rooftop (reference scenario), rooftop and catenary, rooftop and pantograph, and rooftop plus catenary and pantograph. Models were developed for these scenarios, and the results were analysed through radiation pattern, reflection coefficient, half-power beamwidth, and first side lobe level. One observes that in all technologies, the presence of the pantograph and of the catenary leads to the antenna losing its omnidirectional behaviour. Considering that the maximum distance between the pantograph and the antenna for which the surroundings affect the antenna's performance is 20λ, one observes that this is not an issue for LTE-R and BBRS, since this distance is too small and does not occur in reality. The second approach, regarding electromagnetic interference, consisted of analytically determining the minimum Signal-to-Noise-Plus-Interference-Ratio. One used the CST model for the rooftop and catenary scenario to determine the interference power from the catenary, and then to determine the power corresponding to each of the four frequencies (380 MHz, 900 MHz, 2.6 GHz, and 5.9 GHz). The obtained values are significantly above the sensitivity for all systems. However, for certain distances between the antenna and the catenary, such as 1.6 m and 2.8 m, the SNIR is equal to the sensitivity, so the noise from the catenary is not substantial compared with the noise from the environment.

Keywords

Railway Communication, Pantograph, TETRA, GSM-R, LTE-R, BBRS, Electromagnetic Interference.

Resumo

Nas linhas férreas de alta velocidade, existem várias fontes de interferência. A interferência causada pelo pantógrafo, o elemento que coleta a corrente da fonte de alimentação, e a catenária, estrutura que transporta a energia, é uma delas. A sua importância deve-se ao efeito que exerce sobre as comunicações ferroviárias e, consequentemente, na segurança nas ferrovias de alta velocidade. O objetivo principal desta tese foi analisar o desempenho de antenas para quatro sistemas diferentes de comunicação ferroviária, quando influenciados pelo pantógrafo e pela catenária. As tecnologias de comunicação consideradas foram TETRA a 380 MHz, GSM-R a 900 MHz, LTE-R a 2.6 GHz e BBRS a 5.9 GHz. Duas abordagens diferentes foram adotadas para analisar o problema. A primeira, referente à análise de antenas, consistiu no desenvolvimento de um modelo baseado no software CST, onde foram considerados os parâmetros das antenas, bem como as estruturas do pantógrafo / catenária. Identificaram-se quatro cenários diferentes em relação a essas estruturas: somente o telhado (cenário de referência), telhado e catenária, telhado e pantógrafo, e telhado mais catenária e pantógrafo. Os modelos para esses cenários foram desenvolvidos e os resultados foram analisados através do diagrama de radiação, do coeficiente de reflexão, da largura de feixe a meia potência e do nível do primeiro lobo lateral. A segunda abordagem, referente à interferência eletromagnética, consistiu em determinar analiticamente o valor mínimo da relação Sinal-Ruído-e-Interferência. Utilizou-se o modelo CST para o cenário telhado e catenária para determinar a potência de interferência da catenária e, de seguida, determinar-se a potência correspondente a cada uma das quatro harmónicas (380 MHz, 900 MHz, 2.6 GHz e 5.9 GHz).

Palavras-chave

Comunicações ferroviárias, Pantógrafos, TETRA, GSM-R, LTE-R, BBRS, Interferência Eletromagnética.

Table of Contents

List of Figures

List of Tables

List of Acronyms

1G	1st Generation of Mobile Communication Systems
2G	2nd Generation of Mobile Communication Systems
3G	3rd Generation of Mobile Communication Systems
3GPP	3rd Generation Partnership Project
4G	4th Generation of Mobile Communication Systems
5G	5th Generation of Mobile Communication Systems
ABW	Absolute Bandwidth
AC	Alternative Current
AP	Access Point
AuC	Authentication Centre
BBRS	Broadband Radio System
BCC	Backup Control Centre
BS	Base Station
BSC	Base Station Controller
BSS	Base Station Subsystem
BTS	Base Transceiver Station
BW	Bandwidth
CCS7	Common Channel Signalling System No.7 from ITU-T
CCTV	Closed-Circuit Television
CDTA	Cabo de Terra Aéreo
CDTE	Cabo de Terra Enterrado
CSD	Circuit Switch Data
CST	Computer Simulation Technology
D2D	Device-to-Device
DFT	Discrete Fourier Transform
DL	Downlink
DMO	Direct Mode Operation
DMS	Direct Mode Station
DQPSK	Differential Quadrature Phase-Shift Keying
E-UTRAN	Evolved Universal Terrestrial Radio Access Network
EIR	Equipment Identity Register
EIRENE	European Integrated Railway Radio Enhanced Network
eLDA	Enhanced Location Dependent Addressing
EM	Electromagnetic

EMC	Electromagnetic Compatibility
EMI	Electromagnetic Interference
eMLPP	Enhanced Multi-Level Precedence and Pre-emption
EPC	Evolved Packet Core
ERTMS	The European Railway Traffic Management System
ETCS	European Train Control System
ETSI	European Telecommunications Standards Institute
FBW	Fractional Bandwidth
FDD	Frequency Division Duplex
FDTD	Finite Difference Time Domain
FFT	Fast Fourier Transform
FIT	Finite Integration Technique
FNBW	First Null Beam-Width
GGSN	Gateway GPRS Support Node
GMSK	Gaussian Minimum Shift Keying
GPRS	General Packet Radio System
GSM-R	Global System for Mobile Communications – Railway
GTSI	Group TETRA Subscriber Identity
HRL	Home Location Register
HSS	Home Subscriber Service
HST	High-Speed Train
IEEE	Institute of Electrical and Electronics Engineers
IMEI	International Mobile Equipment Identity
IMSI	International Mobile Subscriber Identity
IoT	Internet of Things
ISI	Inter-System Interface
ITSI	Individual TETRA Subscriber Identity
IEV	International Electrotechnical Vocabulary
LCP	Left Circular Polarisation
LDA	Location Dependent Addressing
LoS	Line of Sight
LTE-R	Long-term Evolution - Railway
LS	Line Station
M2M	Machine-to-Machine
MME	Mobility Management Entity
MoM	Method of Moments
MORANE	Mobile radio for Railway Networks
MS	Mobile Station
MSC	Mobile service Switching Centre
MT	Mobile Terminal

NMS	Network Management System
NMU	Network Management Unit
NSS	Network Subsystem
OBU	On-Board Unit
OCC	Operation Control Centre
OFDMA	Orthogonal Frequency Division Multiple Access
OMS	Operation and Maintenance Subsystem
PAMR	Public Access Mobile Radio
PDN-G	Public Data Network Gateway
PEC	Perfect Electric Conductor
PL	Polarisation matching loss
PMC	Perfect Magnetic Conductor
PML	Perfectly Matched Layer
PMR	Private Mobile Radio
PTM-SC	Point-to-Multipoint Service Centre
QoS	Quality of Service
RCP	Right Circular Polarisation
RSSB	Rail Safety and Standards Board
RSSI	Received Signal Strength Indicator
S-GW	Serving Gateway
SAR	Specific Absorptions Rate
SC-FDMA	Single Carrier Frequency Division Multiple Access
SGSN	The Serving GPRS Support Node
SLL	Side Lobe Level
SNIR	Signal-to-Noise-plus-Interference-Ratio
SwMI	Switching and Management Infrastructure
TDD	Time Division Duplex
TDMA	Time Division Multiple Access
THD	Total Harmonic Distortion
TML	Transmission-Line Matrix
TMO	Trunked Mode Operation
TRAU	Transcoding and Rate Adaption Unit
UL	Uplink
UMTS	Universal Mobile Telecommunications System
USIM	Universal Subscriber Identity Module
VBS	Voice Broadcast Service
VGCS	Voice Group Call Service
VLR	Visitor Location Register
VSWR	Voltage Standing Wave Ratio
WLAN	Wireless Local Area Network

List of Symbols

η	Intrinsic impedance
ϵ_0	Permittivity in vacuum
ϵ_r	Relative permittivity
θ	Angle between the positive half of Z-axis and the observation point
λ	Wavelength
φ	Angle between the positive half of X-axis and the observation point projected on XOY plane
Δf	Signal bandwidth
Δ_{max}	Maximum mesh step value allowed
Δ_{min}	Minimum mesh step value allowed
Δx	Mesh dimension for the X axis
Δy	Mesh dimension for the Y axis
ω_0	Fundamental frequency
a_0	Average value of a signal
a_{3dB}	Half-Power Beamwidth
a_i	Incoming wave
a_n	Serie's coefficients
b_i	Outcome wave
b_n	Serie's coefficients
c_n	Exponential Fourier coefficient.
C	Capacitance
d	Height of the transmission line
D	Antennas' directivity
E	Electric field magnitude
E_θ^V	Electric field for a vertical dipole at θ direction
E_φ^H	Electric field for a horizontal dipole at φ direction
f	Frequency of the harmonic
F	Noise figure

$f(t)$	Periodic function.
f_0	Fundamental frequency
G	Gain
H	Magnetic field intensity
h	Antenna height
I	Interfering power
I_0	Maximum current
k	Free space wave number
l	Length of the transmission line
l'	Largest geometrical dimension of the antenna
L_{SLL}	Side lobe level (maximum relative)
P_{harm}	Power of the harmonic
P_{min}	Sensitivity
N_harm	Order of the harmonic
N	Total noise power
N_L^V	Number of lobes for a vertical dipole
N_L^H	Number of lobes for a horizontal dipole
N_{RF}	Average noise power
r	Radius of the transmission line
r'	Distance between the antenna and the observation point
T_0	Period
U	Maximum potential at the transmission line
x	Position in the vertical referential
x'	Electric current in the catenary

List of Software

Antenna Magus	Antenna design software
CST Studio	Electromagnetic simulation software
MATLAB	Numerical Software
Microsoft Paint	Image Editor
Microsoft Word 2016	Text editor software

Chapter 1

Introduction

In this chapter, a brief overview of mobile communications systems evolution is presented, with an explanation of the technologies, as well as the growth in demand for these services. Additionally, a summary of the increasing importance and evolution of railway communications, the high-speed railway market and the purpose of this thesis are provided. At the end of the chapter, the entire thesis structure is given.

1.1 Overview and Motivation

Mobile communications have undergone an impressive evolution in recent decades, not showing any sign of slowing down. They have become a fundamental part of everyday's life, at personal and professional levels.

It all began with the 1st Generation (1G) emerging in the 1980s, which used analogue technology and allowed voice communications only. The 2nd Generation (2G) appears in the early 1990s, using digital technology and enabling data communications, despite being designed for voice. At this point, another two concepts were introduced, capacity and coverage, whose importance in mobile communications systems remains till today. Global System for Mobile (GSM) was the first digital mobile communications system, providing both voice and data services for a more substantial number of users, firstly through circuit-switched technology and then by packet-switching one. The transition to packet transmission was a significant progress in mobile communications, along with the development of General Packet Radio Services (GPRS) and the GSM Evolution (EDGE). This vital step opened the doors to the immense potential that exists in mobile communications, in terms of both network complexity and radio interference [Ribe18].

The need to standardise mobile communications networks led to the development of a project covering cellular telecommunications network technologies, including radio access, a core transport network, and service capabilities, the 3rd Generation Partnership Project (3GPP) [3GPP19]. This way, a complete list of system specifications is provided. The 3rd Generation (3G) of mobile communications appears in 2000, and it focused on data communications. Its main objective was to respond to the increasing demand for Internet services. In Europe, the first 3G system was the Universal Mobile Telecommunications System (UMTS).

In response to the constant evolution of services and the growing need for higher data rates, appears the Long Term Evolution (LTE), in the late 2000s, as the 4th Generation (4G). It respects all 3GPP specifications presented in Releases 7, 8, and 9. The system achieves maximum downlink (DL) peak rates of 300 Mbps and uplink (UL) 75 Mbps. These improvements are due to upgrades on the radio interference and network core performance, as well as Multiple Input Multiple Output (MIMO) antenna technology, interference control, and self-organising networks (SON). These developments brought the possibility of new services that can be used in real-time (e.g., virtual reality, interactive gaming) [Ribe18].

So, as expected, following 4G, the next mobile communications system is the 5th Generation (5G), which is currently under development. It is still an incognita of what exactly 5G fully is, but it aims at higher data rates (peak data rate of 10 Gbps), supporting more Device-to-Device (D2D) and Machine-to-Machine (M2M) communications and better coverage. The objective is the deployment of the Internet of Things (IoT) with lower latency (<1 ms) and less energy consumption. This huge evolution in wireless technologies makes it possible to respond to the increasing demand of communications services for control, operation, and maintenance of smart transportations systems [RGXK17]. 5G technologies will

most likely focus on the development of intelligent transportation systems of terrestrial and aerial vehicles. Nowadays, the demanded communications requirements of quality, capacity, and reliability in transportation systems are rigorous, and one of the best cases of this is the communications systems in high-speed trains (HST) [RGXK17]. In this environment, the existence of critical communication allows the possibility of establishing communications without a cable connections or interoperability an essential asset, since it is important not only for operations but also because of the quality of service provided to passengers.

The reason behind the importance of mobile communications in HST is the increasing demand for this means of transport. According to [SCIV17], a market study from 8 world regions – China, Japan, Korea, Taiwan, Germany, Spain, and Italy, the high-speed railway transport is a growing market. It includes historical data since 2005 and forecasts of market development up to 2025, as Figure 1.1 presents.
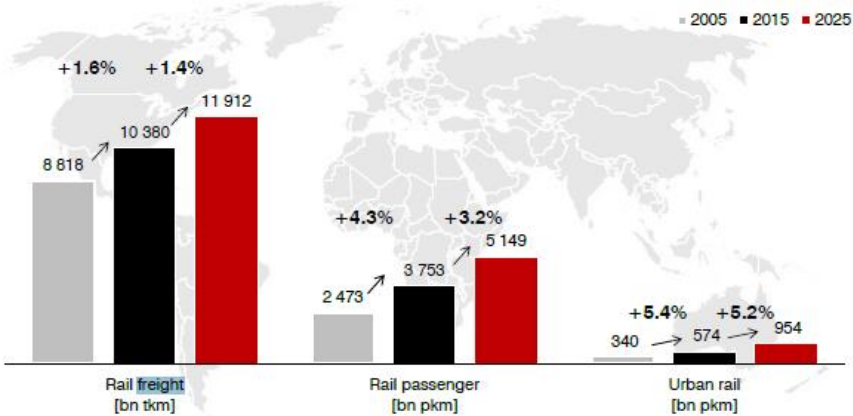
Figure 1.1 Worldwide rail transport performance and CAGR by segment (extracted from [SCIV17]).

It is possible to see a growth of 4.3%, from 2 473 to 3 753 billion rail passengers per km between 2005 to 2015, and a prediction of 3.2% between 2015 to 2025. The data provided by "Rail Transport Markets – Global Market Trends 2016-2025" supports the expectations over the rail market development [SCIV17]. In another study [IRSt18], the authors pointed out that the high-speed traffic's growth worldwide between 2010 and 2016 revealed a raise of 65.3% of passengers per km, Figure 1.2. All of these data support the fact that the level of importance of this means of transportation has been continuously increasing, so trains will likely have a critical role in the future, being worth investing in.

Nowadays, the railway industry still has a lot to grow, as one can see in Figure 1.3, particularly in services, infrastructures, and signalling areas. Some of the main reasons why railways are going to have a major role in the near future are as follows [Kunz17]:

- Energy-efficient: High-speed trains are up to eight times more efficient than commercial planes and four times more energy-efficient than cars over the same distance.
- Rail traffic is clean: The cargo transported by land produces eight times more CO_2 than by trains, and, in terms of passenger transportation, railway companies produced only 1.3% of the total emitted CO_2 in the transportation sector, while aviation is responsible for 12.4%, ships for

12.7%, and road transports for a total of 72.2% of the emissions.

- Safety: A US Department of Transportation study revealed that, in Europe, the number of fatalities in car accidents was fifteen times the number of railway related accidents.
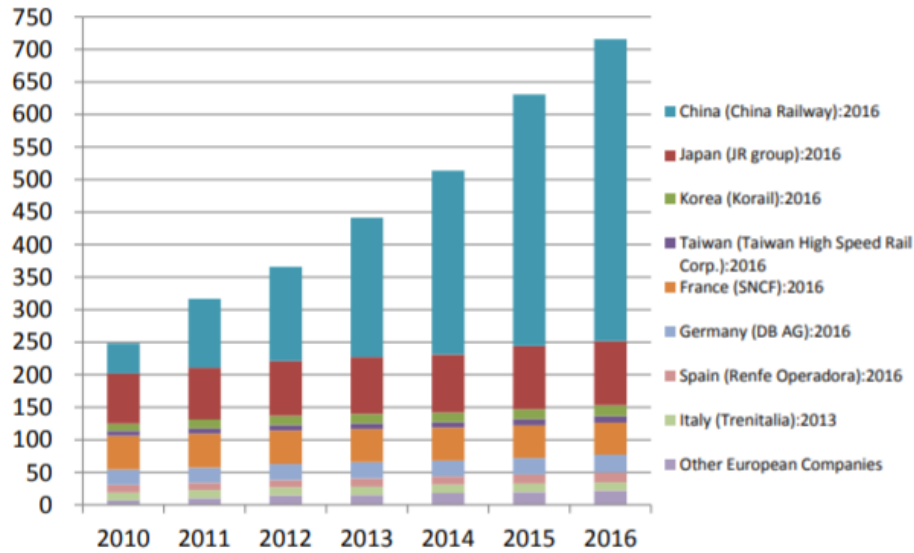
Figure 1.2 High-speed traffic in the world (extracted from [IRSt17]).
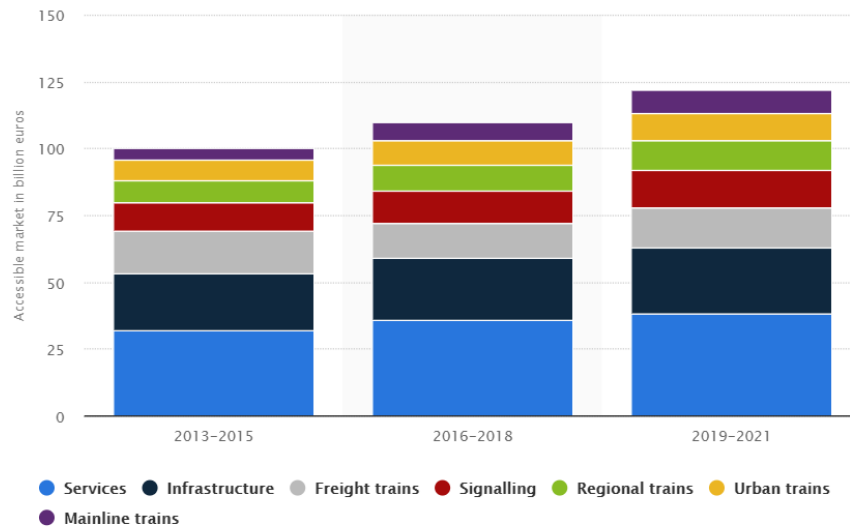
Figure 1.3 Annual average accessible railway market (extracted from [Stat19]).

Railway companies are now investing on the development of better services, either to passengers or to transportation. The increasing complexity of the systems present in the carriage, to improve their performance, result in the emergence of several issues. It is vital to determine how the systems are affected and then determine a way to minimise or solve the problem. One problem is the performance limitation that the antennas placed on the roof of a train suffer due to the structures placed there, like air-conditioning systems, pantographs, and even the form of the carriage itself. The goal of this thesis is to analyse how the pantograph influences the performance of the antennas, affecting, therefore, the

railways communication and endangering the quality of the service provided to passengers and railway operations. This thesis was developed in partnership with Thales, a multinational company that offers services in the transportation market. To do that, a model was developed and implemented using simulation software, the Computer Simulation Technology (CST) Microwave Studio [CST18], allowing the analysis of the situation presented in Figure 1.4.
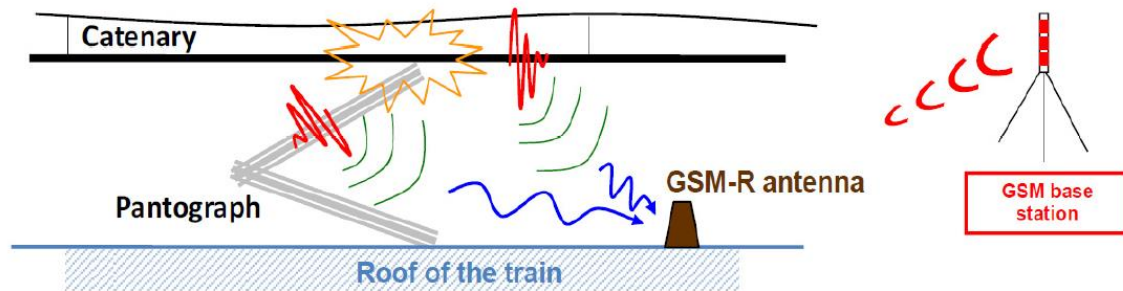
Figure 1.4 EMIs received by GSM-R antenna (extracted from [DDSA12]).

1.2   Contents

This thesis is composed of four chapters, including the present one, Chapter 1, where a brief overview of the evolution of mobile communications systems is presented, as well as the growth in demand for railway services and the report structure.

Chapter 2 presents an overview of the theoretical aspects related to the thesis. The general aspects of TETRA, GSM-R, LTE-R, and BBRS are detailed regarding their network architecture, radio interference and services provided. Afterwards, a description of railway communications requirements and railway scenarios is given. Then, the relevant performance parameters of railway mobile communications and antennas used in the analysis are specified, followed by the software used in the development and implementation of the model. Finally, this chapter ends with an overview of some works related to this thesis.

In Chapter 3, one presents the model developed to reach the main objective of this work, along with the more relevant parameters to be considered and evaluated. Afterwards, the theoretical description of the antennas performance is provided, as well as the considerations for the electromagnetic interference (EMI) analysis. A study to understand the antennas' performance isolated is then performed. Furthermore, a description of the CST Simulation tool is presented, followed by the study focused on the performance of the isolated antenna for the four systems (TETRA, GSM-R, LTE-R, and BBRS), as well as the validation of its behaviour. It ends with a simplified presentation of the model developed, as well as the assessment of the model itself.

Chapter 4 consists of the analysis of the results from both studies: the antenna behaviour analysis and the EMI analysis. This chapter starts by presenting the scenarios considered for both studies, including the most critical parameters that determine the scenario and its values, and an explanation for the perspectives that are relevant to analyse. Firstly, one presents and interprets the results for the antenna behaviour study, assessing how the catenary and the pantograph affect the antenna. This is followed by a study on the harmonics and its influence in the antenna behaviour.

Then, Chapter 5 summarises the main conclusion of this thesis, stating the main achievements and the main findings. One also presents improvements and possible future work to deepen the understanding of the problem.

Additional information to support the decisions made in this thesis along with more detail information is given in annexes. Annex A presents information about the monopoles developed for the four technologies (TETRA, GSM-R, LTE-R and BBRS), such as the mesh cells view, S_{11} performance and far-field patterns for 2D and 3D views. Annex B shows the antenna's performance according to its ground area, presenting the 2D gain pattern, as well as the values for the direction of maximum gain, direction, HPBW and L_{SSL} values for each technology, in the four scenarios. It also presents some intermediate values used in the EMI analysis. Finally, Annex C provides the antennas' specifications used in railway communication systems, presenting specific characteristics for each technology (TETRA, GSM-R, LTE-R, BBRS).

Chapter 2

Fundamental Concepts

This chapter provides an overview of railway communications systems, TETRA, GSM-R, LTE-R, and BBRS, a description of railway communications requirements, and railway scenarios. Also, the relevant performance parameters of railway mobile communications and antennas are defined, followed by a brief description of the software used. Finally, an overview of some works related to the thesis theme is given.

2.1 TETRA

TETRA, standing for TErrestrial Trunked RAdio, was developed and standardised by the European Telecommunication Standards Institute (ETSI), and it is an example of a Professional/Private Mobile Radio (PMR) system, used mainly for professional situations by government or official entities, such as police forces, fire brigades, military forces and even utilities (electricity, gas, water) [Leit09]. This system was standardised to allow one-to-many communications, which means that a series of open interfaces, network interfaces and their services and facilities were defined to enable interoperability, needed in PMR Operations. Also, it emerges as a solution for traffic congestion and the growing demand for speech and data services.

TETRA presents several features, such as a centralised call control that puts though priority call, maintaining the other on hold. The original TETRA standard was first known as TETRA Voice plus Data standard or TETRA Release 1. It is divided into two main interfaces:

- Switching and Management Infrastructure (SwMI): corresponds to the set of all equipment and sub-systems that comprise the network, including base stations.
- Inter-System Interface (ISI): permits infrastructures supplied by different TETRA manufacturers to interoperate with each other, providing interoperability between two or more networks.

Figure 2.1 shows its main components, described as follows [Over18]:

- SwMI: being the core of the TETRA network, it comprises all the switching equipment, base stations, management, and service provision elements. It is constituted by the MT and the Line Station (LS) terminals, the Direct Mode Station (DMS), a Gateway, the Network Management Unit (NMU), and the BS.
- Network Management Unit (NMU): it contains the database with information that allows MTs and its respective services and supported in switching calls coming from and to them. Also, it keeps tracking of the MT connection to the BS and assigns the traffic channels of the BSs.
- Gateway: it is responsible to route and forward calls requested from both the MT and LS, as well as managing data packets, and supports the handovers between BSs.
- Direct Mode Operation (DMO): it allows the direct connection between radio terminals, independently from the SwMI, which is the regular Trunked Mode Operation (TMO).

TETRA provides a series of services, such as group calls. Each subscriber, MT or LS, is identified by their Individual TETRA Subscriber Identity (ITSI), and a group is identified by a Group TETRA Subscriber Identity (GTSI). The MT sends this information to the SwMI upon registration, where this information, as well as the groups, is stored.

TETRA Release 2 appears as a response to the need for more enhanced technology to better satisfy user requirements, future proof investments and guarantees longevity.

TETRA's radio interface is designated by Air Interference in the system's architecture, as seen before. This layer is between the BS and the MT and the DMO interface. It operates in the 400 MHz and 800 MHz bands. Usually, for railway applications, the dedicated frequencies for TETRA are in the 400 MHz band. The band is divided into emergency/governmental services and civil applications.
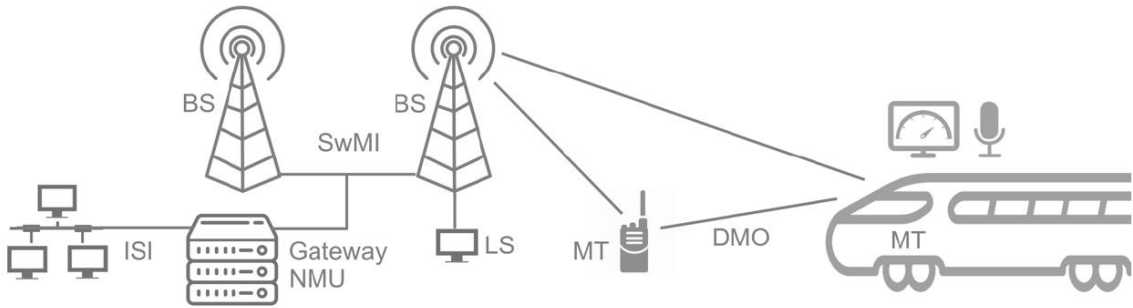
Figure 2.1 TETRA Railway Communication Network (extracted from [Duar18]).

TETRA system uses TDMA technology, so, multiple users share the same carrier. For each 25 kHz carrier, there are four channels, which allows 4 data or voice calls. Both voice and data can be transmitted. The maximum number of carriers for the BS is 8, adding up to 32 times slots.

In terms of modulation, TETRA uses π/4 Differential Quadrature Phase-Shift Keying (DQPSK), which results in a frame structure of approximately 17.65 frames per second. In DL, all slots are typically filled in. However, from the 18 frames per second, only 17 are used for traffic, the 18th being reserved for signalling, short data service messages or synchronisation. The maximum transmitted data is 28.8 kbps, 7.2 kbps for each channel.

2.2   GSM-R

The current section provides an overview of GSM-R's network architecture, as well as a description of the radio interference, based on [Corr18], [Dan08], [GSMR15a], [HAWG16], [LLLW11], [PuTa09] and [Ribe18].

2.2.1 Network Architecture

GSM-R stands for Global System for Mobile Communication for Railways. It is based on the commercial system GSM, but has been specially designed to meet railways' requirements with specific extra features. The primary network elements can be observed in Figure 2.2: the Base Station Subsystem (BSS), the Network and Switching Subsystem (NSS), and the Operation Subsystem (OSS).

On the left side of the architecture, one has the Mobile Station (MS), the interface between the user and the network. Subscribers can control it by choosing the operator that they think provides the best

services, and that responds better to their needs. The identification of each user is acquired through a Universal Subscriber Identity Module (USIM) card, which is inside the MS and possesses the Internal Mobile Subscriber Identity (IMSI) to recognise the subscriber in the network. On the other hand, each MS is identified by the International Mobile Equipment Identity (IMEI). Without a USIM card, the MS only performs emergency calls.
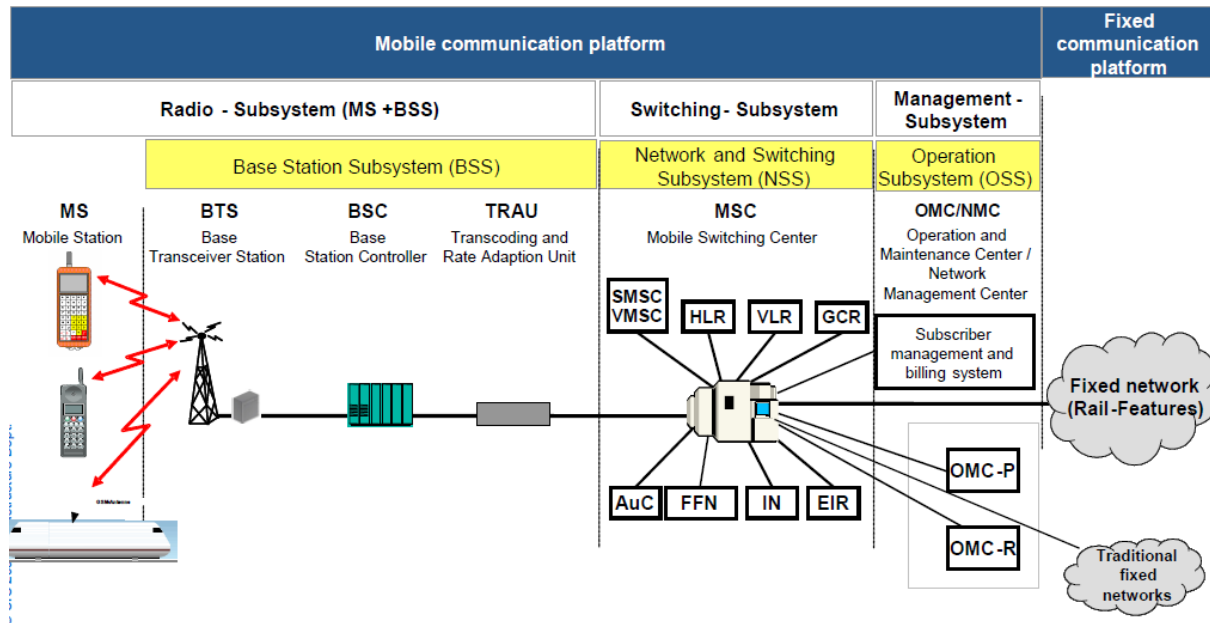
Figure 2.2 GSM-R network architecture (extracted from [Dan08]).

The BSS comprises all the specific radio equipment for a conventional GSM system and is composed of the Base Transceiver Station (BTS), the Base Station Controller (BSC) and the Transcoding and Rate Adaption Unit (TRAU). It is responsible for several functionalities, like handover decisions, coding, encryption, channel assignment, power control and maintenance of link quality. Its components can be described as follows:

- The BTS comprises transceivers and antennas, and it is responsible for the wireless communication between the subscriber and the network and providing continuous GSM-R coverage. Usually, to optimise the capacity of a cell, the transceivers are working at different frequencies regarding the standards for GSM-R. Each BTS is connected to only one Base Station Controller (BSC).
- The BSC is responsible for managing the BTS and their power levels and controls the signalling traffic and handovers. Handovers allow the transference of calls between cells without the loss of communication, which is a fundamental process for a good call experience in railways.
- The Transcoding and Rate Adaptation Unit (TRAU) performs transcoding function (coding and decoding) for speech and the adaption to the user data transmission rate. It is physically located on the BSC or the Mobile-Services Switching Centre (MSC).

The Network Switching Subsystem (NSS) comprises the main switching functions for the network and the databases necessary to assure mobility management. In the GSM-R network, the NSS main

components are: the Mobile Services Switching Centre or Mobile Switching Centre (MSC), the Gateway-MSC (GMSC), the Home Location Register (HLR), the Visitor Location Register (VLR), the Authentication Centre (AuC) and the Equipment Identity Register (EIR) They are described as follows:

- The MSC is the central element of the NSS. It is responsible for the call processing and switching functions. Mainly, it provides the functionality needed to handle a mobile subscriber, like network registration, authentication, location updating, handovers and call routing to roaming subscribers. It also provides an interface to other networks, such as the Public Switched Telephone Network (PSTN), Railway internal networks, and neighbouring GSM-R networks.

- The GMSC works as an interface to other networks and is capable of routing calls across networks.

- The HLR and the VLR are databases. The HLR database contains permanent subscribers' information, along with their last known location. The VLR database holds the subscribers' information that belongs to the MS that is currently in the VLR serving area. The VLR obtains this information from the HLR.

- The AuC is responsible for ensuring that only authorised users have access to the network. It also provides the parameters required for authentication and encryption functions for verification of the user's identity.

- The EIR is a database that decides whether a piece of given mobile equipment may be allowed onto the network. It is used to prevent unapproved, stolen, or defective MS equipment from accessing the network.

The OMC is connected to components of the NSS and the BSC. According to [Puta09], it usually consists of a terminal interface providing direct access to the network operating system, via software applications that are shipped with the network hardware. It is used for the control and monitoring of the GSM network, and it is also used to control the traffic load of the BSS.

According to [PuTa09], an optional feature of GSM-R is the General Packet Radio Service (GPRS). It is a data service that uses radio resources just when data is sent. This way, the channel utilisation for some applications can be more efficient, leading to a more economical use of the bandwidth. GPRS enhances GSM-R data services significantly by providing end-to-end packet-switched data connections. It allows point-to-multipoint (PTM) services, something that is not possible in circuit-switched networks. To add this service, the following infrastructure elements are required: the Serving GPRS Support Node (SGSN), the Gateway GPRS Support Node (GGSN), and the Point-to-Multipoint Service Centre (PTM-SC). The transmission between the BTS and the BSC will remain equal, only requiring a Packet Control Unit (PCU) in the BSC, to control the packet channels.

One of the essential restraints on GSM-R network planning is the available bandwidth in the spectrum. GSM-R allocates a total bandwidth of 4 MHz: 876-880 MHz for mobile station transmissions (UL) and 921-925 MHz for base station ones (DL). In some countries, apart from the 19 channels, this allocation has an additional 200 kHz guard band to protect against interference between the GSM-R band and the adjacent E-GSM band at the upper end. Besides, a 400 – 600 kHz guard band is recommended on the

lower border of frequencies to prevent interference with Private Mobile Radio (PMR) / Public Access Mobile Radio (PAMR) services (e.g., the Terrestrial Trunked Radio). From this guard band, 100 kHz is a part of the UIC band. Figure 2.3 provides an overview (not to scale) of how the spectrum is allocated.
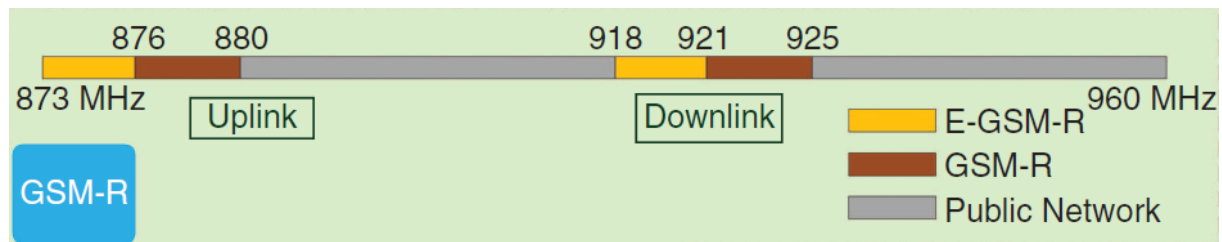
Figure 2.3 The allocation of frequency bands for GSM-R (adapted from [HAWG16]).

It is narrowband compared with other systems, such as, for example, the Long-term Evolution – Railway (LTE-R) system. A narrowband system increases the range and the spectrum efficiency but has a low data rate. GSM-R uses a modulation format called Gaussian Minimum Shift Keying (GMSK) with periodical Time Division Multiple Access (TDMA). The system has a 200 kHz bandwidth, and one TDMA frame corresponds to 4.615 ms and is constituted by 8 time-slots with 156.25 bits each (577 μs). The GSM-R system has a capacity of 22.8 kbps for voice services and 9.6 kbps for data transmission [Corr18]. With GPRS integrated, it provides 56 – 114 kbps.

2.3   LTE-R

In this subsection, an overview of LTE-R's network architecture is presented, the future mobile radio system for railways, based on [Cisc16], [CMAF13], [FRGC15] [HAWG16] and [HoTo11]. Also, a description of the radio interference, as well as the services provided, are given, grounded on [3GPP17], [ACKZ14], [FrFC17], [FRGC15] and [GeRK12].

2.3.1 Network Architecture

In order to provide improved and more efficient transmission for HSR communications, the LTE-R system was chosen one to replace GSM-R. LTE-R is based on an IP based packet switched solution, since IP carries both voice and data services. According to [HAWG16], the LTE standard includes a core network of Evolved Packet Core (EPC) and a radio access network of Evolved Universal Terrestrial Radio Access Network (E-UTRAN). The IP-based EPC supports seamless handovers for both voice and data, and each E-UTRAN cell will support high data and voice capacity by High-Speed Packet Access (HSPA). Therefore, LTE-R has all the important features from LTE, providing an extra radio access system to exchange signals with onboard units (OBUs) and to respond to HSR needs.

As mentioned before, the addition of GPRS to GSM-R offers as much interoperability as possible to the railway communications system. As it can be observed in Figure 2.4, the SGSN node allows LTE-R and GSM-R to work in parallel. The core network of LTE-R is backward compatible with GSM-R.

In the block on the left side, one has the group of all On-Board Units (OBU), which consists of the elements required for the connection in the communications system. Similar to GSM-R with the MSs, the OBUs contain a USIM that identifies and authenticates users and is used to derive security keys for protecting the radio interface transmission.

The Evolved UTRAN (E-UTRAN) block is composed of several nodes E-UTRAN Nodes B (eNodeB or eNB). According to [HoTo11], it is the radio base station that is in control of all radio related functions in the fixed part of the system. The eNodeBs are linked to each other by the X2 interface, and the connection with the EPC is made through the S1 interface. Also, a set of a Mobility Management Entity (MME) and a Serving Gateway (S-GW) is assigned to serve a specific set of eNodesBs. This means that one eNodeB may need to be connected to several MMEs and S-GW at a time, but the OBU is served by only one MME and S-GW, the eNodeB being responsible for tracking the association.
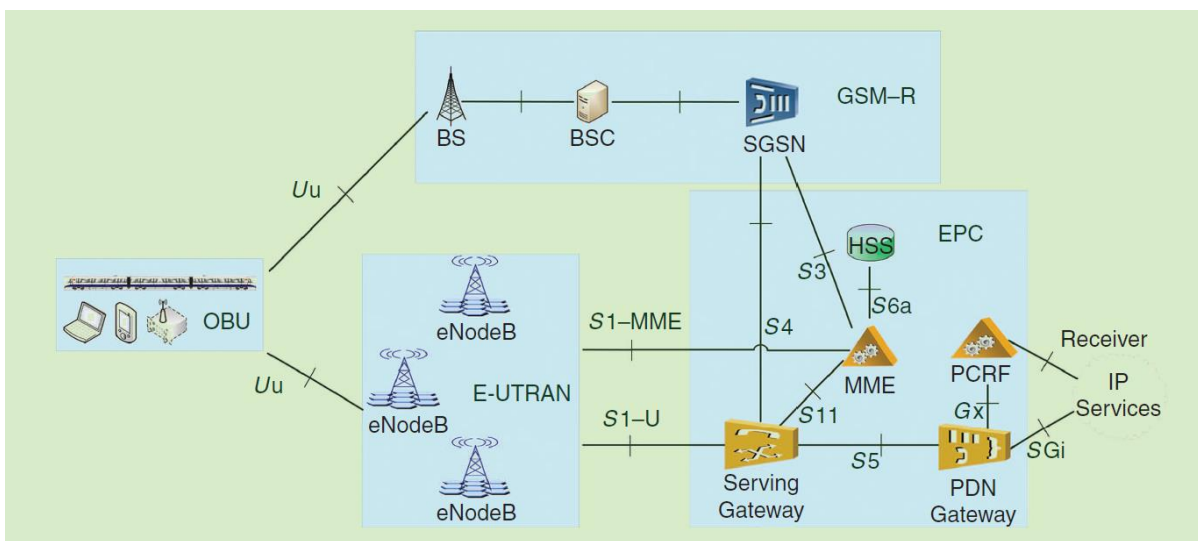
Figure 2.4 LTE-R architecture for HSR (adapted from [HAWG16]).

On the right block, one has the Evolved Packet Core Network (EPC). Like the E-UTRAN block, it represents the IP Connectivity Layer, a sector of the LTE-R core network. The EPC is functionally equivalent to the packet-switched area of the existing 3GGP networks. As presented in Figure 2.4, the primary logical nodes of the EPC are:

- Mobility Management Entity (MME): It is the main control element. It works with eNodeBs (S1), S-GW (S11), HSS (S6a), SGSN (S3), and MMEs from other EPCs. It is the key control-node for the LTE access network. The MME is responsible for the authentication and security, through the HSS, for choosing the appropriate S-GW for a respective OBU and generating and allocating temporary identities for OBUs. It also keeps track of the location of all OBUs.

- Serving Gateway (S-GW): Having a very small role in control functions, the S-GW is only responsible for its resources. All the user's data passes through this node. It works as the local mobility anchor during the mobility between eNodeBs, switching the tunnel from eNodeB to eNodeB according to the MME's command. It also provides tunnelling resources for data forwarding when needed during the radio handover.

- Packet Data Network Gateway (P-GW): Typically, P-GW is responsible for allocating the IP

address to the OBU, which is used by the user to communicate with another IP host in external networks (e.g., the internet). The IP address allocation is always done when the user makes a Packet Data Network (PDN) request. It also performs policy and charging control requests, the control of user plane tunnels for UL and DL data delivery.

- Policy and Charging Resource Function (PCRF): It is the network component responsible for Policy and Charging Control (PCC) and for making decisions on how to handle the services in terms of QoS and information provided to the P-GW and S-GW.

- Home Subscriber Service (HSS): The subscription data repository for all permanent user's data, storing the services that apply to users, the allowed PDN collection, and roaming restrictions.

2.3.2 Radio Interface

With the evolution of services for HSR, there is a need to improve and make transmission for HSR communications more efficient. LTE-R can achieve a higher capacity, a lower latency, and higher reliability compared to GSM-R. According to [3GPP17], it may operate in 70 different frequency bands, either for Frequency Division Duplexing (FDD) or for Time Division Duplexing. The frequency range is from 450 MHz to 2.8 GHz. Presently, most LTE systems work at the bands above 1 GHz, such as 1.8 GHz, 2.1 GHz, 2.3 GHz, and 2.6 GHz, although 700–900 MHz bands are also used in some countries, as presented in Figure 2.5.
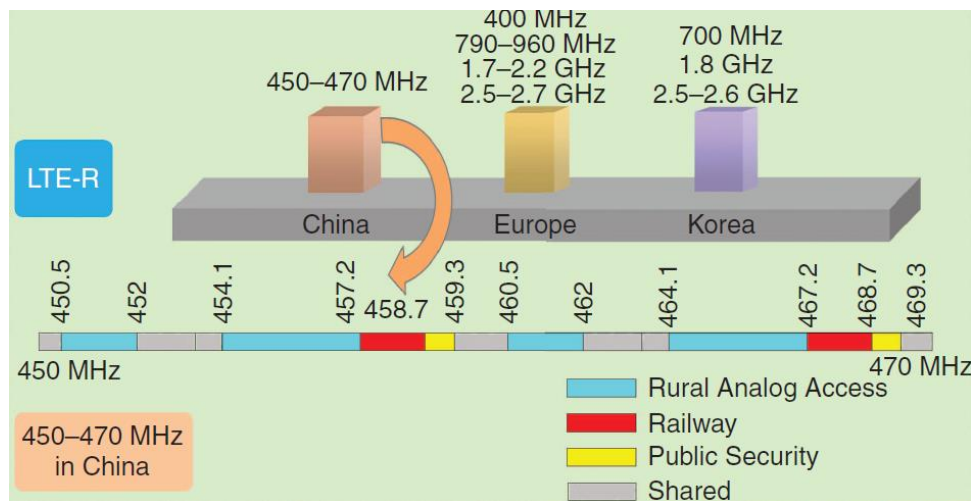
Figure 2.5 The allocation of frequency bands for LTE-R (adapted from [HAWG16]).

The bandwidths are larger, which leads to a higher data rate, but the path loss is also more significant, and signal fading is more substantial. According to [ACKZ14], the higher frequencies exhibit weaker diffraction capability, which is very important for railway dedicated mobile communications. If 2.6 GHz is adopted, with typical transmit power levels, the radius of a cell does not exceed 500 m, resulting in a dense layout of BSs for HSR. This will result in significant investment and frequent handovers. The best solution is to use a dual-band mode. This way, the high priority service is working in the 800 MHz frequency band, and the low priority is working in the 1.8 GHz or 2.6 GHz ones.

LTE DL transmission scheme is based on a multiple access technique named Orthogonal Frequency

Division Multiple Access (OFDMA): the available spectrum is divided into several carriers, called subcarriers, and each subcarrier is independently modulated and transmitted over a high number of closely spaced orthogonal subcarriers. According to [GeRK12], in the time domain, a guard interval is added to each symbol to combat Inter-Symbol-Interference (ISI) due to channel delay spread. This is where the distinction between an OFDM transmission scheme and an OFDMA transmission scheme is made, since OFDMA allows the access of multiple users on the available bandwidth. The overlapping of the subcarriers can happen without any problem because they are orthogonal to each other in the frequency domain. This multiple access technique increases the data rate, lowers the sensitivity to fast fading and since there is no need for a guard-band to prevent ISI it increases spectral efficiency.

The available LTE carrier bandwidth goes from 1.4 MHz, with 72 reserved subcarriers, to 20 MHz, with 1 200 subcarriers, depending on the number of sub-carriers needed with a 15 kHz separation between them. The physical channels are based slots with a duration of 0.5 ms and 12 subcarriers (180 kHz) named Resource Block (RB). Figure 2.6 provides a better understanding of how these physical channels work. The maximum amount of RBs allocated to each user depends on the bandwidth: the lowest bandwidth (1.4 MHz) provides 6 RBs, and the highest one (20 MHz) can afford 100 RBs.
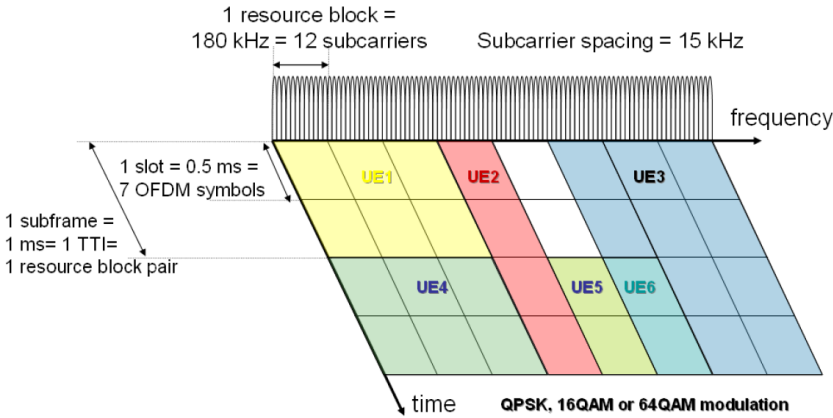
Figure 2.6 Overview of RBs allocation (extracted from [GeRK12]).

Although OFDMA properties are optimum for DL, the same does not happen for UL, due to the weaker peak-to-average power ratio (PARR) properties of an OFDMA signal, which result in worse UL coverage and are a challenge for the power limitations of mobile devices. Thus, to optimise the battery performance, the UL transmission scheme for FDD and TDD node is based on Single Carrier Frequency Division Multiple Access (SC-FDMA) with a cyclic prefix. SC-FDMA signals are a linear combination of all data symbols from a set of subcarriers, and it has better PAPR properties, which decreases costs.

2.4 BBRS (Broad Band Radio System)

This subsection provides an overview of BBRS network architecture, radio interference, and services, based on [BBRS17], [Gonc13], [Maso13], [Mend10] and [Reed18].

2.4.1 Network Architecture

BBRS is a railway communication system provided by Thales. It allows the transmission and reception of data between infrastructures (i.e., stations) and trains. Security systems such as CCTV and the systems for the management of trains are some examples that need BBRS to function. The connection between the radio equipment (APs) and the onboard equipment is created using Wi-Fi technology. It allows bidirectional transmission of data. Figure 2.7 presents the BBRS General Architecture, which has five main functional components: Network Management System (NMS), Gateway Server, Mobility Controller, Static Mesh Nodes and Mobile Mesh Nodes. Each can be described as follows [Gonç13]:

- NMS: It enables live monitoring and management of the entire BBRS network, which is used to allow access to mesh network functions and individual node settings, including security, regulates traffic prioritisation, radio power controls, identifies roaming and handover, detects errors or faults and other features. So, there is redundancy since both the Operation Control Centre (OCC) and the Backup Control Centre (BCC) have the software installed. However, this tool does not perform any vital function for Network operation.

- Gateway Server: It is installed in the Central Equipment Room (CER) in the BCC, and it is used for mobility and traffic management purposes at a specific mesh. It is also responsible for mobility through the different Static Mesh Nodes. Also, for redundancy, each mesh has a main GWS at OCC and a backup at BCC.

- Mobility Controller: It is installed at the CER in the OCC, being used for mobility purposes since it is responsible for the mobility of all meshes, to reduce future problems of handover.

- Static Mesh Nodes: They are placed along the track to guarantee radio coverage, and they are installed on a pole, connected to two-sector antennas.

- Mobile Mesh Nodes: They are installed inside the trains, and they are responsible for establishing the connection between the SMNs antennas, allowing bidirectional transmission between the BCC and the moving trains. Usually, the link between them is done in a two-hop communication system (train-to-infrastructure and intra-car) to avoid the high penetration losses created by carriages (about 25 dB).
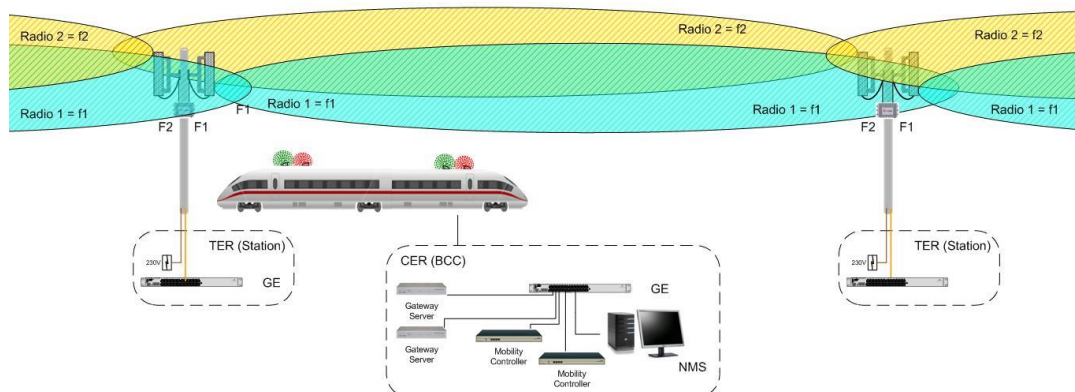
Figure 2.7 BBRS General Architecture (extracted from [Gonç13]).

These five components are connected between them via optical fibre and through wireless connectivity. The handover between the equipment is installed on the track, and it is based on several parameters,

such as RSSI (Received Signal Strength Indicator), throughput, and link quality.

2.4.2 Radio Interface

BBRS is based on the IEEE 802.11n 2x2 standard, using multiple-input multiple-output (MIMO) technology, with two transmitting and two receiving antennas, which enables spatial diversity and spatial multiplexing. Usually, it uses MIMO-OFDM to increase the range and the data transmission rate. And various types of modulation, such as BPSK, QPSK, 16-QAM or 64-QAM, with coding rates between 1/2 to 5/6 as the transmitting data method. The IEEE 802.11n uses 2.4 GHz and 5 GHz bands. It uses channels with a bandwidth of 20 MHz or 40 MHz. Since the wireless network uses an OFDM modulation, it more than doubles the data rate. With a 20 MHz channel, OFDM slices it in 52 subcarriers, 48 of which are used for carrying data. When the channel bandwidth is 40 MHz, the number of subcarriers carrying data increases to 144. This allows a data rate delivery of 65 Mbps for a 20 MHz channel and a total of 135 Mbps for a 40 MHz channel [Maso13]. Table 2.1 presents the different working frequencies for BBRS. It is recommended the use of the non–standard with a license due to security issues and also because the licensed spectrum has 10 to 100 times more signalling power than the unlicensed one, which provides a better link without notable interferences [Reed18].

Wi-Fi allows bidirectional transmission of information packets, making it possible to send and receive any IP traffic. Table 2.2 presents the performance requirements provided by Thales.

Table 2.1 BBRS working frequencies (based on [Thal17]).

Wi-Fi Type	Frequency [GHz]
Standard without license	2.405 - 2.495
	5.150 – 5.825
Non - Standard without a license	5.825 – 5.875
Non – Standard with a license (recommended)	5.875 – 5.925

Table 2.2 BBRS - Performance (based on [Thal17]).

Requirements	Values
Speed	≤ 250 km/h
Rate	70 Mbps ≤ x ≤ 125 Mbps
Handover	< 100 ms
Range	< 1km (300m in an urban environment)

2.5 Services Comparison

According to [HAWG16], the GSM-R network serves as a data carrier for the European Train Control System (ETCS), which is the signalling system for railway control. The main HSR-specific services

offered by this system are as follows [PuTa09]:

- Fast Call Set Up: This feature is essential to support the EIRENE FRS requirement so that railway emergency calls are set up in less than 2 s in 95% of cases.

- Voice group call service (VGCS): orients group calls between trains and BSs or between trackside workers, station staff and similar groups.

- Voice broadcast service (VBS): The BS broadcasts messages to trains and vice-versa, but in this case, only the initiator of the calls can speak, and the others who join the call can only listen. This service is mostly used to broadcast recorded messages or to make train operation announcements.

- Enhanced multilevel precedence and pre-emption (eMLPP): defines the user's priority, and it is used in case of emergency group calls. In case of emergency calls, with higher priority, an appropriation of resources that are being used by a lower-level call can happen, and so can, in worst scenarios, the disconnection of the ongoing call.

- Shunting mode: provides an effective means of communication to a group of personnel who are involved with a shunting operation, which regulates and controls user access to shunting communication.

- Functional addressing (FA): A train can be addressed by a number identifying the function for which it is being used at the time, rather than a more permanent subscriber number.

- Location-dependent addressing (LDA): It is a system of communication between the driver and the controller by merely pressing a bottom or dialling a short code. Calls from a train to certain functions can be addressed based on the location of the train as it moves through different areas of BSs without any concern from the driver.

- Emergency Calls: It informs drivers, controllers, and other concerned personnel about any railway emergency, either train emergency calls (whilst not involved in Shunting operations), or Shunting emergency calls (whilst involved in Shunting operations). A railway emergency call has three phases: Stage 1 – Warning; Stage 2 – Information; Stage 3 – Terminate Railway emergency call.

- Call reselect: Handovers are happening continuously in railway communications, so it necessary to make a reselection of cells while the trains are moving.

Despite the enormous popularity of GSM-R, the responsible railways entities are looking for ways to overcome the barriers imposed by this network. The main limitations are as follows:

- Interference: Interference between GSM-R and public networks is increasing due to both railway and public operators wanting good coverage along rail tracks. This could result in network loss, as well as severe weakening of voice and data communications.

- Capacity: The 4 MHz bandwidth of GSM-R can support 19 channels of 200 kHz width, which is insufficient for the next generation railway system.

- Capability: Being a narrowband system, GSM-R cannot provide advanced services due to its maximum transmission rate (9.6 kbps). This amount of rate is sufficient for applications with low demand, but the delay is so high that it is not possible to achieve any real-time application that a service needs in HSR communications.

Based on these, LTE-R is the most likely to replace GSM-R. Control and safety are two essential concepts in the railway environment. So, LTE-R appears not only as a substitute for GSM-R but also a single integrated solution that can lower operation and deployment cost, while achieves high performance and flexibility. It also brings a complete set of services and applications to be used in railways to improve aspects of security, QoS and network efficiency. In Figure 2.8, it is possible to see the different categories of railway group services.
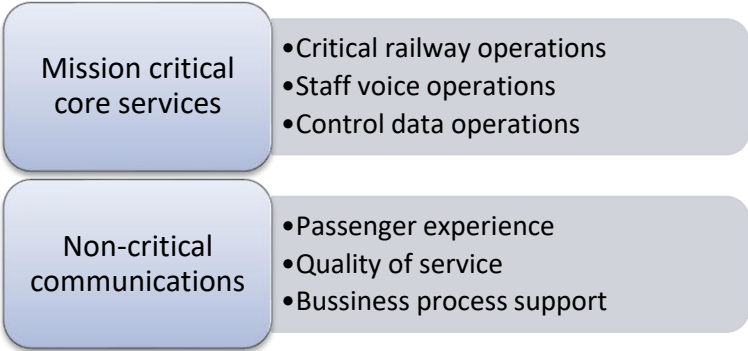
Figure 2.8 Railway services classification (adapted from [CMAF13]).

In Table 2.3, one presents the main characteristics and system parameters of GSM-R and LTE-R. For this transition to take place, its necessary to verify if the LTE-R performs all the services provided by the GSM-R network. One presents the LTE features and mechanisms needed to implement GSM-R railway functionalities.

In the future, it will most likely be necessary services that will be provided by LTE-R to the railway environment. Table 2.4 presents a completed list of those services.

Table 2.3 LTE features that support GSM-R railway functionalities (adapted from [CMAF13]).

LTE	GSM
LTE IMS-based VoIP (VoLTE) + IMS-based Push-to-Talk over cellular (PoC)	Voice group call service (VGCS)
VoLTE + PoC: IP multicast of voice and video services	Voice broadcast calls (VBS)
Access class barring mechanism + policy control rules + QoS mechanisms	Priority and pre-emption (eMLPP)
Session Initiation Protocol (SIP) addressing	Functional addressing (FN)
Localisation services in LTE	Location-dependent addressing (LDA, eLDA)
Emergency and critical safety voice services over IMS in LTE	Railway emergency calls (REC, e-REC)
Very low latency of LTE to support fast exchange of signalling (e.g., IMS-based PoC) + Access class barring	Fast call set up
IMS-based SMS service. Use SG interface between MME and MSC server. MME-based SMS service	Data exchange (SMS, shunting)

Table 2.4 Future railway services (adapted from [CMAF13]).

Passenger experience	Business process support	Operations support
- Trip information: routes, timetables, delay notification - Digital signage - Electronic ticketing - High-speed Intranet access - Personal onboard multimedia entertainment	- High-speed infrastructure for operations staff communications in stations and depots - Remote diagnostics and fleet maintenance - Location-based services	- Real-time video and data for remote driverless operation - Real-time traffic management - Safety services including onboard CCTV, driver look-ahead video - Communication-based train control and signalling - Legacy voice communications

Due to the constant evolution of the services provided in trains, the amount of services provided by BBRS is considerable and continues to grow in the direction of the Internet of Trains. According to [BBRS17], the main applications provided by BBRS are the following:

- Train Maintenance System: It provides real-time notifications such as alarms and warnings of any anomalies on the systems onboard.
- Onboard live CCTV: It allows the visualisation of video streaming in real-time of every camera onboard.
- Platform cameras visualisation: It allows a real-time display of platform chambers from the trains driver's cab.
- Passenger Information System: It increases the interaction between the passenger and the train, allowing the sending of audio messages, text messages, and video content to the train.
- Internet for passengers: It gives internet access to passengers.

These services have the objective of improving the experience and QoS in the users' perspective.

2.6   Railway Communications

In this subsection, a description about the main features of railway communications is given based on [AGRK15], [BFML10], [FDGH13], [FrFC17], [GSMR15a], [GSMR15b], [Palu13], [PuTa09], [TMGA01a] and [XZAZ16].

2.6.1 Requirements

According to [PuTa09], the Council Directive 96/48/EC of 23 July 1996 for High-Speed Lines (HSL) defines the six subsystems that constitute the railway network: Control and Command, Infrastructure, Energy, Rolling Stock, Operation and Maintenance. Control and Command are the most important ones for railway communications. In Europe, the entity responsible for these sub-systems is ERTMS, the most common signalling system in Europe. It ensures high performance concerning interoperability, safety, accessibility, cost, and maintenance. Based on [Palu13], the benefits of ERTMS are as follows:

- Safety: Safety increases due to the constant speed monitoring, the signals received in the cabin by the crew and the sending of Temporary Speed Reductions (TSR) to the network.
- Cost: There is a decrease in the costs, once the number of physical signals and track magnets with cable connections also decreases, as well as an improvement in traffic management.
- Accessibility: Error recovery is faster, and the number of systems is reduced.
- Interoperability: Due to the standardisation of both architecture and information, as well as the uniformisation of the technical interfaces between the sub-system.
- Maintenance: Maintenance decreases because, once the systems are standardised, there are fewer critical safety interfaces, and there are several suppliers on the market.

So, ERTMS is an international standard program that was created so that there is a common interoperable platform for railways and signalling systems. The command and control system chosen is a standardised, interoperable Automatic Train Protection system, the European Train Control System (ETCS). This system is the main component of signalling and train control. ETCS is divided into different functional levels. According to [Palu13], the levels can be defined as:

- ETCS LEVEL 0: When the ERTMS/ETCS is adopted, one significant advantage is the removal of lateral signals. However, when an ETCS vehicle is used in a non-ETCS route without a train borne Specific Transmission Module (STM), the train driver only has access to the maximum speed, so he must observe the trackside signals.
- ETCS LEVEL 1: The *Eurobalise* radio beacons, fixed between the rails, pick up signal aspects from the trackside signals via signal adapters and telegram *LEU Encoders*, and transmit them to the train as a *Movement Authority*, with permission to cross one or more block sections, together with route data at fixed points. The computer on board is responsible for monitoring and calculating the maximum speed and the braking curve from this data in continuous time. So that this transmission is continuous, an additional infill should be added due to the occasional interruptions. Because of the spot transmission data, the train must travel over the *Eurobalise* beacon to obtain the next movement authority. Figure 2.9 presents a scheme of ECTS level 1.
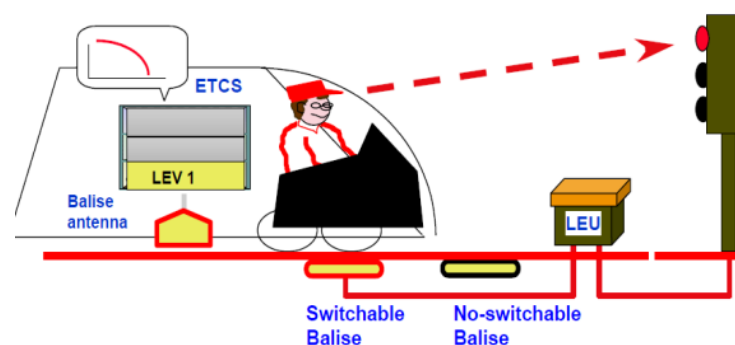
Figure 2.9 ECTS Level 1 (extracted from [Palu13]).

- LEVEL 2: This is a digital radio-based signal and train protection system. The Radio Block Centre (RBC) provides information to the train, such as Movement Authorities, speed restrictions, and route data. The GSM-R network is used by all trains, so they can automatically report their exact position and direction of travel to the RBC. At this level, the *Eurobalises* are used as passive positioning beacons, and between two beacons, the train determines its

position via sensors. They are used to correct distance measurement errors. The onboard computer continues monitoring the transferred data and the maximum permissible speed. Figure 2.10 presents a scheme of the ECTS level 2, and, as it can be observed, there is no need for trackside signals, since the driver has access to all the information in the panel.
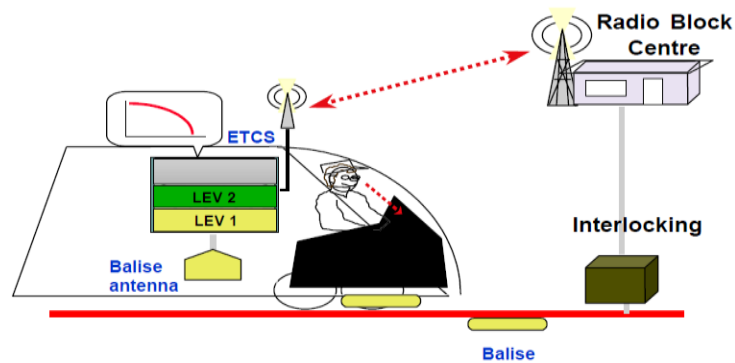
Figure 2.10 ECTS Level 2 (extracted from [Palu13]).

- LEVEL 3: Delivers an implementation of full radio-based train spacing. Following the same model as LEVEL 2, trains determine their position through the beacons and via sensors and must also be capable of determining train integrity onboard. The track is no longer divided into fixed sections because the position of a train is based on its distance from the next one. This method is called absolute braking distance spacing or moving the block and aims to optimise the capacity of the track. Figure 2.11 presents a scheme of the ECTS level3.

According to [FrFC17], in order for GSM-R to follow the last EIRENE specifications, the network should fulfil all the requirements that guarantee the interoperability of the railway system. The general and functional requirements can be allocated to four categories: Mandatory for Interoperability (MI), Mandatory (M), Optional (O), or Not Applicable (NA). The placement depends on the type of radio. In Table 2.5, one presents the classification of services according to the categories presented before.
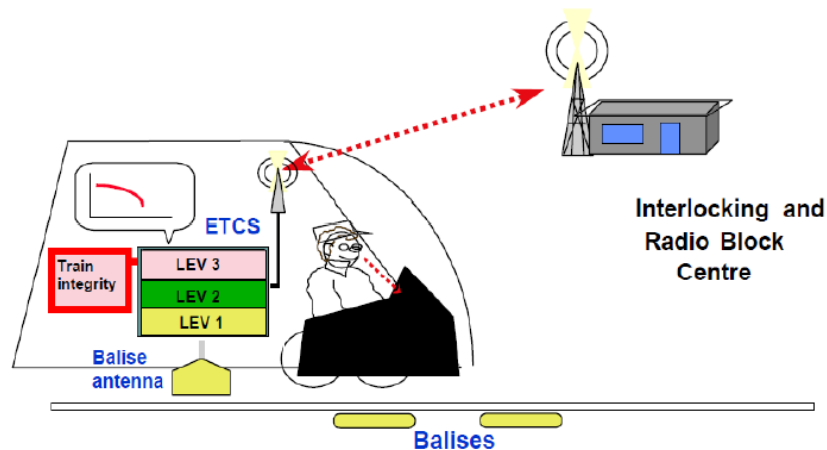
Figure 2.11 ECTS Level 3 (extracted from [Palu13]).

Table 2.6 presents the threshold for the call setup required times, and they must be achieved in at least 95% of the cases (MI). Also, the call setup time cannot be more than 1.5 times the required call setup time for 99% of the cases (MI).

Table 2.5 Services to be supported according to the radio type (adapted from [FrFC17]).

Service Group	Type of Service	Cab	ETCS Data Only	General Purpose	Operational	Shunting
Voice - Call	Point-to-point	MI	NA	M	M	M
	Public emergency	M	NA	M	M	M
	Broadcast	M	NA	M	M	M
	Group	MI	NA	M	M	M
	Multi-party	MI	NA	O	O	M
Data	Text message	MI	NA	M	M	M
	General data applications	M	O	O	O	O
	Automatic fax	O	NA	O	O	O
	ETCS trains control	NA	MI	NA	NA	NA
Specific features	Functional addressing (FA)	MI	NA	M	M	M
	Location dependent addressing (LDA)	MI	M	O	O	O
	Direct mode	NA	NA	NA	NA	NA
	Shunting mode	MI	NA	NA	NA	M
	Multiple driver communication within the same train	MI	NA	NA	NA	NA
	Railway emergency calls	MI	NA	O	M	M

Table 2.6 GSM-R call setup time requirements (adapted from [FrFC17]).

Call Type	Call Setup [s]
Railway emergency call	4 (M)
High priority group calls	5 (M)
Group calls between drivers in the same area	5 (M)
All operational and high priority mobile-to-fixed calls not covered by the above	5 (O)
All operational and high priority fixed-to-mobile calls not covered by the above	7 (O)
All operational mobile-to-mobile calls not covered by the above	10 (O)
All other calls	10 (O)

According to [FrFC17], the GSM-R network is in charge of guaranteeing mandatory services, so it must satisfy all QoS requirements. However, even though the network's ability to manage QoS policies according to the traffic types, it is not enough for real-time applications. Strict latency requirements are needed for continuous operations, such as train status and location, and the connectivity must be uninterrupted at 500 km/h. Table 2.7 summarises the main QoS parameters and their availability.

Table 2.7 Main GSM-R QoS requirements (adapted from [FrFC17]).

Requirements	Value
Connection establishment delay of mobile originated calls	<8.5s @ 95%, ≤10s @ 100%
Connection establishment error ratio	$<10^{-2}$ @ 100%
Connection loss rate	$<10^{-2}$/h @ 100%
Maximum end-to-end transfer delay	≤0.5s @ 99%
Transmission interference period	<0.8s @ 95%, <1s @ 99%
Error-free period	>20s @ 95%, >7s @ 99%
Network registration delay	≤30s @ 95%, ≤35s @ 99%, ≤40s @ 100%
Call setup time	≤10s @ 100%
Emergency call setup time	≤2s @ 100%
Duration of transmission failures	<1s @ 99%

The handover success rate should be at least 99.5% over train tracks according to [GSMR15a], and this process must be optimised. The handover for voice calls is 350ms in 95% (M) of cases and 500ms in 99% of cases (M). Also, to reduce the handover break period to about 150ms, the synchronous handover capability is advisable. It consists of having the BTS transmissions in different cells synchronised. Each authority decides if it is implemented.

According to [XZAZ16], an increase in the train's velocity causes a high Doppler shift and spread. It is necessary to consider the fast-varying channel and inter-carrier interference (ICI), particularly for OFDM technology. The ratio between the energy of the direct path and the multipath is relatively large, and the delay of multipath is relatively small. Therefore, the Doppler shift is the one that needs to be considered. However, its variation is so tiny that the Doppler shift can be estimated with certainty and compensated, allowing an accurate determination of the train's velocity and its location.

Another aspect that must be considered in network planning is the coverage, meaning the field strength at the antenna on the train. In Table 2.8, one presents the values of coverage and speed-limitations required for ER-GSM band frequencies. Each location interval has a length of 100 m, and the coverage levels consider a maximum total loss of 6 dB, 3 dB between the antenna and the receiver input, and a margin of 3 dB for, for example, ageing.

Table 2.8 Coverage and speed limitation requirements (based on [GSMR15a]).

Services	Coverage probability [%]	Coverage level [dBm]	Velocity [km/h]
Voice and non-safety critical data	95	-98	-
ETCS levels 2/3	95	-95	≤ 220
ETCS levels 2/3	95	-92	≥ 280
ETCS levels 2/3	95	[-95; -92]	]220; 280[

2.6.2 Railway Scenarios

The different scenarios that exist in railway tracks must be considered since there may exist specific parameters that influence the propagation of the signal. In railway communications, the main scenarios are bridges, viaducts, tunnels, water, terrain cuttings and embankments, urban, suburban, and rural areas, mountains, and railway stations, which cause reflection and scattering of the signal and influence network performance. The positioning of the antennas is something that has also to be considered. For example, in an onboard rooftop antenna, placed outside the train, the elevation and the azimuth plane pattern give the ability to analyse the way that the antenna radiates in all directions.

Also, there are several ways to power a railway, and nowadays, the railway electrification system is the most used to supply trains. The power provided to the moving trains is made through a nearly continuous conductor that runs along the track, and it usually takes one of these two forms: an overhead line or a third rail. While the overhead line is suspended from poles along with the track or tunnel ceilings, the third rail (or even a fourth rail) is an additional line that is at the same level as the track. In the overhead line mode of power transmission, the structure that is used to collect power is a pantograph, and it is installed on the train's roof.

There are various sources of Electromagnetic interference (EMI) in a railway environment, the emissions from the pantograph and overhead line being two of them, as presented in Figure 2.12.
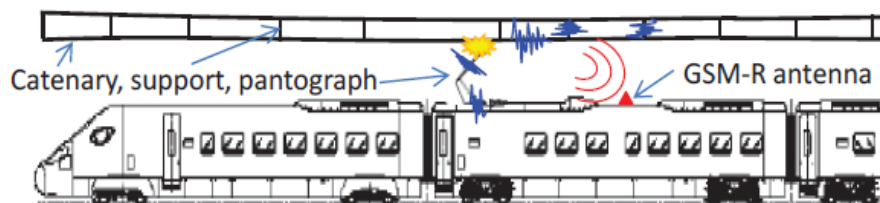
Figure 2.12. EMI from Line-Pantograph interaction (extracted from [FDGH13]).

EMI in electric railway operation is considered more and more important since it constitutes a significant disturbing agent of signalling and telecommunication installations, from third party facilities, and the standardisation of European railway systems [FDGH13]). So, understanding the EMI received by antennas placed on the train roof is imperative.

In Portugal, there are two types of power supply systems: 1500 V DC, used in the line of Cascais, and 25 kV at 50Hz, in the remaining rail network [THAL09]). According to [REFE15], the 25 kV power supply is comparable to a typical star distribution configuration. In this case, the transformer feeds the catenary with a rated voltage of 25 kV. For the transport of energy at 25 kV, three systems are possible [REFE15]: ST, RT, and AT. In the catenary, these systems can be recognised by the aerial ground cable (CDTA) and/or the feeder, as presented in Figure 2.13.

So, being the emission of magnetic fields in high frequencies an important characteristic in these systems, being aware of its behaviour is fundamental [REFE15]:

- In ST, the traditional and simplest system, the overhead contact line is only composed of the contact wire and, possibly, a support cable. The power circulates in large meshes, so the emission of magnetic fields is quite high.

- In RT, the traction current and land return system is based on rails, a continuous overhead cable (CDTA), and at least a buried earth cable (CDTE). Here, a considerable part of the traction return current circulates in the CDTA, so the magnetic field produced by these currents partially cancels the magnetic field produced by the current circulating in the catenary, hence, the magnetic field is smaller compared to the one in ST.

- In AT, two transformers and a feeder are added. A part of the current circulates in the feeder, and the magnetic field produced by this current partially cancels the magnetic field of the current in the catenary, reducing the emissions (that are relatively lower than those provided by RT). This system is the best option for high-speed trains.

(a) ST   (b) RT   (c)AT
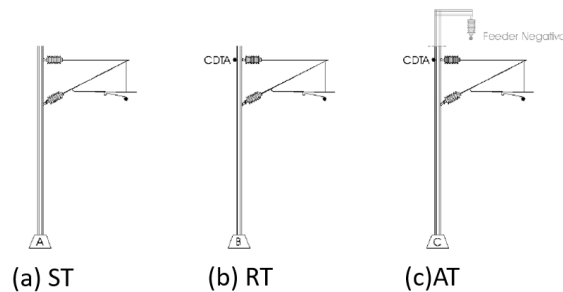
Figure 2.13 Catenary configurations (extracted from [REFE15]).

Since this is an environment where the equipment performs critical functions, it is necessary to have electromagnetic compatibility (EMC) standards for railway applications. In Europe, the standards applied to characterise the EM environment in the railway context are the EN50121. Some of these standards are presented in Table 2.9.

Table 2.9 List of EMC standards applied to railway domain (adapted from [DDSA12]).

EN 50121 parts 1-5	Railway Applications Electromagnetic Compatibility
CISPR/C/116/CDV	Interference from overhead power lines, high voltage equipment and electric traction system.
GM/RC 1500	Code of Practice for EMC between the Railway and its Neighbourhood.
EN 55011 (CISPR 11)	ISM radio-frequency equipment – Radio disturbance characteristics – (CISPR 11) Limits and methods of measurement.
UMTA-MA-06-0153-85-6	Conductive Interference in Rapid Transit Signalling Systems Suggested Test Procedures for Conducted Emission Test Vehicle
UMTA-MA-06-0153-85-8	Inductive Interference in Rapid Transit Signalling System Suggested Test Procedures for Inductive Emissions of Vehicular Electrical Power Subsystems, Rail-to-Rail Voltage from 20Hz to 20 kHz.
UMTA-MA-06-0153-85-11	Radiated Interference in Rapid Transit Signalling System Suggested Test Procedures for Broadband Emissions of Rapid Transit Vehicles from 140 kHz to 400 MHz.

The standard EN 50121 indicate the methodologies and the limits to apply, regarding the EM emission and immunity of railway equipment, vehicles, and infrastructures.

Additionally, railway lines can be classified into four classes: urban, urban/inter-city, inter-city and/or high speed. Table 2.10 presents the differences between them. Figure 2.14 shows the different communication scenarios that were defined: trains-to-infrastructure, inter-car, intra-car, inside station and infrastructure-to-infrastructure.

Table 2.10 Main characteristics of different line types (adopted from [FrFC17]).

Characteristics	Urban	Urban/Inter-City	Inter-City	High-Speed
Maximum speed [kph]	s ≤ 70	70 < s ≤ 160	160 < s ≤ 250	250
Line length [km]	l ≤ 20	20 < l < 100	100 ≤ l < 250	l ≥ 250
Parallel tracks [units]	1	2	3	4
Train stations	1-5	6-20	21-50	51+
Passengers per km of line	n < 100,000	100,000 ≤ n < 200,000	200,000 ≤ n < 500,000	n ≥ 500,000
Range of services	Single	Small diversity	Multiple variances	Extremely varied
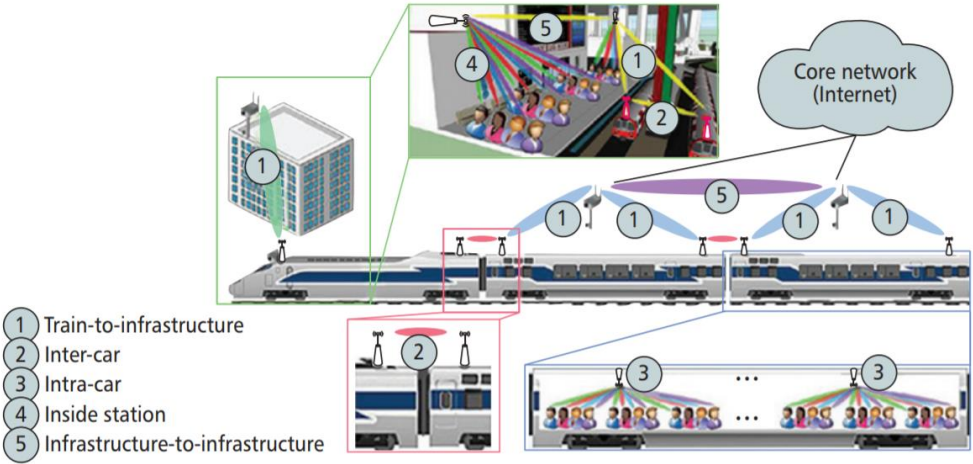
Figure 2.14. Connectivity scenarios (extracted from [FrFC17]:

Each scenario can be described as follows [FrFC17]:
- Train-to-infrastructure: A bidirectional connection between the access points (APs)/ transceivers of the train and the closer BS allows streaming with high data rates and low latency. If the moving speed of the train is 350 km/h or more, the communication has to provide latencies lower than 100 ms, and the availability of 98% to 99%.
- Inter-car: A wireless or optical fibre connection between adjacent cars, the former being the most practical in terms of train reconfiguration. High data rates and low latency are required in this scenario. In the wireless method, the APs are organised in each car such that each one passes as a client station for the AP in the previous station, and as an AP for all the stations

within its vehicle. For this reason, connectivity with a high data rate and low latency is required.

- Intra-car: In this scenario, a wireless connection is provided to passengers or sensors inside the car by the APs in the carriage. Low latency is required.

- Inside station: A wireless link between APs and users. Usually, a crowded scenario, the usage of MIMO technology is an excellent choice to achieve high spectral efficiency, high data rates, high energy efficiency, and more capacity.

- Infrastructure-to-infrastructure: A real-time bidirectional link between infrastructures with high data rates and low latency. Information is transmitted between cameras or other IoT infrastructures and APs deployed on trains, stations, platforms, and wayside along rail tracks.

2.7   Performance Parameters

In this section, a description of the significant parameters of antennas, EMI and mobile communications is presented, based on [Bala05], [Corr17], and [HAWG16].

2.7.1 Antenna's Parameters

To have a good connection between BSs and MT, one needs to analyse all the losses and gains that exist. One of the most essential aspects to considerer is path loss, which depends on several parameters, and there are several propagation models to make the best estimation like the free space propagation model, the "Flat Earth" propagation model for short distances, the Knife-Edge propagation model for obstacles with dimensions much larger than the wavelength, the COST 231 – Okumura-Hata propagation model for more considerable distances, and COST 231 – Walfish-Ikegami propagation model for small distances as well as urban environments [Corr17]. Most of the models require parameters like frequency, the distance between terminals and the height of antennas. Also, some correction factors may be added due to specific environmental conditions.

Also, it is necessary to understand what happens specifically in the antenna, how the electromagnetic field behaves. Usually, the space surrounding an antenna is divided into three regions: reactive near-field, radiating near-field (Fresnel), and far-field (Fraunhofer).

The reactive near-field region is the closest to the antenna and where the EM field behaviour is more erratic due to the reactive oscillation and the non-radiating energy strength. Then, one has the reactive near-field region. This region is defined as being the transition from the near-field region and the far-field one, in which radiation fields predominate, and the angular field distribution depends on the distance from the antenna [Bala05]. Finally, the far-field region is where the angular field distribution is no longer dependent on the range. This last scenario is the most important to be considered, since the terminal is usually far from the antenna.

To analyse an antenna, a coordinate system is defined to represent graphically or analytically the radiation properties in the space surrounding the antenna, usually (r, θ, φ). However, since three-dimensions analysis can be very complicated, two-dimension graphics are easier to understand the antenna's characteristics, so they are mainly used (e.g., polar and rectangular radiation patterns).

According to [Bala05], a radiation pattern has lobes that can be classified as major, minor, side and back. In Figure 2.15, one presents a symmetrical three-dimensional polar pattern. The major lobe is defined as "the radiation lobe containing the direction of maximum radiation". The minor lobes are the remaining ones. A side lobe is any lobe in a different direction than the intended. A back lobe in one whose axis makes an angle of approximately 180º concerning the main beam. Usually, it is on the opposite side of the major lobe.

IEEE defines the First Null Beamwidth (FNBW) as the angular separation between the first nulls of the pattern. The Half-Power Beamwidth (HPBW), α_{3dB}, is defined as, in a plane containing the direction of the maximum of a beam, the angle between the two directions in which the radiation intensity is half the value of the beam, i.e., 3 dB difference.
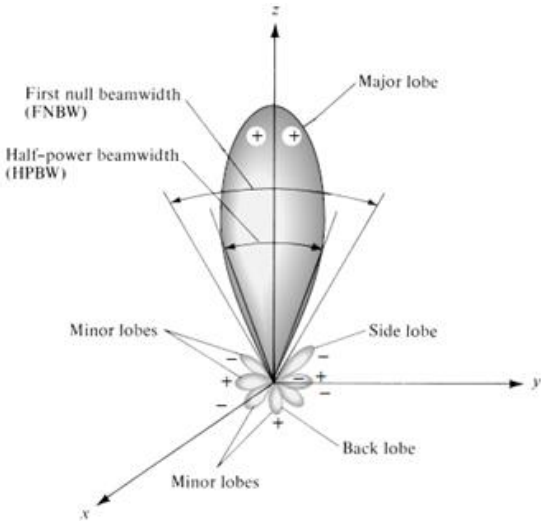
Figure 2.15 Radiation lobes and Beamwidths of an antenna pattern (adapted from [Bala05]).

The radiation pattern can be classified as isotropic, described by a uniform radiation configuration in all directions; omnidirectional, defined by a uniform signal in all directions for a given plane, and finally, directional, that has a clear main lobe.

The radiation intensity in a given direction is another parameter that allows the determination of the antenna's efficiency. The directivity is defined as being the ratio between the radiation intensity in a particular direction, and the radiation intensity averaged over all directions.

The maximum effective area of an antenna also affects the received signal. The effective antenna's aperture, where maximum directivity occurs, without dielectric and ohmic losses that could be a consequence of the polarisation conditions, provides the ratio of the power delivered at the antenna's

terminals to the power flux density of a plane wave incident on the antenna from a particular direction.

Also, one must consider the impedance characteristics. The formation of resonant wire antennas occurs when the load impedance is not the same as the characteristic impedance of the line – mismatch. This will cause reflections [Bala05]. To avoid reflection of the radiation, the resistance needs to be equal to the generator resistance that is connected to the antenna. The Voltage Standing Wave Ratio (VSWR) is used to measure the reflected power.

The polarisation of a wave radiated by the antenna is also an essential parameter since, according to the reciprocity theorem, in case both terminals are not set with the same polarisation, the signal will not be received. So, this property of an electromagnetic wave, which describes the time-varying direction and relative magnitude of the electric field vector, allows one to understand the antenna's transmission or reception waves. The polarisation can be classified as linear (vertical or horizontal), circular (right or left), and elliptical (right or left). The possibility of using two independent channels to occupy the same spectral space (e.g., Right Circular Polarisation (RCP) and Left Circular Polarisation (LCP)) increases spectral efficiency. The polarisation matching loss (PL) is the ratio between the received power and the maximum value possible when there is a perfect polarisation match.

Another parameter that one must consider is the type of technology of the antenna. The different types are described as follows [Bala05]:

- Wire antennas: Popular in vehicles, ships, aircraft, trains, and so on, it is a wire antenna that presents various shapes such a straight wire (monopole or dipole), loop and helix. The loop antenna may take the form of a circle, rectangle, square, ellipse, or any other form.
- Aperture antennas: They are commonly used in aircraft and spacecraft because they can be very conveniently flush-mounted on the surface of the aircraft. Also, they can be easily covered with a dielectric material to protect them from several conditions, such as the environment.
- Microstrip antennas: Usually used for government and commercial applications, these antennas consist of a metallic patch that can have several configurations, patch on a grounded substrate. The most popular patches are rectangular and circular due to the ease of analysis and fabrication. These antennas are low profile, comfortable to planar and nonplanar surfaces, inexpensive and straightforward to manufacture using the modern printed-circuits technology.
- Array antennas: It consists of the aggregation of radiating elements in an electrical and geometrical arrangement. The arrangement of the array may be such that the radiation from the components adds up to give a radiation maximum in a particular direction or directions and minimum in others.
- Reflector antennas: These types of antennas were created to achieve the high gain required to transmit or receive signals from considerable distances.
- Lens antennas: Primarily used to collimate incident divergent energy to prevent it from spreading, transforming the received divergent power into plane waves. They can be used in most of such applications as parabolic reflectors, mainly ate higher frequencies.

2.7.2 EMI Parameters

The tendency is to electrify all railways, so EM radiations need to be understood. Their influence in the telecommunications systems put the management of the railway network in jeopardy. According to [DDSA12], trains are being more and more equipped with systems potentially sensitive from an EMC point of view. Some definitions regarding EMC and present in the International Electrotechnical Vocabulary (IEV) are as follows [DDSA12]:

- Electromagnetic environment: The totality of EM phenomena existing at a given location.
- Immunity: Immunity to a disturbance is the ability of a device, equipment, or system to perform without degradation in the presence of EM disturbance.
- Susceptibility: Electromagnetic susceptibility is the ability of a device, equipment, or system to perform without degradation in the presence of an EM disturbance.
- Immunity level: The maximum level of a given EM disturbance incident on a particular device, equipment, or system for which it remains capable of operating at a required degree of performance.

The EMC problem can be divided into three parts: the source intentionally or unintentionally produces the emission, a coupling path that transfers that emission to the receiver, and the receiver itself that can be susceptible if the emission's energy is more prominent than its immunity. EM disturbance refers to radiated or conducted signals that can lead to system malfunctions, which can be voltages, currents or electromagnetic fields. Generally, the higher the frequency of EM disturbances, the more efficient the coupling path. Both source and receiver can be classified as intended or unintended. For example, if one considers a system that transmits and receives EM fields in some frequencies, both the antenna and the equipment around it will operate under its influence. Depending on the antenna's coverage and the level of EM disturbances, communication can be affected or even interrupted [DDSA12].

EM disturbances can be coupled to the receiver by either radiated or conductive paths, and coupling mechanisms can be classified as follows [DDSA12]:

- Conductive: It can be viewed as a standard impedance coupling, occurring when source and receiver are physically connected by a conductor and share a common-impedance path.
- Magnetic: When two objects transfer energy between one another through their varying or oscillating magnetic fields.
- Electric field: Capacitive coupling occurs due to the voltage difference between conductors. It is mainly present in high-impedance circuits and can be represented by mutual impedance.
- Electromagnetic field: Being the most observed mechanism, it is a combination of electric and magnetic fields. It occurs when the source and the receiver are separated by a significant distance, typically more than a wavelength, source and receiver behaving as antennas.

2.7.3 System Parameters

To evaluate QoS, three main parameters must be measured: coverage, capacity, and interference. They are all correlated and need to be defined according to system requirements. To have a system that has

excellent performance, cellular planning is necessary. Both the signal estimations as the morphology of the terrain must be considered to choose an appropriate propagation model and optimise the placement of the BSs, which provide the best coverage and minimise interference.

In terms of estimates of signal behaviour, it can be classified as slow (long-term) or fast (short-term) fading. A slow fading signal depends mostly on distance through a Log-normal Distribution, and fast fading signal is related to moving terminals, associated with the Rice Distribution. To assess QoS it is fundamental to have a prediction of BSs' coverage area. This way, it is possible to know the receiving power at a specific location and distance by only considering slow fading and neglecting the fast one.

Typically, cellular planning is done considering hexagonal/circular cells, using the omnidirectional antenna coverage theory. However, this does not happen in railway communications, since the path that trains travels is well-known. In this case, a frequency reuse cluster is done for linear coverage with directional antennas. Figure 2.16 presents the predicted coverage areas for both cases, and it is possible to observe that for the linear cell, performance has increased.
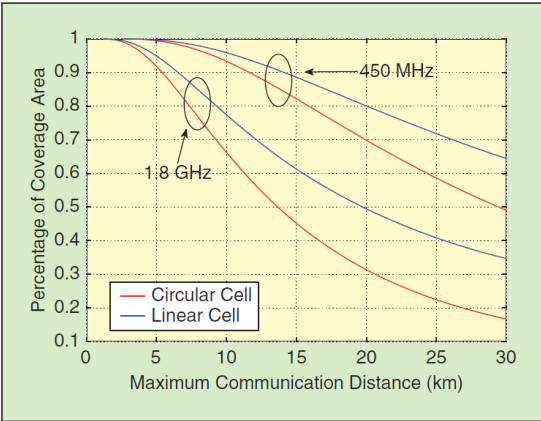
Figure 2.16 Coverage area for Linear and Circular cells (extracted from [HAWG16]).

2.8 State of the Art

An overview of research related to the subject of the thesis is presented in this subsection, where one shows the work that has been developed regarding the influence of the pantograph and catenary in railway communications. The main focus of this thesis is the analyses of the antennas' signal parameters and their behaviour in the presence of pantographs.

[FDGH13] presents a thorough analysis of the electromagnetic interference generated by trains. This paper focus on the modelling of EMI received by antennas placed on the train roof. The switch-on transients, when the pantograph touches the contact wire and the switch-off when detaches, closing and opening the circuit respectively, creates interference and generates an electric arc. The angle between antenna and pantograph also has to be considered while analysing this scenario. It presents a modelling methodology to examine the effect of pantograph arcing in GSM-R antennas. The

measurements were performed in Spain, on a train of the Spanish railway company CAF. The stationary train was equipped with antennas placed on the roof 10 m back from the pantograph. The antenna used for the measurements had a range from 500 MHz to 6 GHz, and it was placed laterally onto the train's side at 1.5 m. It was then moved along the train to perform the measurements. The researchers tried to reproduce the four different stages of the pantograph, by switching on and off the High-Speed Circuit Breaker (HSCB) and connecting and disconnecting the pantograph from the catenary. The Computer Simulation Technology (CST) tool was used to modulate the most representative train components.

In [TMGA01a], the researchers pointed out the importance of understanding EMI in electric railways due to the interaction between pantograph and overhead contact line. They wanted to understand the contributions from switch-on and switch-off transients. A high-voltage 4 kV DC power system supplied the catenary through a 39 mH inductor that simulates the inductance of the supply line, as presented in Figure 2.17. In [TMGA01b], the same authors present the results of a measurement campaign aimed at investigating EMI phenomena.
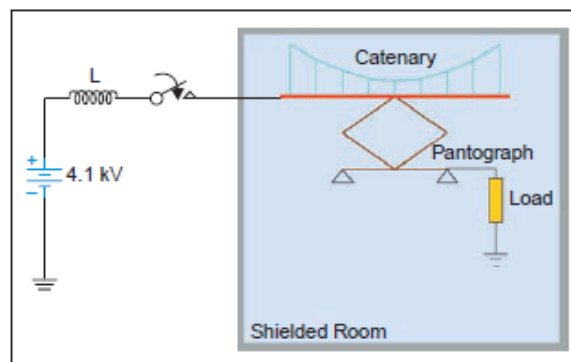
Figure 2.17 The measurement setup assembled (extracted from [TMGA01a]).

In [DFHR13], the authors' objective was to understand the transient disturbances produced by the pantograph in the train's roof and analyse the EMI disturbance received by GSM-R antennas. The measurements were made on the OARIS high-speed train provided by a Spanish rolling stock company, with four cars, each with 24.8 m long. The measurements were performed with the antennas placed on the second car and an additional one on the side of the train, 0.9 m lower than the rest. The measurements that were made for the EM disturbances coming from the catenary-pantograph were the main focus. This analysis was supported by the CST Microwave Studio tool.

In [GMT01], the authors discuss the contribution of the arc channel to the total emission and present experimental evidence that this contribution is negligible compared to that of the rest of the circuit. The radiated fields associated with electrical discharge (ESD) events must be considered. The main objective was to determine whether electromagnetic emission can be associated with only the arc or with the all-electric and geometric characteristics of the circuit in which the discharge takes place.

[MBST09] presents an overall explanation of the consequences of pantograph arcing in the AC traction system. It approaches the distortion of the sinusoidal waveform caused by the pantograph arcing, as well as the harmonics and inter-harmonics and the conducted and radiated electromagnetic emission, which can cause interference in several radio-based communication systems. Figure 2.18 presents the

frequency spectrum of the conducted and radiated emission from pantograph arcing and associated railway system with their frequency bands. An experimental investigation to study this phenomenon is presented, where an original test setup was developed for this purpose.
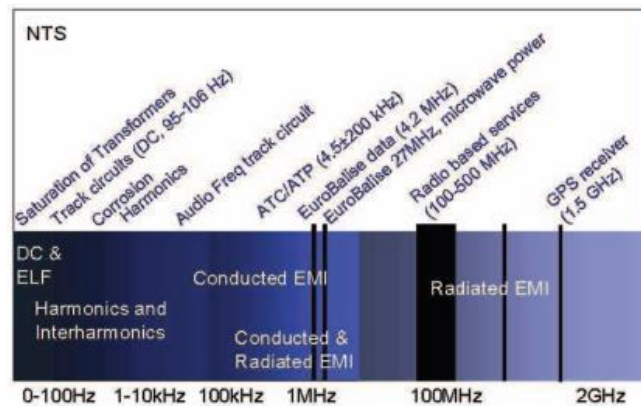
Figure 2.18 Pantograph arcing and associated frequency spectrum (extracted from [MBST09]).

In [MUMi07], the authors assess the low-frequency electric and magnetic field of 25 kV / 50 Hz power supply systems. Measurements of the electric field strength were performed and compared with the calculation's results, which have shown a good agreement. The system is a single-track catenary system with two return rails, which is similar to the scenario that one is going to model.

André Ribeiro's thesis [Ribe18] is the work that is closest to the current thesis, since it aims to continue his search. In [Ribe18], the main goal was to analyse the performance of antennas on trains and understand the impact of the different available positions to install the antennas depending on the surrounding environment, to optimise and improve services for railway operations and passengers' experience. The author chose the simulation software CST Microwave Studio, where it was possible to import similar 3D models of trains and train antennas of different mobile communications systems and to perform a complete analysis of the antenna's parameters; an example can be seen in Figure 2.19. However, André Ribeiro's thesis does not consider the influence of the pantograph, something that is carried out in this thesis.

(a) Farfield at "Position 1" and 100 mm of depth.

(b) Farfield shifting the BBRS antenna to the left.

Figure 2.19 BBRS antenna 3D far-field performance at different positions (extracted from [Ribe18])..

Chapter 3

Models and Simulator

This chapter includes the problem methodology and the most important aspects that are considered for simulations. A description of the software and the implementation of the antennas and scenarios are also presented.
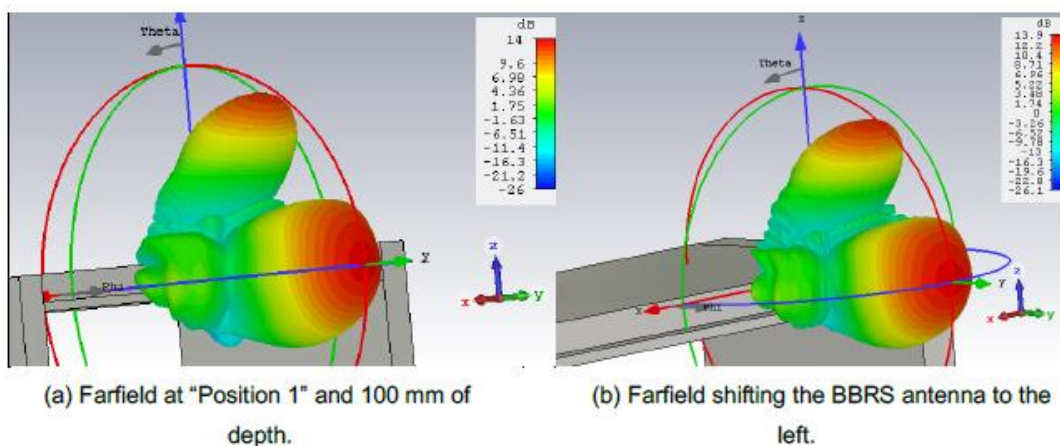
3.1 Model Overview

This section shows the general perspective of the approach taken for the analysis of antennas' performance and the model used. Figure 3.1 presents the model overview, with the path used to reach the final results.
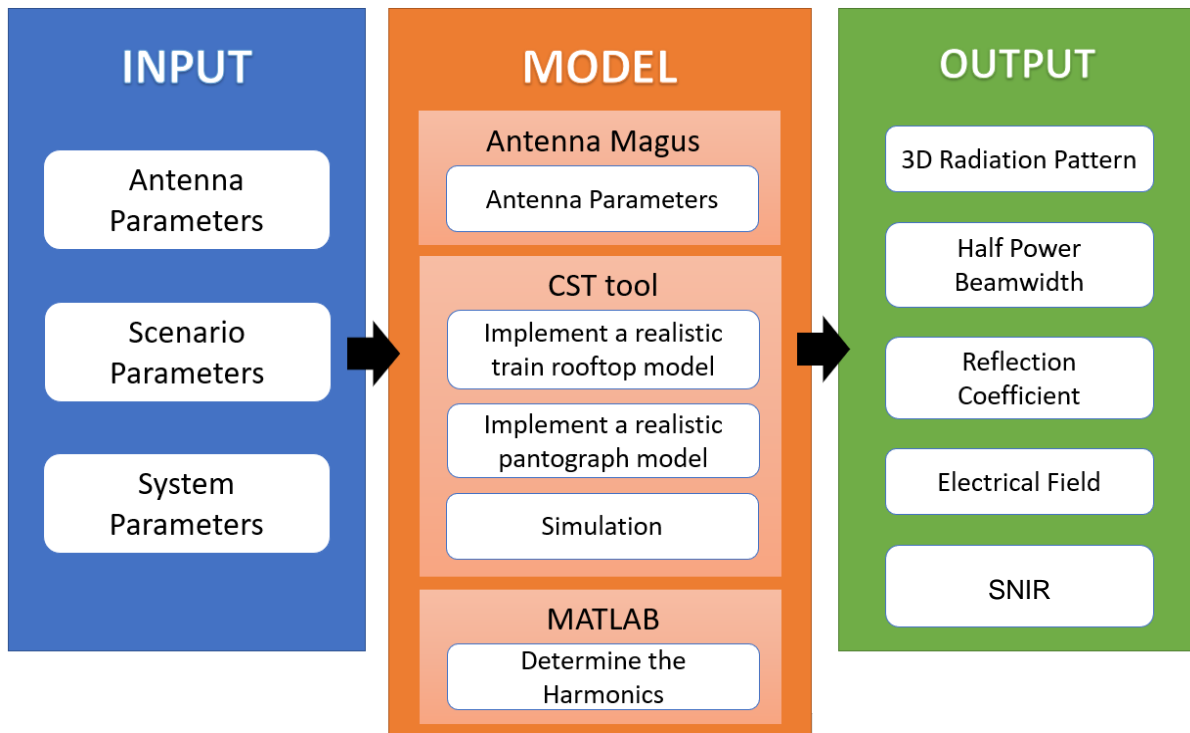
Figure 3.1 Model overview.

The corresponding steps for the modelling phase are as follows:
- Design of the antenna using Antenna Magus.
- Implement a realistic model of the composition train/pantograph/catenary using the CST tool.
- Implement the antenna on a specific distance from the pantograph.
- Run the simulation.
- Determine analytically, using MATLAB, the power produced by harmonics, and the minimum Signal-to Noise-plus-Interference-ratio using data from simulation.

The main goal of this thesis is the development of a model for the analysis of the influence of pantographs in railway communications. The objective is the study the behaviour of specific parameters of the antennas in the train while in the presence of pantographs and different scenarios. Two main issues were considered: the presence of the pantograph and the catenary as metallic structures, and the electric field from the catenary due to energy passing through. To complete the thesis, a methodology constituted by four phases was established. Primarily, it is fundamental to perform a

theoretical presentation based on previous studies. The second phase consisted of the development of the model and the scenarios considered necessary during the first phase; this model was used to evaluate the performance of the antennas in different scenarios. In the third stage occurs the implementation of the model, and finally, in the fourth phase, one aims to analyse the results obtained.

There are several input parameters that the model must consider regarding the antennas and the pantograph, as well as the surrounding environment, that may affect the behaviour of the radiation pattern. In this thesis, the most critical antennas' parameters are the gain, the polarisation type, and the working bandwidth, which depends on the system (TETRA, GSM-R, LTE-R, and BBRS). Besides these electrical properties, one needs to consider the mechanical properties and their dimension, the pantograph parameters and their dimension, as well as the different railway power systems.

After all these input parameters are defined, the proposed model consists of using the CST tool to understand the interferences regarding the pantographs. For that purpose, one must create a representative 3D model of the trains' rooftop, the pantograph, and the catenary. The Antenna Magus software was used to design the antennas. Finally, CST provided the needed outputs so that the study can be done through 3D or 2D plots of radiation patterns, α_{3dB}, S_{11} coefficients, as well as SLL properties.

3.2   Antenna analysis

Antennas are usually placed near an infinite plane conductor, which creates a direct effect on their radiation features. In this case study, the antenna is placed on the train's rooftop, which is also considered a plane. The transmitted and received waves of a radiating element that are directed to the ground suffer a reflection that has different behaviours depending on the geometry of the problem, the ground characteristics, and the frequency, or antennas' specifications. To simplify the problem, one considered the roof of the train as a flat infinite ground and a Perfect Electric Conductor (PEC). The material can be viewed as a PEC when its electric conductivity is around 10^7 [Ribe18]. The imaging method is the most ideal to understand the reflected electrical field behaviour near a PEC.

The space surrounding an antenna is divided into three regions with the following boundaries [Bala05]:
- Reactive near-field region:

$$0.62 \sqrt{\frac{{l'_{[m]}}^3}{\lambda_{[m]}}} > r'_{[m]} > 0 \tag{3.1}$$

- Radiating near-field (Fresnel) region:

$$\frac{2{l'_{[m]}}^2}{\lambda_{[m]}} > r'_{[m]} \geq 0.62 \sqrt{\frac{{l'_{[m]}}^3}{\lambda_{[m]}}} \tag{3.2}$$

- Far-field (Fraunhofer) region:

$$r'_{[m]} \geq \frac{2l'^2_{[m]}}{\lambda_{[m]}}$$ (3.3)

where:

- l': largest dimension of the antenna
- λ: wavelength
- r': distance between the antenna and the observation point

According to [Bala05], the total electric field for a vertical dipole can be written as:

$$E^V_\theta {}_{[V/m]} \cong j\eta_{[\Omega]} \frac{kl'I_0 e^{-jkr'}}{4\pi r'} \sin\theta_{[\circ]}{}^2 \left[2 \cos k_{[m^{-1}]} h_{[m]} \cos \theta_{[\circ]}\right], z \geq 0$$ (3.4)

where:

- η: intrinsic impedance (120π Ω for free-space)
- $k_{[m^{-1}]} = \frac{2\pi}{\lambda}$: the free space wave number
- $I_{0[A]}$: maximum current
- θ: angle between the positive half of z-axis and the observation point
- h: antenna height to the PEC plane

The total field is equal to the product of the field of a single source positioned symmetrically about the origin and a factor which is a function of the antenna height and the observation angle. The array factor provides a relation between the radiation pattern and the antenna height. The number of lobes equal to the integer that is closest to:

$$N^V_L \cong \frac{2h_{[m]}}{\lambda_{[m]}} + 1$$ (3.5)

Using the same approach as before, the expression of the total electric field for a horizontal dipole, valid only above the ground plane ($z \geq h; 0 \leq \theta \leq \frac{\pi}{2}, 0 \leq \Phi \leq 2\pi$), can be expressed as:

$$E^H_\varphi {}_{[V/m]} \cong j\eta_{[\Omega]} \frac{kl'I_0 e^{-jkr'}}{4\pi r'} \sqrt{1 - \sin\theta_{[\circ]}{}^2 \sin\varphi_{[\circ]}{}^2} \left[2j \sin(k_{[m^{-1}]} h_{[m]} \cos \theta_{[\circ]})\right]$$ (3.6)

where:

- $\varphi_{[\circ]}$: angle between the positive half of x-axis and the observation point projected on xOy plane

For this reason, the number of lobes can be expressed as:

$$N^H_L \cong \frac{2h_{[m]}}{\lambda_{[m]}}$$ (3.7)

3.3 EMI analysis

In an electrical system, the main objective is to have a sinusoidal voltage at a reasonably constant magnitude [KALS10]. However, this is difficult to obtain due to the loads on the system that produce harmonic currents. These harmonics will cause distorted voltages and currents, as shown in Figure 3.2, which will have an impact on the system. In [MBST09], the authors present the problems caused by the pantograph arcing such sinusoidal wave distortion and the appearance of harmonics and inter-harmonics that will interfere with several radio-based railway services. Therefore, the detection of these harmonics and their frequencies is critical.
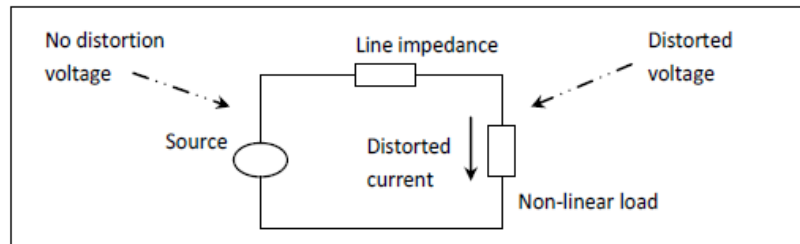
Figure 3.2 Distorted current and voltage (extracted from [KALS10]).

In this system, the signal that one considers passing through the catenary and pantograph corresponds to the sum of the original signal, a 25 kV AC with $f_0 = 50$Hz, and the harmonics, whose frequency is 380 MHz, 900 MHz, 2.6 GHz, and 5.9 GHz. It can be expressed as:

$$x'(t)_{[V]} = \sum_{n=0}^{N\_harm} \frac{25000}{N\_harm} \cdot \sin(2\pi \cdot N\_harm \cdot f_{0_{[Hz]}} \cdot t) \tag{3.8}$$

where:

- x' – electric current in the catenary
- N_harm – order of the harmonic
- f_0 – fundamental frequency

To determine the harmonics, one uses the Exponential Fourier Series. A periodic time-domain signal can be represented as a sum of sinusoidal signals. The Fourier Series, Trigonometric and Exponential, of a periodic function $x'(t)$, can be expressed as:

$$x'(t) = a_0 + \sum_{n=1}^{\infty}\left(a_n \cos\left(\frac{2\pi nt}{T}\right) + b_n \sin\left(\frac{2\pi nt}{T}\right)\right) = \sum_{n=1}^{\infty} c_n e^{jn\omega_0 t} \tag{3.9}$$

where:

- a_0 - average value of a signal
- a_n, b_n - coefficients of the series
- c_n - exponential Fourier coefficient
- $\omega_{0_{[rad/s]}}$ - fundamental frequency.

Considering any periodic $f(t)$ with period T_0, it is possible to compute the coefficients of its EFS using the following expression:

$$c_n = \frac{1}{T_0} \int_0^{T_0} f(t)e^{-jn\omega_0 t}\, dt \qquad (3.10)$$

By getting these coefficients, one can determine the electric field originated from the harmonics having only the electric field from the fundamental frequency.

To calculate the theoretical value of the electric field, one considers this scenario equivalent to a cylindrical conductor parallel to a ground conductor, as presented in Figure 3.3, so the expressions of the capacitance and the electric field are used.

$$C_{[F]} = 2\pi \cdot \epsilon_{0[F/m]} \cdot \frac{1}{\log_{10}\left(\frac{d_{[m]}}{r_{[m]}} + \sqrt{(d_{[m]}/r_{[m]})^2 - 1}\right)} \qquad (3.11)$$

$$E_{[V/m]} = \frac{C_{[F]} \cdot U_{[V]} \cdot d_{[m]}}{\pi \cdot \epsilon_{0[F/m]} \cdot l_{[m]} \cdot (x_{[m]}^2 - d_{[m]}^2)} \qquad (3.12)$$

where:

- C – capacitance
- E – electric field magnitude
- ϵ_0 – permittivity in vacuum
- d – height of the transmission line
- r – radius of the transmission line
- U – maximum potential at the transmission line
- l – length of the transmission line
- x – position in the vertical referential
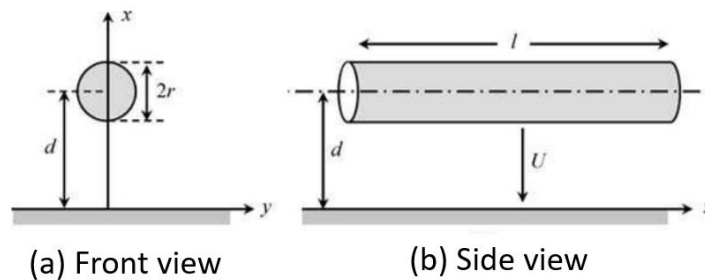

(a) Front view (b) Side view

Figure 3.3 Cylindrical conductor above ground (adapted from [Bran08]).

To determine the power of each interfering harmonic, one uses the following expression [Corr18]:

$$P_{harm[dBm]} = -77.21 + E_{[dBuV/m]} + G_{[dBi]} - 20\log(f_{[MHz]}) \qquad (3.13)$$

where

- P_{harm} – power of the harmonic
- f – frequency of the harmonic
- G – gain

To estimate the average noise power N_{RF}, the following expression is used [Corr18]:

$$N_{RF\ [\text{dBm}]} = -174 + 10\ log_{10}(\Delta f_{[\text{Hz}]}) + F_{[\text{dB}]}$$ (3.14)

where

- Δf – signal bandwidth
- F – noise figure

In this thesis, the total noise power $N_{[\text{dBm}]}$ is taken as N_{RF}. Once having both the noise power and the power of the interfering signals, one can determine the minimum power of the desired signal at the receiver [Corr18]. Having the minimum signal-to-noise-and-interference-ratio stated, it is possible to find the minimum power at the receiver that guarantees the quality of the signal. To do so, the following expression is used:

$$\rho_{min[dB]} = \frac{P_{min|Nenv+Ncat\ [dBm]}}{N_{[dBm]} + I_{[dBm]}}$$ (3.15)

where

- ρ_{min} – minimum Signal-to-Noise-plus-Interference-Ratio
- P_{min} – sensitivity
- N – total noise power
- I – interfering power

3.4 CST Simulation Tool

The 3D Electromagnetic Simulation software allows the user to investigate the EM properties of several structures, from specific components such antennas, sensors, and chips to complete systems such as aircraft and smartphones, in various frequency ranges, from statics to optical frequencies. Computer Simulation Technology (CST) provides an accurate and efficient computational solution for simulating electromagnetic design and analysis. The 3D EM simulation software allows the user to choose the most appropriate method for the design and optimisation of devices [CST18].

There are several ways to approach electromagnetic problems on the developments and applications of computational methods [CSTH18]. The computational EM methods can be divided into numeric methods and analytical methods for high frequencies [Ribe18]. For the first part of this thesis, the antenna analysis, the best option is the numeric method, since it allows a detailed analysis of electromagnetic fields behaviour. The Method of Moments (MoM) is based on the resolution of integrals

in the frequency domain, but it has some efficiency problems when compared with volume discretisation methods, like the Finite Integration Technique (FIT). FIT is the best technique to analyse antennas' parameters, like the radiation pattern, gain, S-parameters, and so on. This method is applied in CTS Microwave Studio

CST 2018 [CST18] has a system named Project Wizard that allows users to adopt the best project settings to achieve the most accurate simulation results. The first step is to create a new project template, where one must choose one application area from the five available: MW & RF & Optical, EDA / Electronics, EMC/EMI, Charge particles Dynamics and Statistics and low frequencies. For this thesis, the MW & RF & Optical is the best option for the analysis of the antennas. Within this application, one must select a specific workflow from six: Antennas, Circuits & components, Radar cross-section, Biomedical/Exposure/SAR (Specific Absorptions Rate), Optical applications and Periodic structures. After selecting the Antennas workflow, more specifications of the workflow will be asked all the antennas' types: Waveguide, Planar, Wire, Phase array/Unit cell, Mobile phone/Integrated, Reflector, Dielectric resonator, and RFID. In this situation, the wire is the one selected. Afterward, one must choose the best solver for the problem in question. Figure 3.4 presents all these three stages.

Although six different solvers (Time domain solver, Frequency-domain solver, Eigenmode solver, Integral equation solver, Asymptotic solver, and Multilayer solver) are presented in the manual, there are only three solvers available in CST Microwave Studio, as presented in Figure 3.4. Each is described as follows and can be seen in more detail in [CSTH17], [CST18] and [Ribe18]:

- Time-domain solver: There are two types of time-domain solvers: Transient and Transmission-Line Matrix (TML). Both are based on hexahedral meshes. They simulate problems to study the electromagnetic field behaviour and are capable of showing the broadband frequency-domain effects through S-parameters, which are essential for understanding the performance of the antennas. Furthermore, it also simulates the radiation pattern, with possibilities of analysis of residences inside the simulated spectrum.
- Frequency-domain solver: Its main features are to display the near and far-field electromagnetic performance and the S-parameters. This solver is the best choice for a small range of frequencies, since the results would have better accuracy and lesser simulation time
- Integral equation solver: The main focus of this solver goes to large electrically structures, which are mainly constituted by metal, such as cars and trains. It provides data from the S-parameters as well as the far-field pattern.

Analysing the characteristics of each of these solvers, the most suitable is the transient solver since it is based on the FIT. CST produces a hexahedral mesh constituted by small variable size cuboids (Δx, Δy, and Δz), named grid cells, discretising the problem with a specific electric (**E**) and magnetic (**H**) field behaviour for each cell. The cells are based on YEE cell, which has the electric and magnetic fields spatially organised so that each element of **E** is surrounding by four elements **H,** and each element **H** is surrounding by four elements **E**. As it is possible to observe in Figure 3.5, the elements of E are positioned on the central point of the Yee cell edge of the facet, and the H elements are located on the central point of each cell facet.
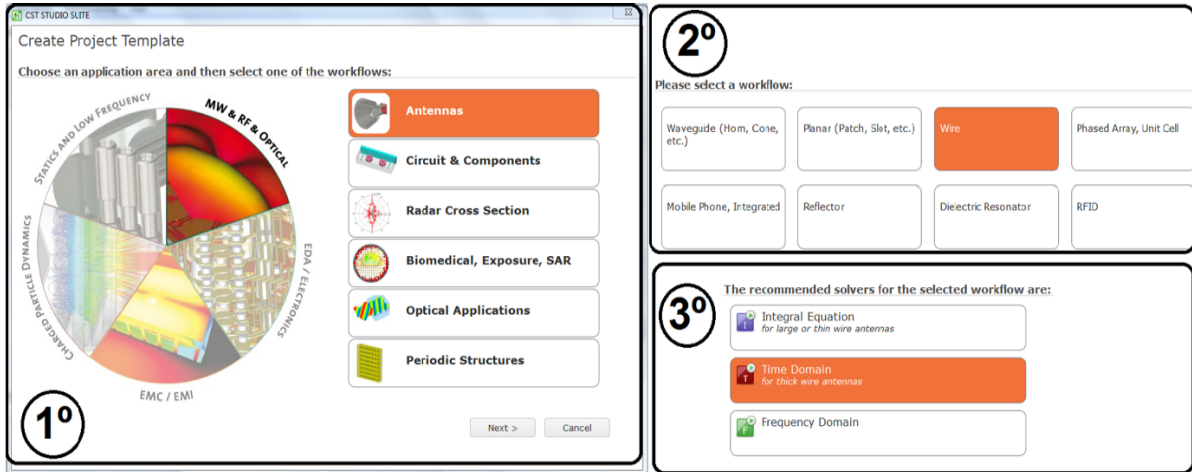
Figure 3.4 CST Project Wizard template (extracted from [Ribe18]).

For the second part of this thesis, the use of CST EM Studio is more suitable, since it is an easy tool for the analysis of static and low frequency structures [CSTH17]. Despite featuring five electromagnetic solvers (Magnetostatic Solver, Electrostatic Solver, Stationary Current Solver, LF Frequency Domain Solver, and LF Time Domain Solver), the most fitting solver for this problem is the Electrostatic solver, since it can be used for a static problem. In the corresponding CST Project Wizard template, the application and workflow are Statics and Low Frequency and High Voltage / Heavy Current, respectively.

The other fundamental decision is the definition of the best mesh type for the problem. There are two ways to define a hexahedral mesh without doing it manually [Ribe18]. One is the "Automatic Mesh Generation with an Expert System", which is an automatic mesh generator capable of creating a proper mesh through the identification of relevant features of each structure. The other option is the "Adaptive Mesh Refinement" that discovers the mesh by a loop, where an initial mesh is created, then with a local error estimation, the mesh is refined. If the result starts to diverge below a certain accuracy level, the process stops. To optimise the mesh generation, some settings may be defined. The main properties to take into account are:

- Lines per wavelength (M_{LW}): It is directly linked to the wavelength of the upper frequency set for simulation, expressing the minimum number of mesh lines in each coordinate vector. A suitable value for an acceptable conciliation between computation time and accuracy is about 10.

- Lower mesh limit (M_{LL}): It defines the maximum mesh step (M_{MS}) to be applied for the mesh formation. The relation between the M_{LL} and the M_{MS} is:

$$M_{MS} = \frac{\sqrt{3}\, D_{SBF}}{M_{LL}}$$

(3.14)

where:

- D_{SBF}: Smallest box face diagonal.
- Mesh line ratio limit (M_{RL}): This provides a relation between the maximum (dy_i) and the minimum (dx_n) allowed values of meshes steps, Figure 3.6.
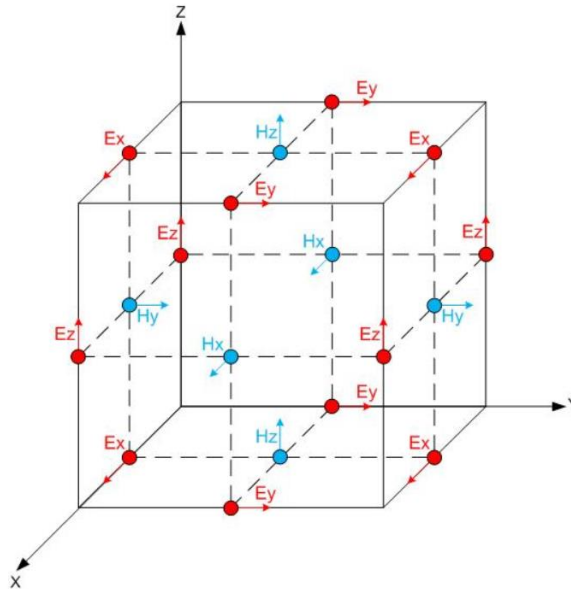
Figure 3.5 Yee Cell with the position of each field component (extracted from [CSTH17]).

The number of cells per wavelength in the mesh properties has a direct influence on the simulation time and its accuracy. It defines the maximum number of cells for the smallest wavelength or the highest frequency of the working band. To avoid space, discretisation a minimum of 10 cells per wavelength is recommended.

It is also important to understand how the boundaries conditions are considerate in CST, since, in the computational perspective, all simulations require a finite expansion. A rectangular grid system is used, and it can be defined by maximum and minimum positions – X_{max}, X_{min}, Y_{max}, Y_{min}, Z_{max}, Z_{min} - in each coordinate direction to identify the six boundary surfaces. There are seven available conditions for the high-frequency properties, presents in Figure 3.7. They can be described as follows [CSTH18]:

- Electric: Operates as a perfect electric conductor (PEC), meaning all tangential electric fields and normal magnetic fluxes are set to zero.
- Magnetic: It behaves like a perfect magnetic conductor (PMC), so all the tangential magnetic fields and normal electric flux are set to zero.
- Open (PLM): It extends the touching geometry virtually to infinity by using a perfectly matched layer (PML) boundary. It allows waves to pass this boundary with minimal reflection.
- Open (add space): It is the same as Open (PML), except it adds some extra space for far-field calculation. This option is the one recommended for antenna problems, since it automatically adapts the centre frequency of the working bandwidth.
- Periodic: It connects two opposite boundaries with a definable phase shift, so that the calculation domain is simulated to be periodically expanded in the corresponding direction, hence, changing one boundary to this type will automatically change the opposite one.
- Conducting Wall: This boundary acts as a lossy conducting wall.
- Unit Cell: It is similar to the Periodic boundary, where a two-dimensional periodicity other than the direction of the coordinate axes may be set.
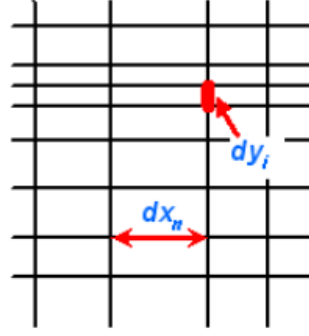
Figure 3.6 Different mesh step widths (extracted from CSTH18)

(a) Electric   (c) Open (PLM)   (e) Periodic   (g) Unit Cell

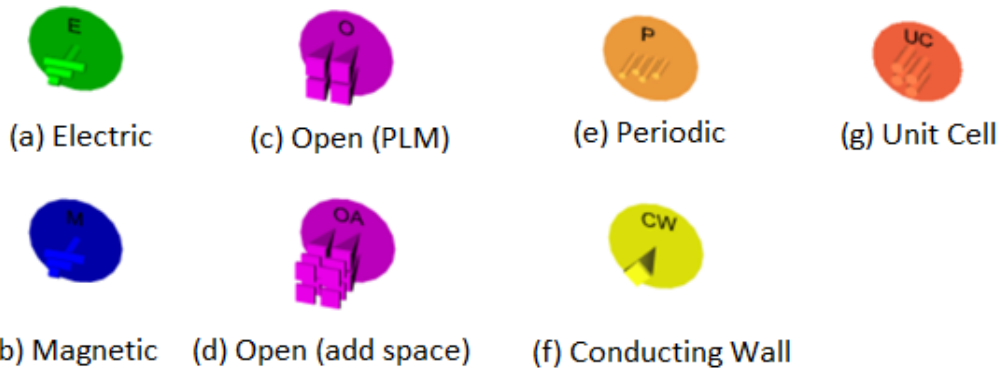(b) Magnetic   (d) Open (add space)   (f) Conducting Wall

Figure 3.7 Icons representing the types of boundaries conditions (adapted from [CSTH18]).

Regarding the analysis of the antennas' performance, there are some fundamental far-field properties of CST that are required: Directivity and Gain. Firstly, it is necessary to understand that the radiated power of an antenna is directly related to its far-field region through:

$$U(\theta,\varphi)_{[W]} = \frac{r^2_{[m]}}{2\eta_{[\Omega]}}\left|\boldsymbol{E}(r,\theta,\varphi)_{[V/m]}\right|^2 \cong \frac{1}{2\eta_{[\Omega]}}\left[\left|E_\theta^V(\theta,\varphi)_{[V/m]}\right|^2 + \left|E_\varphi^H(\theta,\varphi)_{[V/m]}\right|^2\right] \tag{3.15}$$

The directivity can be easily determined through:

$$D(\theta,\varphi)_{[dBi]} = 10log_{10}\left(4\pi \cdot \frac{U(\theta,\varphi)_{[W]}}{P_{rad_{[W]}}}\right) \tag{3.16}$$

where:

- P_{rad}: Total radiated power.

The Gain is defined as:

$$G(\theta,\varphi)_{[dBi]} = 10log_{10}\left(4\pi \cdot \frac{U(\theta,\varphi)_{[W]}}{P_{in_{[W]}}}\right) \tag{3.17}$$

where:

- P_{in}: Input or received power.

The realised gain, which includes impedance mismatches (reflection losses) and polarisation

mismatches within the information of the "S-Parameters Balance" graph, is as follows:

$$G_{realised_{[dBi]}} = G(\theta, \varphi)_{[dBi]} \cdot (1 - B^2), \qquad 0 \le B \le 1 \tag{3.18}$$

where:

- B: S-parameter balance given by the square root of the summed power leaving the structure through all ports. The balance should be one for structures that do not have any losses and is closed (without open or lossy boundary conditions).

To have a clear knowledge of the most significant directions that have a stronger signal regarding the antenna's radiation pattern, the $\propto_{3dB}$ is a fundamental parameter to study. Considering θ=0° the maximum lobe direction, $\propto_{3dB}$ is given by:

$$E\left(\theta = \frac{\propto_{3dB}}{2}\right)_{[V/m]} = \frac{E_{max_{[V/m]}}}{\sqrt{2}} \tag{3.19}$$

where:

- E_{max}: Maximum electric field of the main lobe.

The L_{SLL} is usually used to measure how well the power is concentrated into the main lobe, and it is given by:

$$L_{SLL_{[dB]}} = 20log_{10}\left(\frac{E_{SL\ [V/m]}}{E_{\max\ [V/m]}}\right) \tag{3.20}$$

where:

- E_{SL}: Maximum value of the lobe adjacent to the major one.

Before analysing the antennas' parameters, it is mandatory to recognise if the antenna is well-adapted. To do that, one needs to understand the S_{11} reflection coefficient of the specific antenna under evaluation. In general terms, for a network with n-ports, there are incoming (a_i) and outgoing (b_i) waves associated with each port given by:

$$a_{i_{[V]}} = \frac{1}{2}\left(\frac{V_{i_{[V]}}}{\sqrt{Z_{i_{[\Omega]}}}} + \sqrt{Z_{i_{[\Omega]}}}I_{i_{[A]}}\right) \tag{3.21}$$

$$b_{i_{[V]}} = \frac{1}{2}\left(\frac{V_{i_{[V]}}}{\sqrt{Z_{i_{[\Omega]}}}} - \sqrt{Z_{i_{[\Omega]}}}I_{i_{[A]}}\right) \tag{3.22}$$

where:

- V_i: Voltage of port i.
- I_i: Current of port i.
- Z_i: Characteristic impedance of port i.

The relationship between the outgoing and incoming waver of a particular n-port network leads to the following **S**-matrix:

$$\begin{pmatrix} b_1 \\ b_2 \\ b_3 \\ \vdots \\ b_n \end{pmatrix} = \begin{pmatrix} S_{11} & S_{12} & S_{13} & & S_{1n} \\ S_{21} & S_{22} & S_{23} & \cdots & S_{2n} \\ S_{31} & S_{32} & S_{33} & & S_{3n} \\ \vdots & \vdots & \vdots & \ddots & \vdots \\ S_{n1} & S_{n2} & S_{n3} & \cdots & S_{nn} \end{pmatrix} \begin{pmatrix} a_1 \\ a_2 \\ a_3 \\ \vdots \\ a_n \end{pmatrix} \tag{3.23}$$

The main diagonal elements express the reflection coefficients of that particular port, and the other elements are transmission factors between two specific ports considered in that network. When the element holds only reciprocal material, and if the characteristic impedances are real, the **S**-matrix is symmetric: $S_{ij} = S_{ji}$.

Another way to determine the efficiency of a certain port i is through the total accepted power, via:

$$P_i = |a_i|^2 - |b_i|^2 \tag{3.24}$$

3.5   Isolated Antenna Performance

To understand the behaviour of the antennas' parameters, the same approach used in [Ribe18] is used, so a $\lambda/4$ resonant monopole is chosen because of the rooftop morphology, and also because a monopole working above an infinite ground plane is the equivalent to a $\lambda/2$ resonant dipole. This approach is suitable because monopoles are usually installed inside an aerodynamic structure.

In Figure 3.8, it is possible to observe a design draft, as well as the corresponding dimensions exported to CST for different communication systems in Table 3.1. One considered a 380 MHz working frequency for TETRA, 900 MHz for GSM-R, 2.6 GHz for LTE-R, and 5.9 GHz for BBRS. The antenna's radius is 1 cm for all technologies, since this is a common dimension in railways.
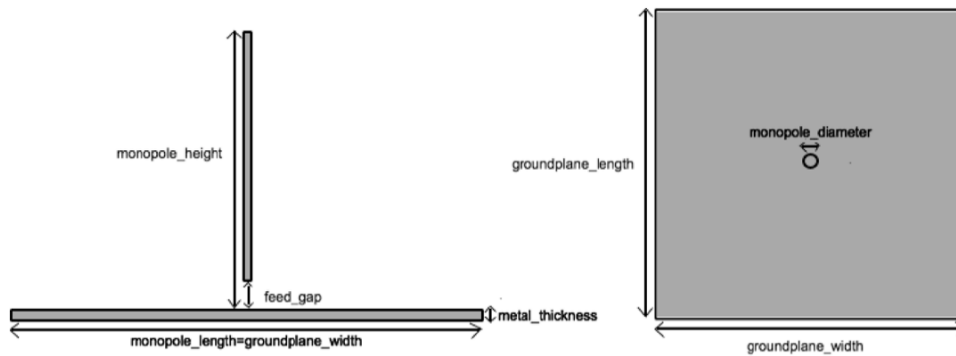

Figure 3.8 Sketch of a $\lambda/4$ monopole above a square conducting plane.

Table 3.1 Monopole dimensions for TETRA, GSM-R, LTE-R and BBRS technologies.

Parameters	Dimensions [mm]			
	380 MHz	900 MHz	2.6 GHz	5.9 GHz
Wavelength centre	788.93	333.10	115.30	50,81
Monopole height	180	77	27.3	11.9
Metal thickness (λ/100)	7.89	3.33	1.15	0.51
Feed gap (monopole height/100)	1.8	0.77	0.27	0.12

The antennas used a custom monopole with a circular ground plane, were previously designed in Antenna Magus during the development of André Ribeiro's thesis [Ribe18]. Some specific antenna parameters, such as the centre working frequency, the minimum and maximum frequencies, the directivity or the realised gain, and the port impedance characteristics, such as S_{11} and the characteristic impedance Z_0, were set. In this case, de impedance of the λ/4 monopole is only resistive (36.5 Ω), with zero reactive impedance (inductance or capacitance contributions).

These four antennas were imported to CST, where the simulation was run. The main objective was to understand if the obtained performance results are similar to the theoretical ones. All the simulations were based on the Time Domain Solver and the global properties set at "Hexahedral" [Ribe18]. Regarding the mesh cells, the standards option was selected, 3-15 cells per wavelength near and far from the model. Also, these two local mesh groups were created for the Port 1, identified in Figure 3.10 within a red marker, and for the antenna itself.

Regarding simulation time, the most critical case is the 5.9 GHz, due to the smallest wavelength, creating 251 464 mesh cells. The simulation took about 21 hours, which is acceptable. Following the same approach as André Ribeiro [Ribe18], all the boundaries were defined as "open (add space)" apart from Z_{min}, which was fixed as a "conducting wall". The purpose of this is to have the theoretical characteristics of a λ/4 monopole at an infinite ground plane. Figure 3.9 presents the mesh view of the λ/4 monopole operating at 5.9 GHz. All simulations performed in this work were executed using a laptop equipped with an Intel Core i7-7700HQ CPU with 16 GB of RAM.

The theoretical directivity value of a λ/4 monopole is twice the one of a λ/2 dipole, 5.15 dBi. The radiation pattern of the former can be seen in Figure 3.10, and the remaining are shown in Annex B. In every situation, the directivity is equal to the gain, which implies that there are no losses from the accepted power of the structure. In the worst case, the antenna has a slight difference of 0.12 dBi, which can be explained by some technical aspects of the antennas' design.

Figure 3.11 S11 parameter of the λ/4 monopole operating at 5.9 GHz presents the reflection coefficient S_{11} of the λ/4 monopole operating at 5.9 GHz.
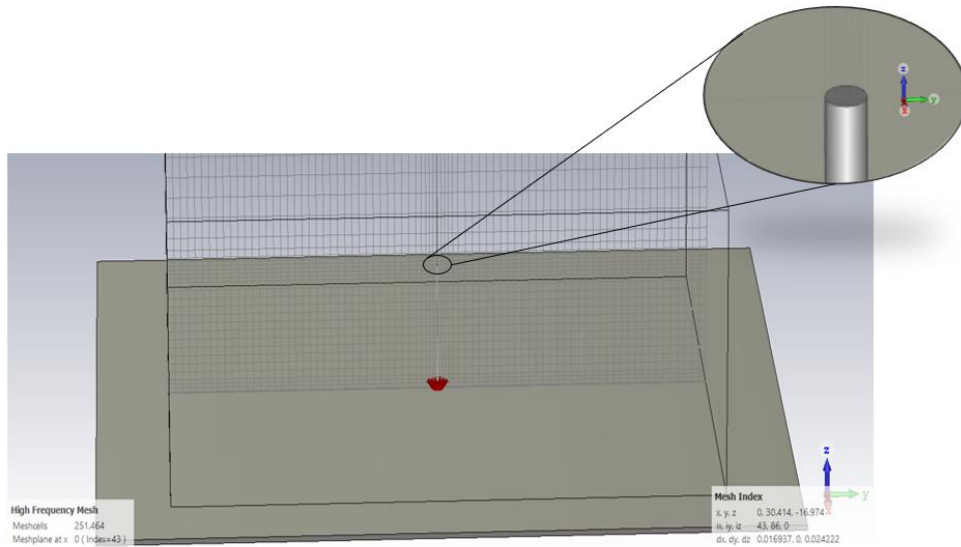
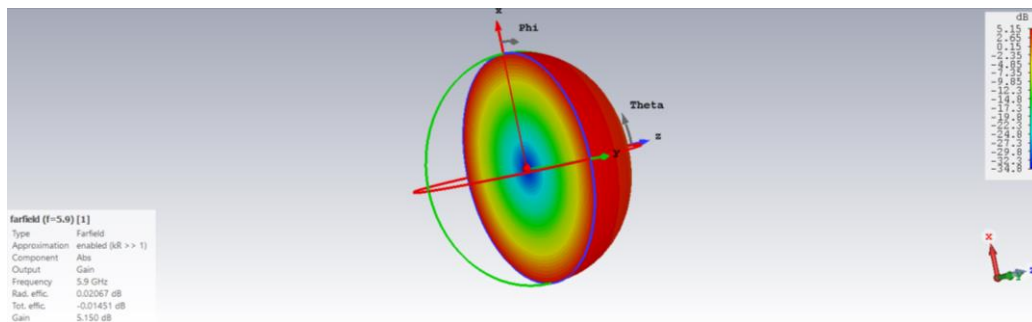Figure 3.9 Mesh view $\lambda/4$ monopole operating at 5.9 GHz

Figure 3.10 3D far-field view of a $\lambda/4$ monopole operating at 5.9 GHz
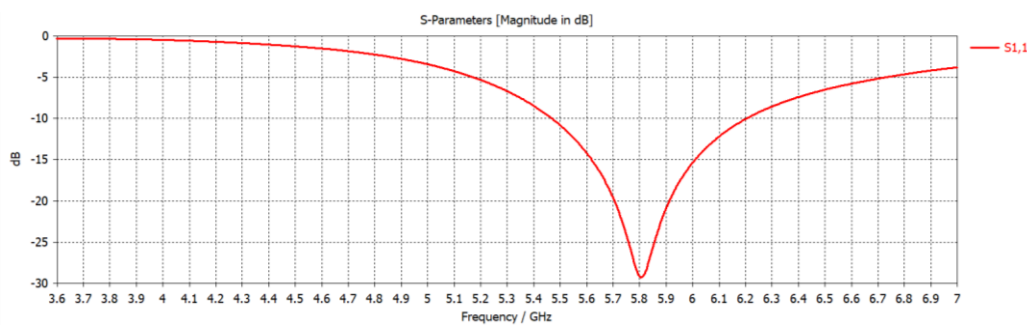

Figure 3.11 S_{11} parameter of the $\lambda/4$ monopole operating at 5.9 GHz

3.6   Train and Pantograph Model

In terms of the scenario that is analysed, the train, the pantograph, and the catenary are the main structures that one is going to focus on. The CST model needed to represent the scenarios presented in Figure 3.12. To do that, a CST model prevenient from a CAD database was used.

Figure 3.12 Pantograph and Catenary – Azambuja's station.

However, the simulation time regarding this model, presenting a complete carriage, and the pantograph was taking more than 10 hours to simulate. So, to decrease the simulation time, one focused on the rooftop, pantograph and catenary. The second model that one used to perform the simulations and the radiation pattern obtained after simulation can be observed in Figure 3.13.
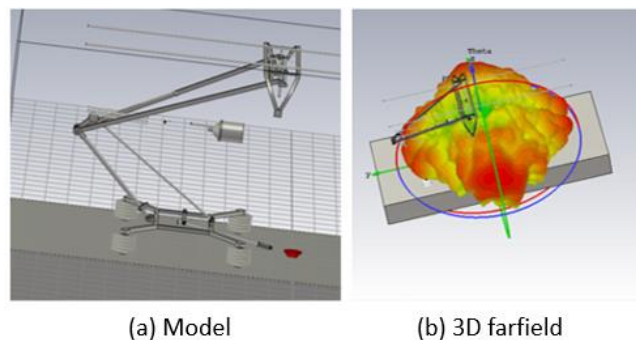
(a) Model   (b) 3D farfield
Figure 3.13 CST view of the pantograph and the catenary.

However, since the simulation time was rounding the three days for higher frequencies, one decided to simplify the model, as presented in Figure 3.14. Here, the pantograph structure was completely changed, having fewer details, which diminish the simulation time significantly.
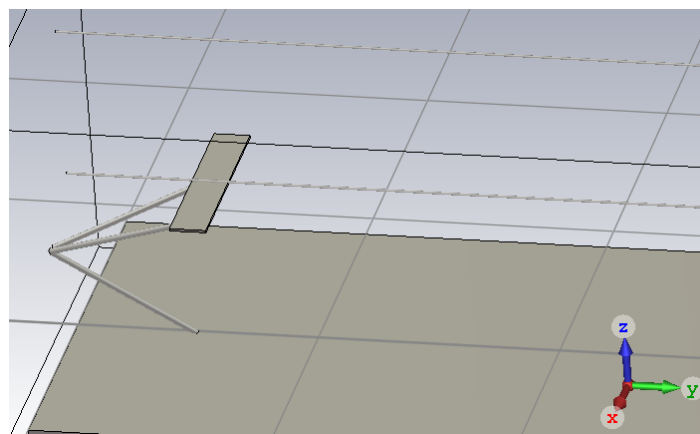

Figure 3.14 Simplify CST model for the pantograph and the catenary.

3.7 Assessment

Regarding the antenna analysis, to understand if the model selected to evaluate the behaviour of the antenna in the presence of the catenary and pantograph is correct, one had to analyse the simulation results. Analysing the reference scenario, where the only structure besides the antenna is the train rooftop, one can observe that the gain obtained in the simulation, 5.273 dBi, is similar to the theoretical one, 5.19 dBi, as presented in Figure 3.15. This means that the presence of the antenna in the train's rooftop is not significant, so all the results obtained with the catenary and the pantograph are mainly affected by these.

For the EMI analysis, one took the theoretical approach first. Using the theoretical expression on MATLAB, one determined the exponential coefficients for the harmonic corresponding to each technology and the value of the electric field for the reference distance, 1.4 m. The result, $E = 6\ 338$ V/m, corresponds to the electric field originated from the fundamental frequency, 50 Hz. Having both pieces of information, one can determine the value of the electric field from each harmonic and then its power.
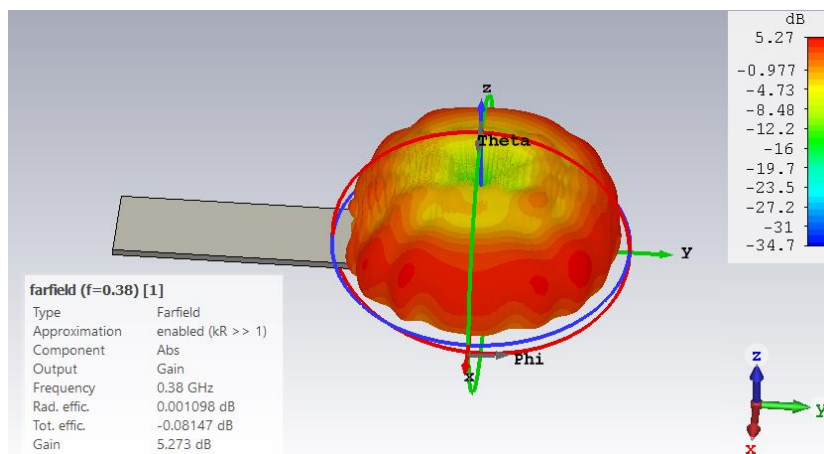

Figure 3.15 3D far-field view of a $\lambda/4$ monopole operating at 380 MHz.

In the simulation approach, one used the CST to simulate this same scenario and determine the maximum value of the electric field, as presented in Figure 3.16. The value obtained in the simulation was E_{max}=4 481.7 V/m, which divided by $\sqrt{2}$ provides the average time value of $E = 3\ 446$ V/m. The difference in the results may be due to CST, assuming that the potential between the catenary and the train's rooftop is continuously 25 kV, when theoretically is periodic. Also, the train's rooftop is not an infinite structure as it is theoretically assumed, so this may also be affecting the results. Figure 3.17 presents the power of each interfering harmonic for different distances between the train's rooftop and the catenary, *d_sup_cat*. It is possible to see that when *d_sup_cat* decreases, the CST value obtained for the power of each interfering harmonic is more and more close to the theoretical one, so one can assume that the model is a good approximation of the reality.

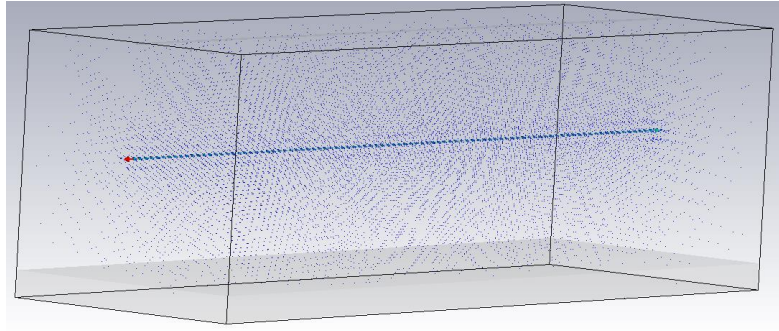Figure 3.16 CST model of the catenary and train's rooftop with the representation of the electric field.

(a) d_sup_cat=2.8m

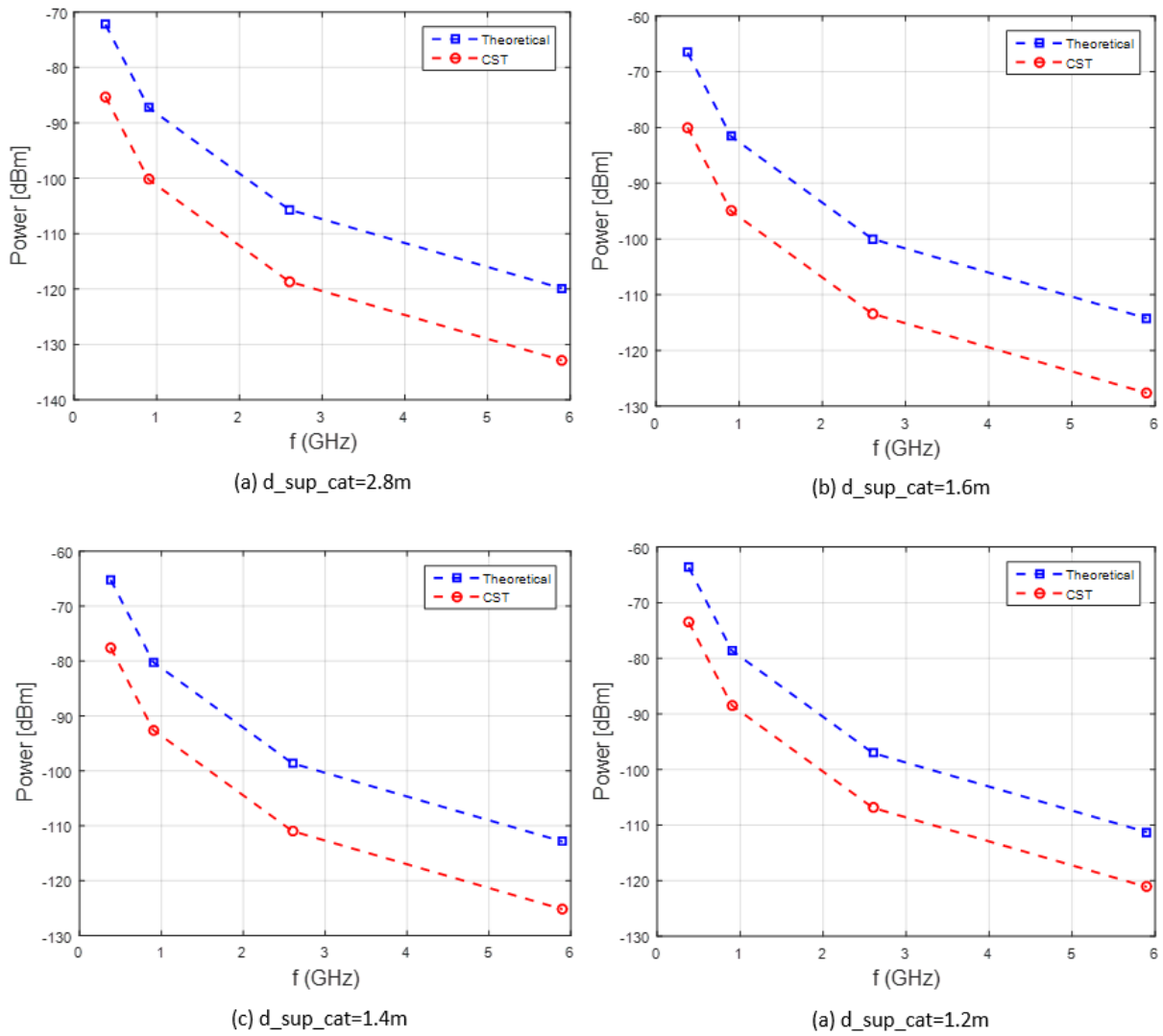(b) d_sup_cat=1.6m

(c) d_sup_cat=1.4m

(a) d_sup_cat=1.2m

Figure 3.17 Interfering power prevenient from each harmonic.

Chapter 4

Results' Analysis

This chapter includes the problem methodology and the most important aspects that was considered for the simulations. A description of the software and the implementation of the antennas and scenarios are also presented.

4.1 Scenario Description

In this section, a description of the reference scenario for both the antenna analysis and the EMI study is provided.

4.1.1 Antenna Analysis Scenario

Generally, the train rooftop is a curved ground with specific dimensions. However, since the goal of this work is to analyse the antenna's performance in the presence of the pantograph and catenary, one has considered that the train's rooftop is a plane rectangular metallic structure. The dimensions for the scenario are presented in Figure 4.1.
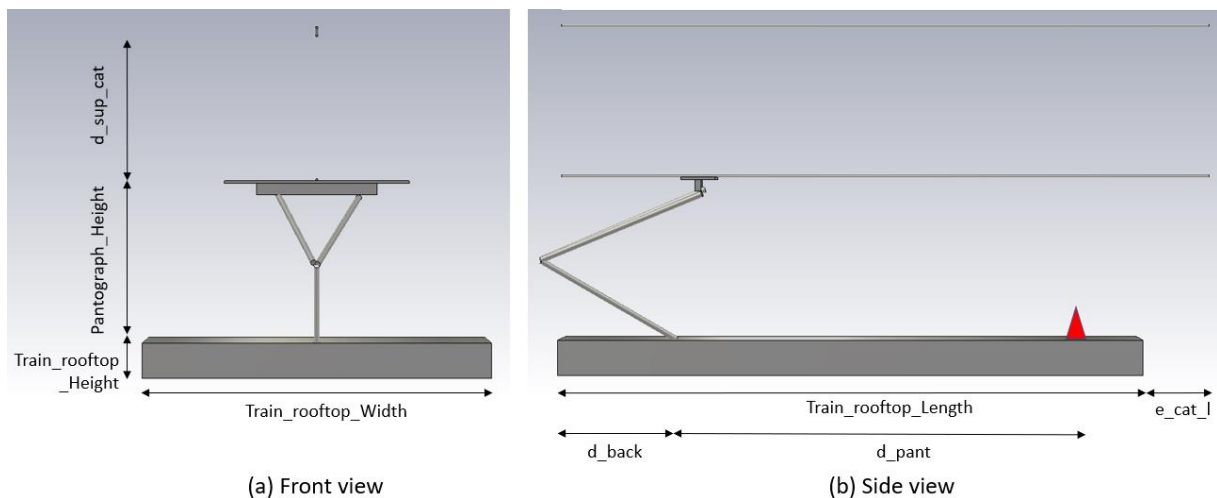

Figure 4.1 Train's rooftop-pantograph-catenary model

Each dimension is defined as follows:

- d_sup_cat: Distance between catenary and the support line.
- d_pant: Distance between the front of the carriage and the pantograph.
- d_back: Distance between the back of the carriage and the pantograph.
- e_cat_l: Extra catenary length, about 5λ.
- Pantograph_Height: Height of the pantograph.
- Train_rooftop_Height: Height of the train's rooftop, 30cm.
- Train_rooftop_Length: Length of the train's rooftop, variable.
- Train_rooftop_Width: Width of the train's rooftop, 3m.

For the antenna analysis, the values for each of these dimensions, according to each system are presented in Table 4.1 (based on [Trai19]). One has also chosen three distances between the antenna and the position of the pantograph (d_pant) for each technology: one outside the 20λ limit, and the other

two inside. This is done since, according to [Pals13], it is considered as a good approximation to analyse the surrounding environment up to 20λ of distance from the antenna. This way, it is possible to assess what the behaviour of the antenna is, when the pantograph is outside and inside of the antenna's influence radius. The selected distances are presented in Table 4.2.

Table 4.1 Model dimensions for antenna analysis

f [MHz]	380	900	2600	5900
d_sup_cat [m]	1.3			
d_back [m]	1			0
e_cat_l [m]	4	1.7	0.6	0.3
Pantograph_Height [m]	1.4			
Train_rooftop_Height [cm]	30			
Train_rooftop_Length [m]	18	9	5	4
Train_rooftop_Width [m]	3			

Table 4.2 Distances between the antenna and the pantograph position

f [MHz]	20λ [m]	d_pant [m]		
380	15.8	16	10	5
900	6.7	7	4	1
2 600	2.3	3	2	1
5 900	1.0	1.25	1	0.5

Concerning the analysis of the signal received at the antenna, one can distinguish two placements for the antennas: the on-track radios and the on-board radios, which are explained in more detail in André Ribeiro's thesis [Ribe18]. The BSs are placed parallel to the railway, equally distanced, and the MSs are usually at each extremity of the carriage, as shown in Figure 4.2. Each distance is defined as follows:

- d_bs_bs: Distance between the BSs.
- d_bs_ms: Distance between the BS and the MS.
- d_ms_ms: Distance between the MSs placed at each extremity of the train.
- d_0: Distance between the BS and the railway track.
- L: total length of the train.

Although these parameters are important when approaching the problem, the main focus when analysing the antenna resides on the two perspectives between an antenna and the BSs: the vertical perspective (elevation plane) and horizontal plane (azimuth plane) [Ribe18]. The elevation plane provides information regarding the elevation angle θ, which is measured between the BS and the antenna. When θ = 0°, it means that the antenna is passing right under the BS, and when θ = 90°, both antennas are at the same height, which may be due to terrain morphology. The azimuth plane gives the direction and positioning of the antenna relative to the BS from angle φ. For example, if φ = 0° V φ = ±180°, then the BS would be on the right or left side of the train, and when φ = 90° V φ = 270°, the BS respectively in the same direction of the movement of the train or the opposite direction [Ribe18]. This

information is relevant to decide which angles are important to assess the antennas' behaviour, as one presents in the following section. In this study, one is going to assess two sets of angles.
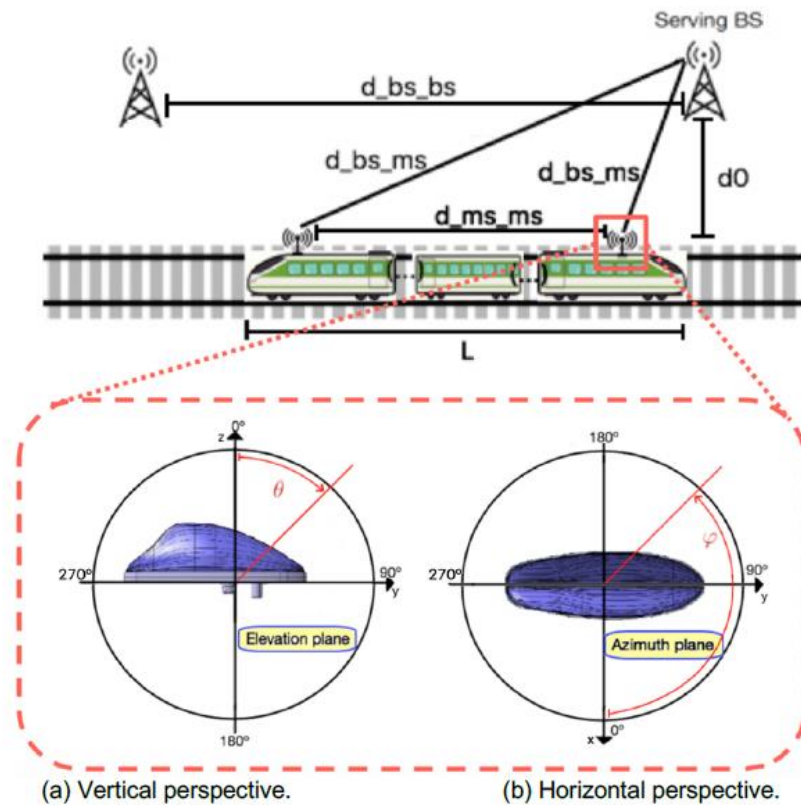

Figure 4.2 Reference scenario with two perspectives of an antenna (extracted from [Ribe18]).

For the first part of this study, the four scenarios that one considered are the following, all of them presented in Figure 4.3:

- only rooftop (R),
- rooftop with catenary (R+C),
- rooftop with a pantograph (R+P),
- rooftop with catenary and pantograph (R+C+P).

These last three are compared with the reference scenario, R, where there is only the antenna placed on the rooftop. Regarding the problem formulation, one has analysed three different perspectives in the azimuth plane: $\varphi = 0°$ (lateral view), $\varphi = 90°$ (no pantograph obstruction), and $\varphi = 270°$ (possible pantograph obstruction).

For the second part of this study, one considered only the R+C+P scenario. Regarding the problem formulation, one has analysed eight different perspectives in the azimuth plane: $\varphi = 45°$, $\varphi = 60°$, $\varphi = 75°$, $\varphi = 90°$, $\varphi = 270°$, $\varphi = 285°$, $\varphi = 300°$ and $\varphi = 315°$; and different elevation angles in the interval [60°;90°], with a step size of 5°. This set of angles was chosen because the most important scenario is when trains are between BSs, when the performance of the antenna can be more critical due to the distance to the BS that is serving, as shown in Figure 4.4.
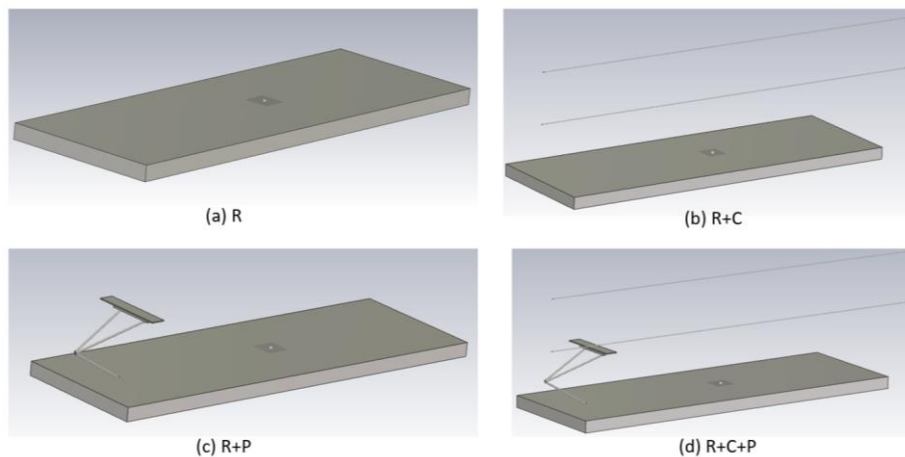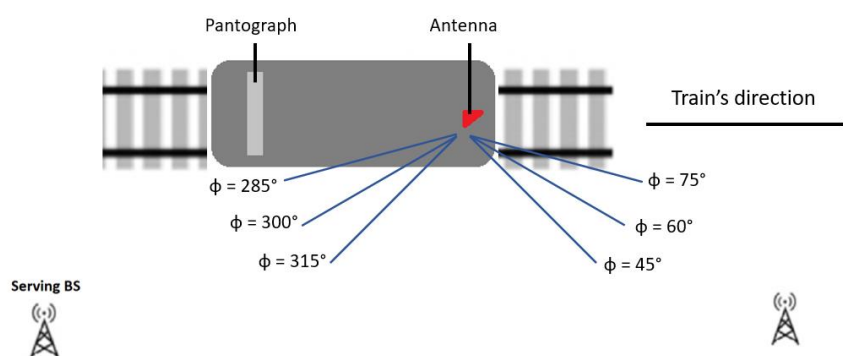
Figure 4.3 CST models

Figure 4.4 Train horizontal perspective

4.1.2 EMI Scenario

In the EMI study, the values for the parameters presented in Figure 4.1 are presented in Table 4.3. One has chosen 4 different pantograph heights, according to reference values for the minimum and maximum heights of the pantograph. This way, one can analyse how this distance influences the antenna's behaviour.

Table 4.3 Model dimensions for EMI analysis

d_sup_cat [m]	1.3			
e_cat_l [m]	0			
Pantograph_Height [m]	1.2	1.4	1.6	2.8
Train_rooftop_Height [cm]	30			
Train_rooftop_Length [m]	10			
Train_rooftop_Width [m]	3			

In Table 4.4, one presents the values for the parameters presented in Chapter 3, such as the noise figure, the carrier bandwidth, and the sensitivity, for each system, provided by Thales.

Table 4.4 EMI input parameters

f [MHz]	380	900	2600	5900
NF [dB]	8	8	7	5
Δf [kHz]	25	200	15	384
P_{min} [dBm]	-103	-104	-94	6Mbps: -90 54Mbps: -73

4.2   Antenna Analysis

In this section, an analysis is performed to determine the effect that the pantograph and the catenary, have on antennas' performance. The height of both structures is variable, however, one decided that 1.4 m between them would be a reasonable one. Two studies were performed in this section: one comparing four different scenarios and another varying the distance between catenary and pantograph.

To have an acceptable simulation time, specific dimensions are different among technologies. This is due to the frequency that each antenna operates since the wavelength is lower for higher frequencies, which leads to more variation and more calculations for the CST tool. When passing from a simulation with a lower frequency to a simulation with a higher one, the simulation time increases rapidly. For example, using the same model for a TETRA antenna and a BBRS antenna, the simulation time of 30 minutes for the first one becomes more than 36 hours for the second one. To avoid this issue, one defined that the length of the rooftop would decrease when going to higher frequencies. This does not affect significantly the results, since the distance for which the surroundings have an influence on the performance of the antenna 20λ is, in most part, respected. In total, CST was run 48 times within four scenarios and four d_pant distances for each system. The results of these simulations are available in Annex B, where one presents the 2D monopole performance for each set of specifications.

4.2.1 TETRA

One started the simulations in CST using TETRA, with an operating frequency of 380 MHz. The simulations were ran using the four scenarios presented before and the three distances d_pant: 16 m, 10 m, and 5 m. For the first part, one has chosen to analyse the results for d_pant=10 m, within the 20λ boundary, which are presented in Figure 4.5. When φ=0° (side view), the antenna's performance is very similar in the four scenarios. One observes a slight variation of 1.26 dB in the gain, along with an α$_{3dB}$ between 39.5° and 49°. The direction of maximum gain decreases 8-11° in the scenarios with a pantograph and/or catenary relatively to the reference. This may not be relevant since, for the most part, the BSs are at the front or the back of the train. For φ=90° (front view), one observes a significant improvement in the antenna's performance when in the presence of pantograph and/or catenary, increasing about 5 dB. However, this growth is accompanied by an increase in the direction angle, which means that these structures lead to the reflection of electromagnetic waves in this direction, increasing

the gain. The directions of maximum gain, between 83-88°, mean that the antenna is directed in a straight line in this direction, which can be unfavourable, especially on terrain with irregular morphology.

When φ=270° (back view), one observes that only in the R+C+P scenario, the performance of the antenna is significantly above the reference, increasing 5.14 dB, along with a low α_{3dB}. The low dispersion of the electromagnetic waves increases the gain. Thus, in the presence of both structures, the directivity of the antenna increases, affecting its omnidirectional behaviour. Also, in the R+P scenario, the direction angle is expressively lower than the reference one, along with a maximum gain slightly below the reference. This means that the pantograph reflects the EM waves propagation in all directions except for this one, in particular, in the opposite direction, which may lead to communication problems with the BS behind the train.
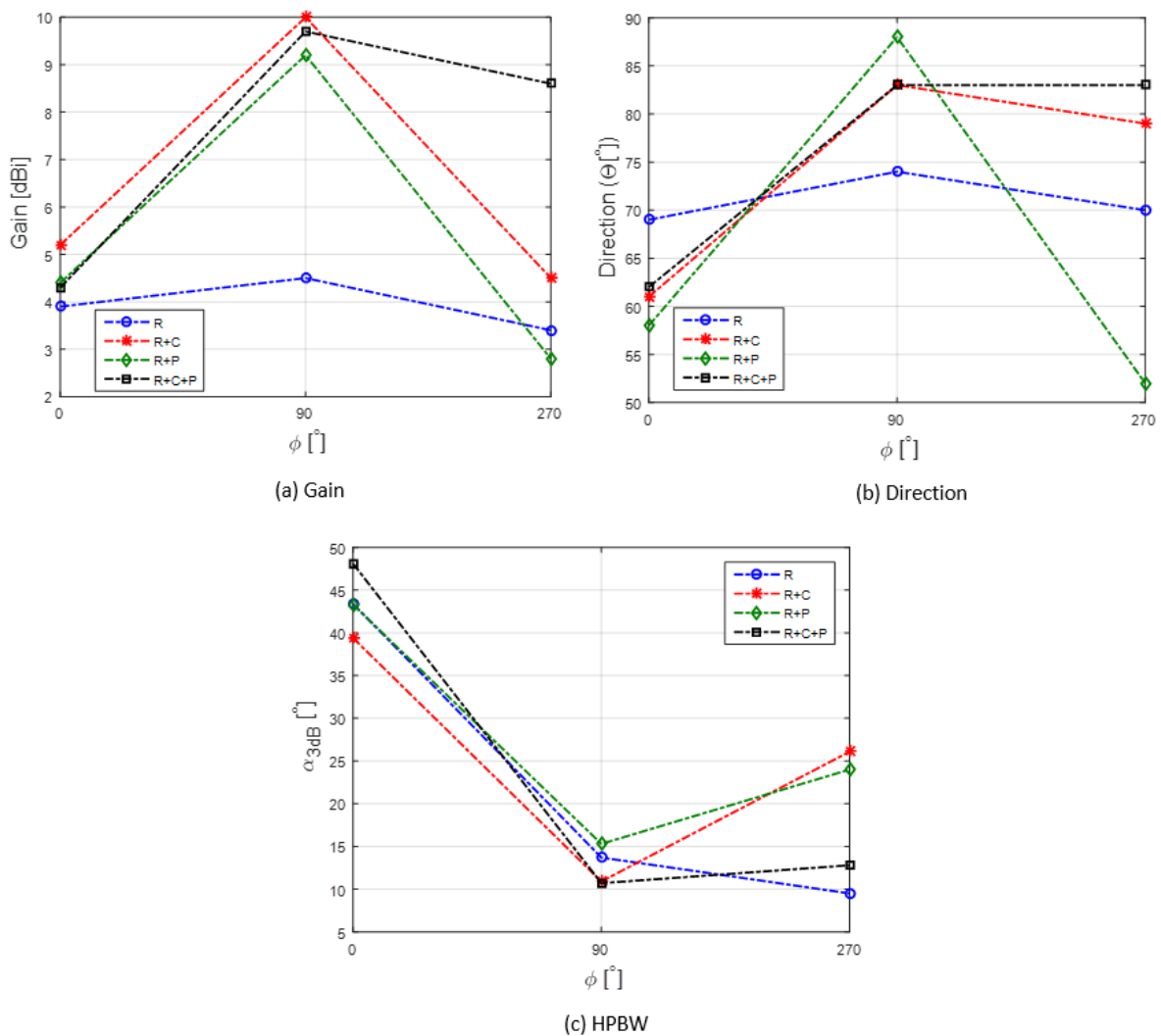

(a) Gain

(b) Direction

(c) HPBW

Figure 4.5 Comparison between the four scenarios' performance at 380 MHz.

To understand the behaviour of the antenna when varying the pantograph positioning, regarding the antenna in the R+C+P scenario, a set of angles were selected to determine the variation of the generalised gain and its standard deviation. Figure 4.6 Comparison between azimuth views at 390 MHz and Figure 4.7 present the results obtained for the three distances in eight azimuth angles: four

corresponding to the front of the train, and the other four to the back of the train, respectively, as well as the standard variation. One observes that at distances d_pant equal to 5 m and 10 m, within the influence range of 20λ, the behaviour of the antenna is very close to the reference scenario for the φ=45° and φ=60°, decreasing less than 1 dB, and increasing from 1.5 dB to 2.5 dB for φ=75° and φ=90°, so the pantograph improves the antenna's performance. For d_pant equals to 5 m and φ=75° and φ=90° perspectives, the standard deviation is between 4 dB and 5 dB, so the antenna's directivity increases when the antenna is in the presence of the catenary and pantograph. When moving away from the antenna, still inside the 20λ boundary, the standard deviation decreases, so the antenna is no longer as directive as before, which leads to a decrease in the gain. For d_pant equal to 16 m, the gain decreases significantly, verifying that the presence of the pantograph is no longer felt. However, the catenary is still above the antenna, which leads to a significant decrease in φ=90°. In the back part of the train, where the pantograph is placed, the equivalent happens for symmetric angles, the gain for φ=285° being slightly more significant than in its front part, but then the tendency is to get closer to the reference, as the antenna moves away from the pantograph. However, when φ=285°, the standard deviation of the gain increases, which means that the reflection from the catenary is being felt and leading to a more directive antenna's behaviour.
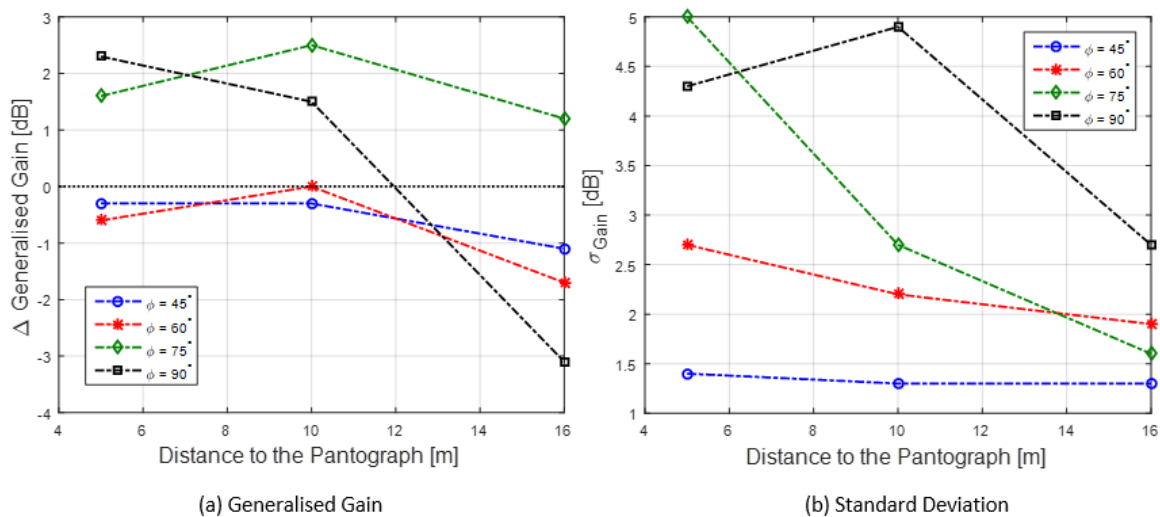

(a) Generalised Gain   (b) Standard Deviation

Figure 4.6 Comparison between azimuth views at 390 MHz at the front of the train

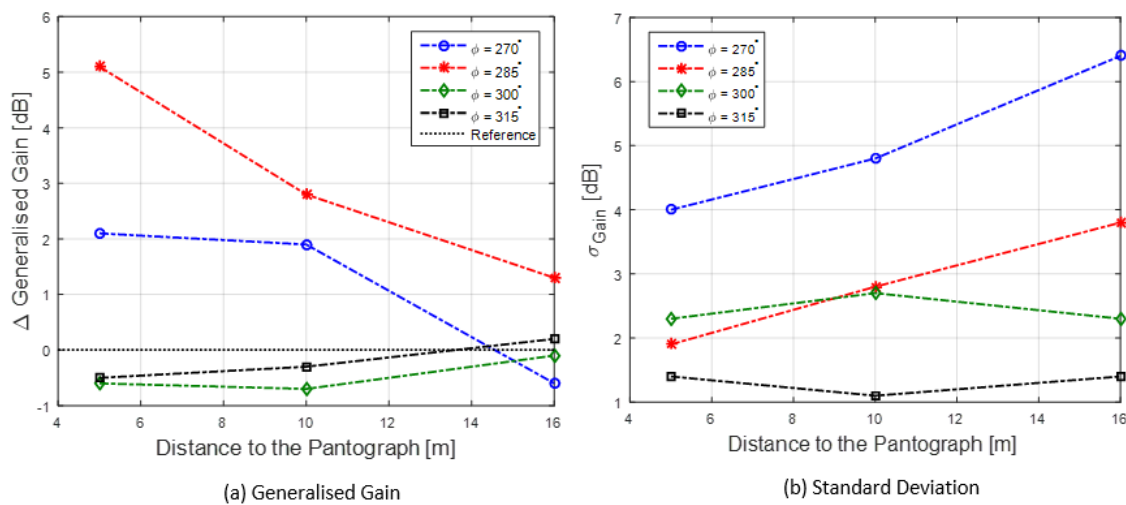(a) Generalised Gain   (b) Standard Deviation

Figure 4.7 Comparison between azimuth views at 390 MHz at the back of the train

4.2.2 GSM-R

For GSM-R, one has used an antenna operating at 900 MHz. The simulations for the four scenarios and three distances were run in CST. Figure 4.8 presents the comparison of the antenna's performance for the four scenarios when the antenna is at 4 m from the pantograph base. Note that at this distance the antenna is nearly in the middle of the train's rooftop and inside of the 20λ boundary. One observes that once again, in the lateral view (φ=0°), the maximum gain increases meaningfully comparatively to the reference, intensifying 7-9 dB, accompanied by a huge growth in the direction's angle, with the antenna pointing much lower, between 65-70°, so the presence of the catenary and/or pantograph reflects the EM waves in this direction. However, α$_{3dB}$ decreases 1.1° and 2.5° for the R+C and R+C+P scenarios, respectively, and it remains practically constant in the R+P one, so the catenary is responsible for decreasing the waves dispersion, leading to a more directive antenna. Once again, this may not be an issue for this perspective, since the BS is right beside the carriage and its power is very high.

In the front view (φ=90°), one observes that the presence of the catenary continues to increase the maximum gain in this perspective, along with a high direction and an α$_{3dB}$ below reference, so the antenna still has a directive behaviour. However, in the R+P scenario, one observes a clear decrease in the gain with an α$_{3dB}$ 2.9° above the reference, so the dispersion of EM waves increases, which could lead to interference problems regarding other signals. For φ=270°, the back view, one observes that, in terms of gain, only in the R+P scenario, it equals the reference, along with an α$_{3dB}$ of 10.1°, so the reflection at the back of the train is very dispersive, due to the pantograph.

Regarding the generalised gain and the standard variation for the front and back part of the train, the results can be observed in Figure 4.9 and Figure 4.10, respectively. At the front part of the train, one observes that for φ=45° and φ=60°, the generalised gain is very close to the reference for all distances from the pantograph, varying about 1 dB, so the catenary and the pantograph do not have a significant effect on the antenna's behaviour for these perspectives. For φ=75° and φ=90° in the two distances within 20λ boundary, the generalised gain is about 4 dB to 6 dB above the reference, so the antenna has a very directive behaviour. When d_pant equals to 7 m, the generalised gain for φ=75° decreases significantly, and remains almost constant for φ=90°, so the EM waves are mostly reflected in this direction. Regarding the standard deviation, inside the 20λ limit, it is clear that, for φ=45° and φ=90°, the lobe is very irregular. When d_pant equals to 7 m, outside the 20λ boundary, σ_{Gain} tends to zero, so the effect of the pantograph is much more significant than the catenary. At the back part of the train, one observes that, when the antenna is moving away from the pantograph, σ_{Gain} increases for φ=270° and φ=285°, so the influence of the catenary is much more significant when the pantograph is not close to the antenna. In terms of σ_{Gain}, one observes that for φ=270°, when d_pant is too close to the pantograph, it is about 3 dB, but when it moves away but and is still inside the 20λ boundary, it increases to almost 8 dB, so the lobe is much more irregular, due to the reflections in the pantograph. When d_pant equal to 7 m, the influence is no longer felt, so σ_{Gain} decreases again.
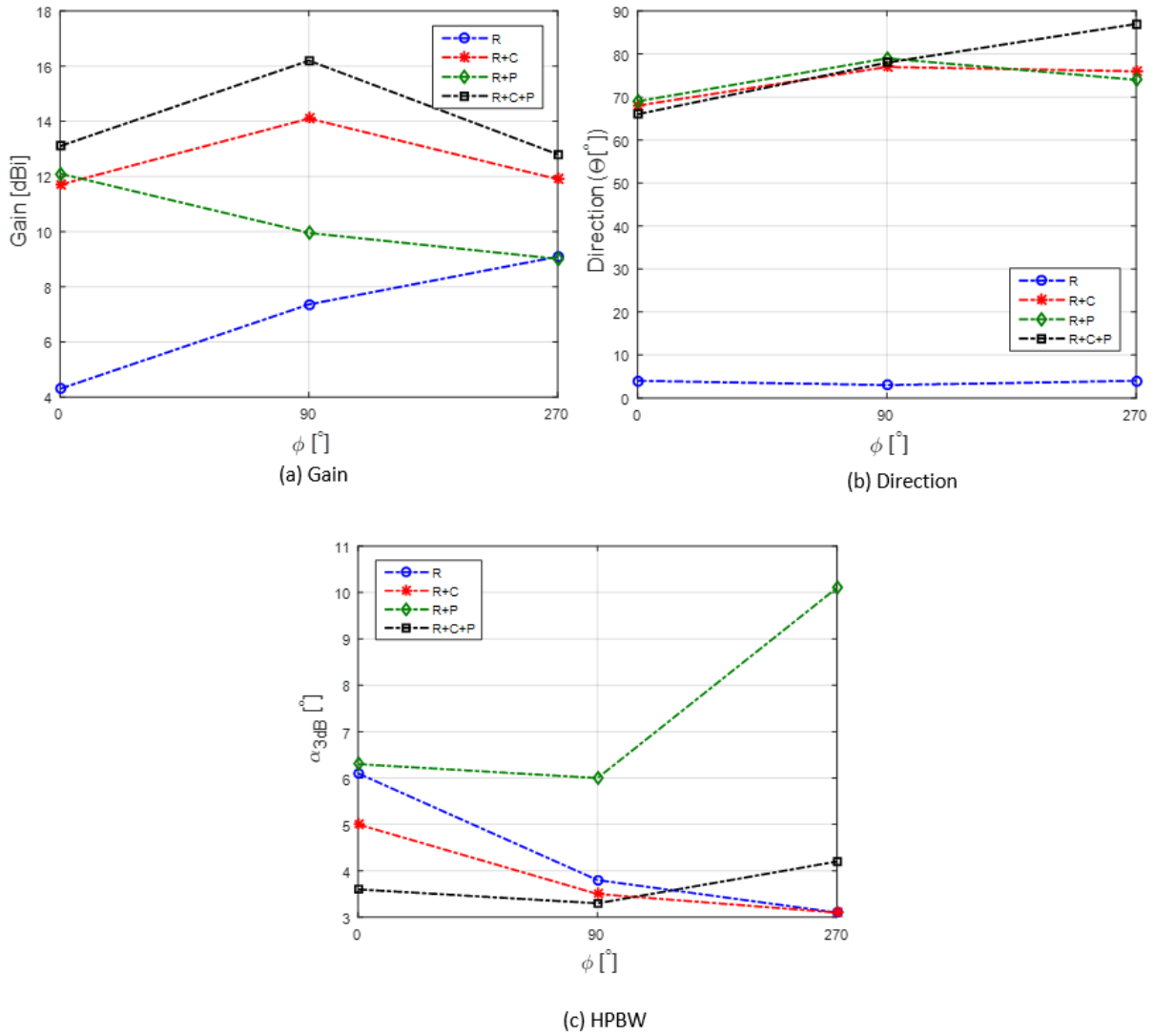
(a) Gain

(b) Direction

(c) HPBW

Figure 4.8 Comparison between the four scenarios performance at 900 MHz.

(a) Generalised Gain

(b) Standard Deviation
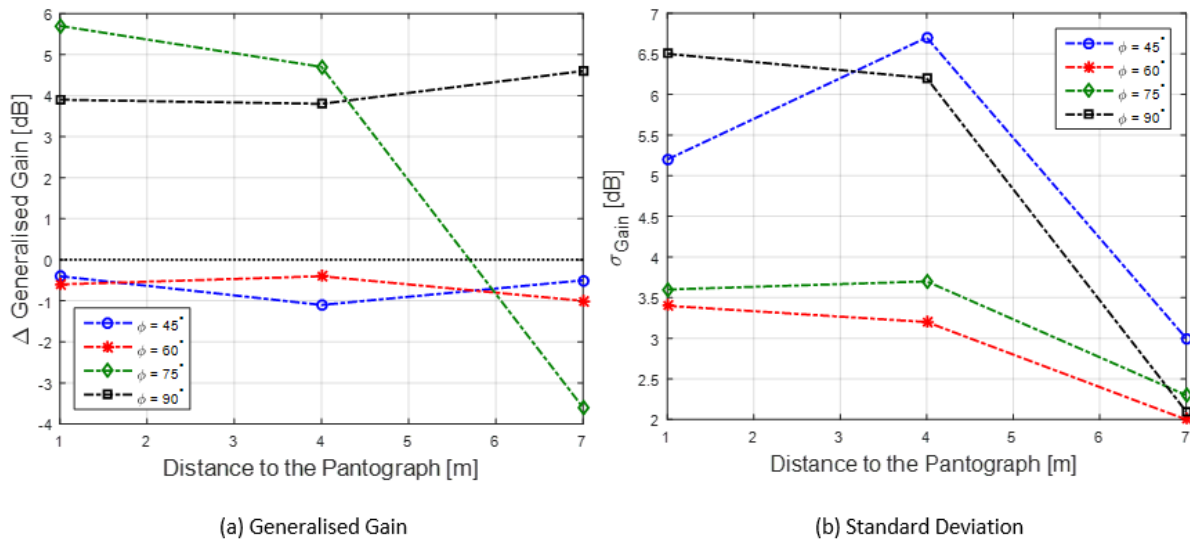
Figure 4.9 Comparison between azimuth views at 900 MHz at the front of the train.
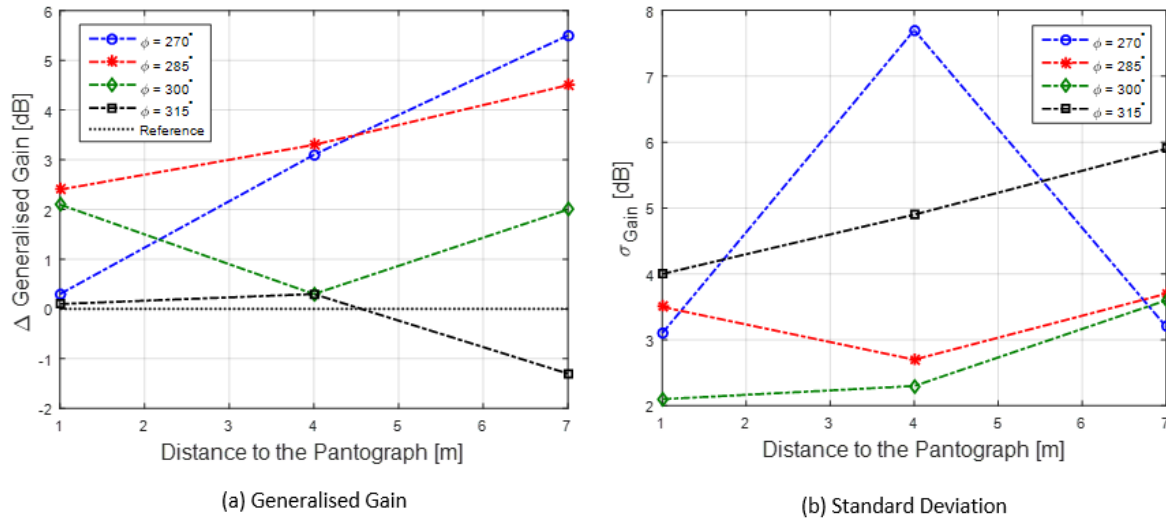
(a) Generalised Gain

(b) Standard Deviation

Figure 4.10 Comparison between azimuth views at 900 MHz at the back of the train.

4.2.3 LTE-R

For LTE-R, the antenna is operating at 2.6 GHz. The results for d_pant=2m, in the three perspectives, are presented in Figure 4.11. For φ=0°, one observes that in the R+P scenario, the gain increases about 2 dB relatively to the reference, along with a 5° increase in the direction, and a decrease of 5.8° in the α_{3dB}, so the antenna has a more directive behaviour comparatively to the reference. The pantograph reflects the EM waves in a way that there is less dispersion, which increases the gain. For the R+C and R+C+P, the existence of the catenary leads to an even more significant increase in the gain and in the direction, and a decrease of the α_{3dB}, so the antenna is even more directive in the presence of the catenary. One observes that for both φ=90° and φ=270°, the maximum gain for all the three scenarios with the structures is below the reference, so the antenna is too close to the pantograph, and the EM waves are being reflected the sides (φ=0° and φ=180°). This could be a very significant issue, since, as mentioned before, the BSs are mostly at the front or the back of the train, so the pantograph and the catenary are considerably damaging the performance of the antenna in these views. One also observes that for the front and the back view, the direction is more or less equal, except for the R+C scenario, but this is because the antenna is very close to the back end of the train car (3 m) comparatively with the 7 m in the opposite direction. Regarding the α_{3dB}, one observes that, for φ=0°, its value is much lower in scenarios with a pantograph and/or catenary, which supports the conclusion of the gain increasing on the sides, making the antenna more directive in that perspective.

Regarding the variation of the generalised gain and the standard variation, one presents its results for the front and back in Figure 4.12 and Figure 4.13, respectively. One observes that, in the perspectives at the front part of the train, the generalised gain is, for the most part, below the reference. In particular, when the antenna is outside of the boundary of the pantograph's influence, in φ=60°, φ=75°, and φ=90° perspectives, the generalised gain decreases significantly. This means that the catenary is harmful to the antenna's performance, especially in this range of angles, and that the pantograph reduces its

impact. As one has mentioned before, the transitioning from one BS to another is the most critical scenario due to the distance between the antenna and the BSs themselves, so when having a low gain in these perspectives, some railway operations may be vulnerable. One also observed that for φ=75° and d_pant equals to 3 m, σ_{Gain} increases meaningfully, so the antenna is very directive in this direction.
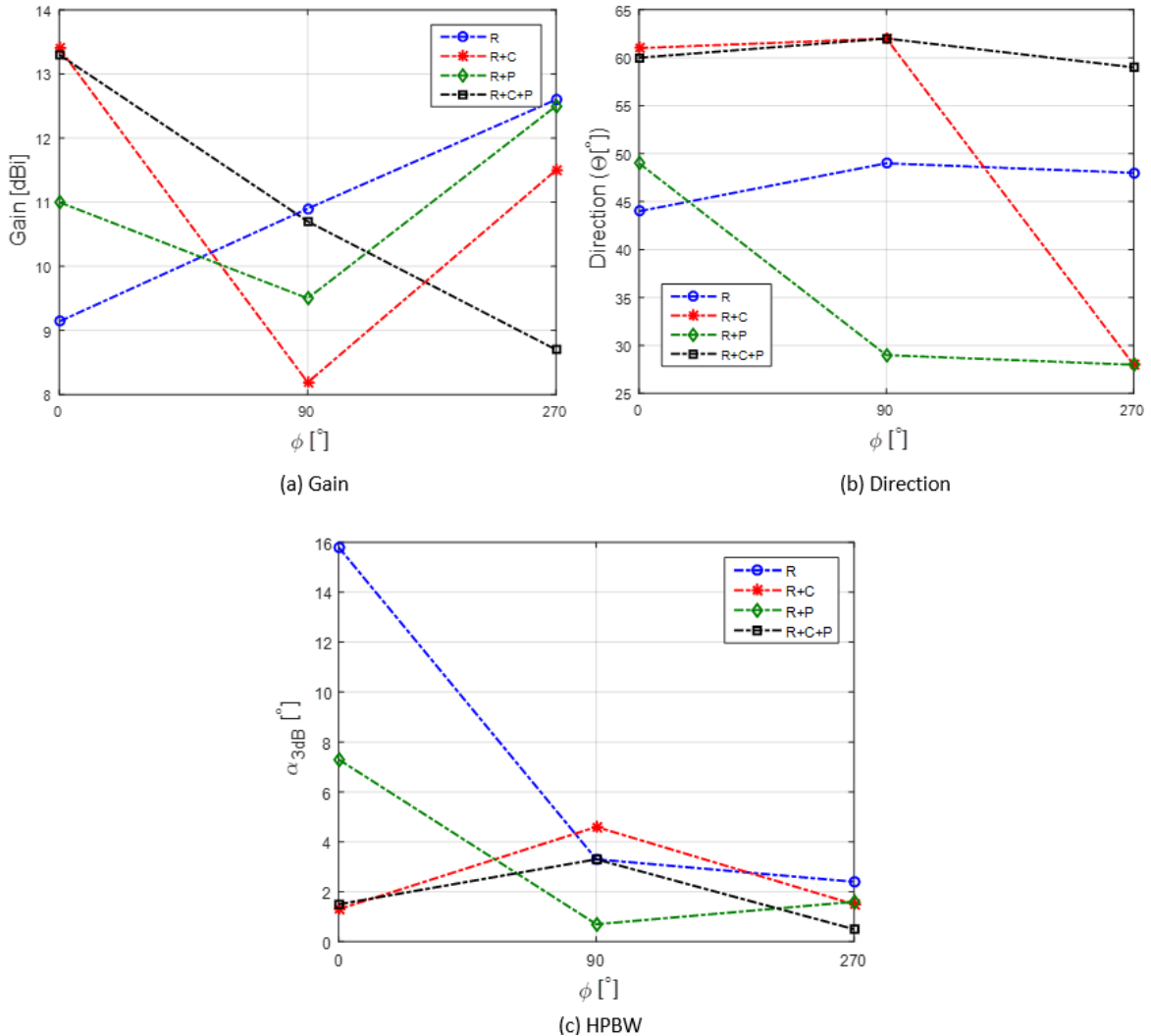

(a) Gain

(b) Direction

(c) HPBW

Figure 4.11 Comparison between the four scenarios' performance at 2.6 GHz.

In the back part of the train, one observes that when the antenna is 1 m from the pantograph, the generalised gain for φ=270° and φ=285° is below the reference, so the antenna is so close to the pantograph that the EM waves are mostly reflected in the opposite direction (φ=90°). This means that when the train is going away from the BS, the railway operation may suffer a severe quality decrease. As the antenna moves away from the pantograph, one noticed that for φ=270°, the generalised gain increases, being significantly above the reference when outside the 20λ limit, so the reflection of EM waves is significant in this direction. The proximity to the pantograph is substantial here, because it either damages the antenna performance, resulting in communication issues, or it improves it, which leads to possible interference issues. Regarding σ_{Gain}, one observes that for a very close distance, its value is high for φ=270°, so the antenna is directive in this direction, and for a d_pant=3 m, it is high for φ=300°.

(a) Generalised Gain

(b) Standard Deviation
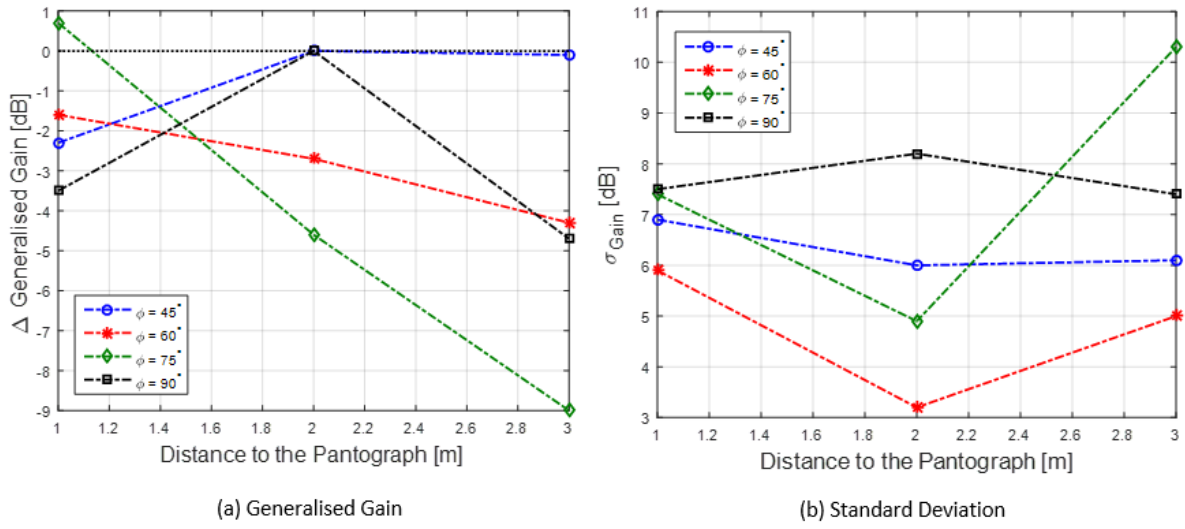
Figure 4.12 Comparison between azimuth views at 2.6 GHz at the front of the train.

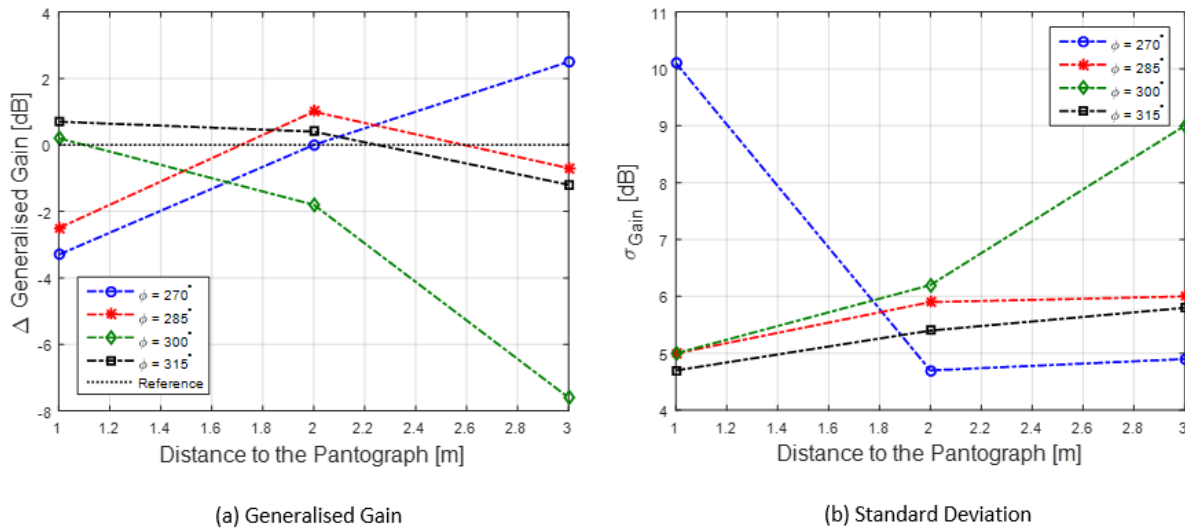(a) Generalised Gain

(b) Standard Deviation

Figure 4.13 Comparison between azimuth views at 2.6 GHz at the back of the train.

4.2.4 BBRS

One finally simulated CST, using a BBRS antenna operating at 5.9 GHz. Figure 4.14 presents the results obtained for a distance between the antenna, and the pantograph equals to 1 m. For φ=0°, one observes an improvement in the antenna's performance. The maximum gain is approximately 2 dB above the reference in the scenarios where the catenary is present, and 4.25 dB above when there is only the pantograph. However, in the R+C+P scenario, the antenna is pointing in the 70° direction, while in R+C is pointing upwards. This, along with an $α_{3dB}$ below the reference, means that the antenna has a more directive behaviour, losing an omnidirectional performance. As explained before, this may not be a significant issue since, in this case, the train is very close to the BS, so there would be performance problems. For φ=90°, the gain decreases, being slightly above the reference for R+P and R+C+P scenarios, whereas for R+C it is 0.75 dB below. This means that the antenna is so close to the pantograph, virtually underneath it, so there is not as much reflection of the EM waves in that

perspective. In terms of the direction of maximum, the presence of the pantograph prevails over the one of the catenary, being 8°, which means that it is pointing up. This is a real issue, since this perspective is critical when the train is between two BSs, so when the direction of maximum is up, the antenna is not directed to the BSs on the terrain, especially with this technology, where the BSs are about 1 km apart. The most common interval for the elevation angle would be from 60° to 90°, so this would result in severe link problems. For φ=270°, one observes that the performance of the antenna improves comparatively to the reference in all the scenarios, particularly the R+C+P scenario, where the gain magnitude increases 2.66 dB. Also, the direction of the maximum is very close to the reference, from 13° to 30°, along with a low α$_{3dB}$, so the antenna is very directive, and has its maximum pointing up. However, this case is not very realistic because the scenario that was used to run the simulation has the pantograph on the edge of the car, so the reflections of the EM waves in the rooftop are not considered. Also, the proximity of the antenna is not realistic.

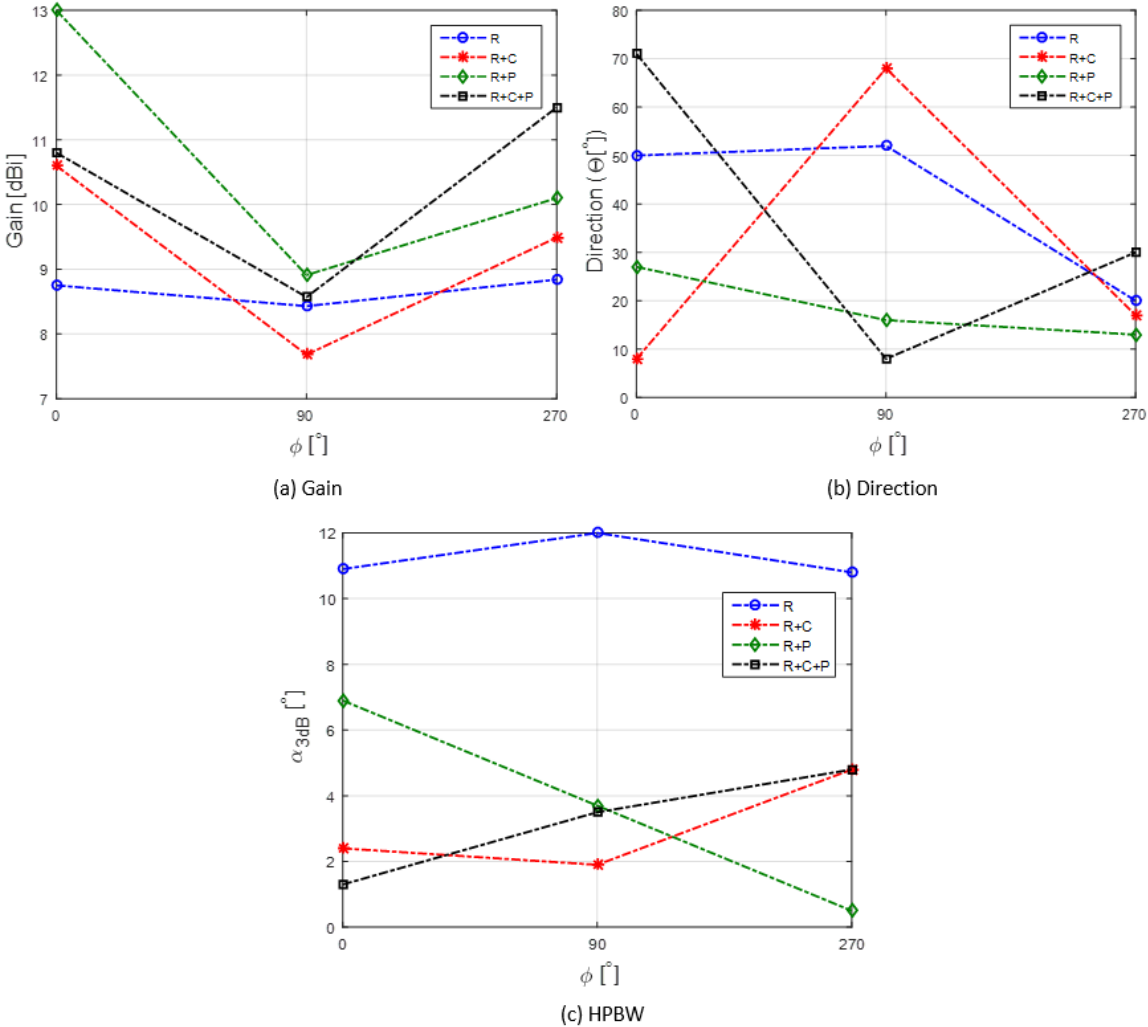(a) Gain

(b) Direction

(c) HPBW

Figure 4.14 Comparison between the four scenarios performance at 5.9 GHz.

Regarding the variation of the generalised gain and its standard variation, one presents the results for the front and back part of the train in Figure 4.15 and Figure 4.16, respectively. One observes that in both figures, the results for d_pant=0.5m and d_pant=1.25m are similar, so the behaviour of the antenna

is the same when it is very close to the pantograph and outside of the 20λ boundary. This supports the fact that at a certain distance, the presence of the pantograph is no longer felt by the antenna. For the front part of the train, when φ=45° and φ=60°, the generalised gain is about 2.5 dB above the reference, but when φ=75° and φ=90°, it is between 5-6 dB below, so the performance of the antenna is significantly damaged in the presence of the catenary and the pantograph, since these angles are significant when the trains are between BSs. As expected, one observes that for d_pant equals to 1 m, the value of the generalised gain tends to the reference, since the antenna is almost at the limit of 20λ, and the reflected EM waves almost do not affect the antenna's behaviour.
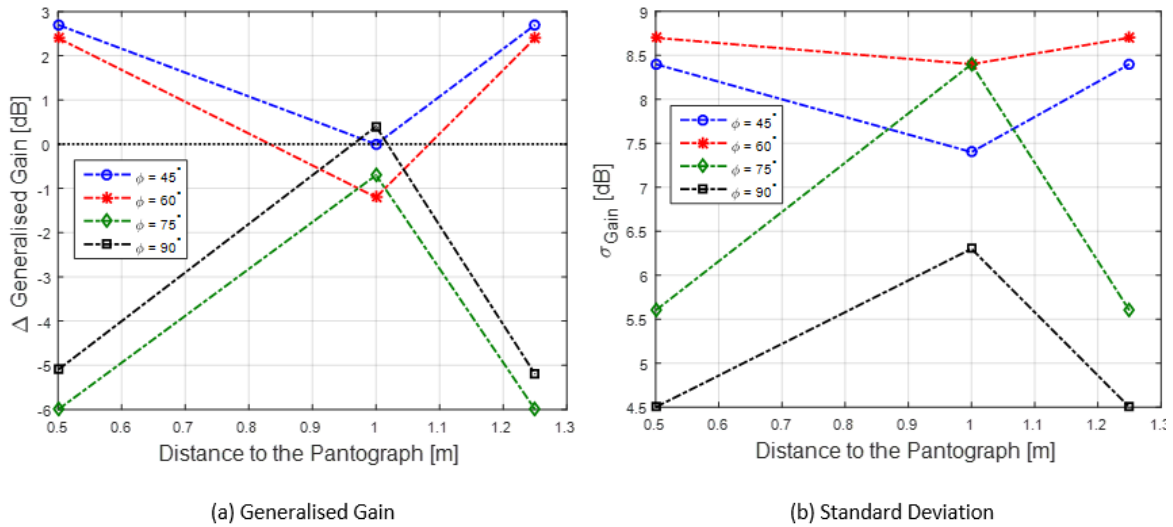

(a) Generalised Gain   (b) Standard Deviation

Figure 4.15 Comparison between azimuth views at 5.9 GHz at the front of the train.

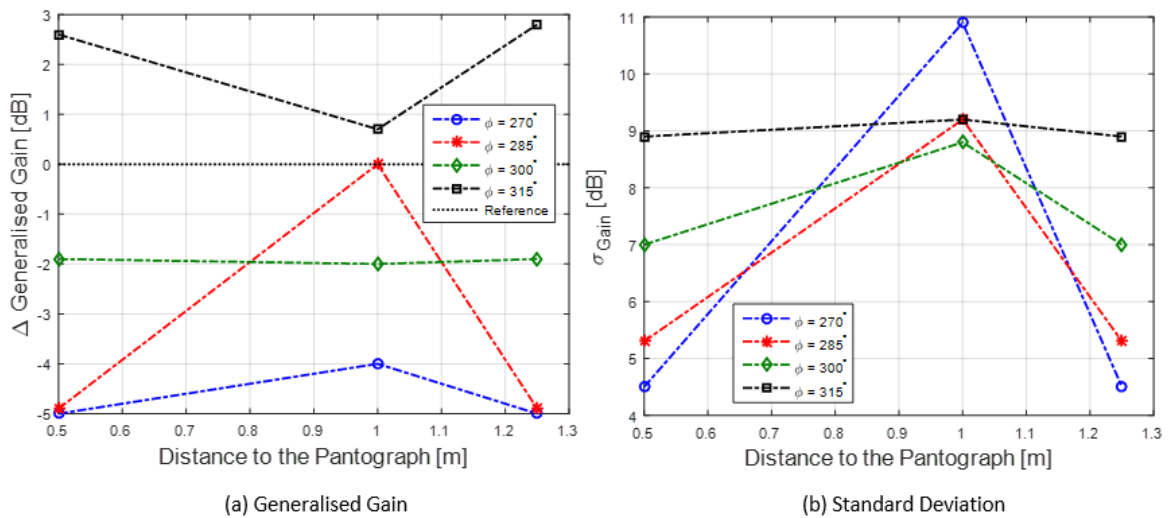(a) Generalised Gain   (b) Standard Deviation

Figure 4.16 Comparison between azimuth views at 5.9 GHz at the back of the train.

At the back part of the car, where the pantograph is placed, for d_pant=0.5 m and d_pant=1.25 m, one observes that for all the azimuth angles, apart from φ=315°, the generalised gain is at or below the reference, along with a high σ_{Gain}. This means that the antenna is very directive and that is affected by the catenary. For d_pant equals to 1 m, one observes an improvement in the generalised gain for

φ=270° and φ=285°, so the pantograph is reflecting EM waves in these directions. Once again, this could lead to severe communications problems, due to the reason presented before, but the probability of this scenario being deployed is very slim.

4.3 EMI Analysis

In this section, an analysis regarding the EMI is performed to determine how the harmonics originated by the catenary signal affect the communication systems. The interference provided by the catenary is considered to be noise, since no information is being transmitted. The results obtained for Signal-to-Noise-plus-Interference-ratio are presented in Figure 4.17.

(a) d_sup_cat=2.8m

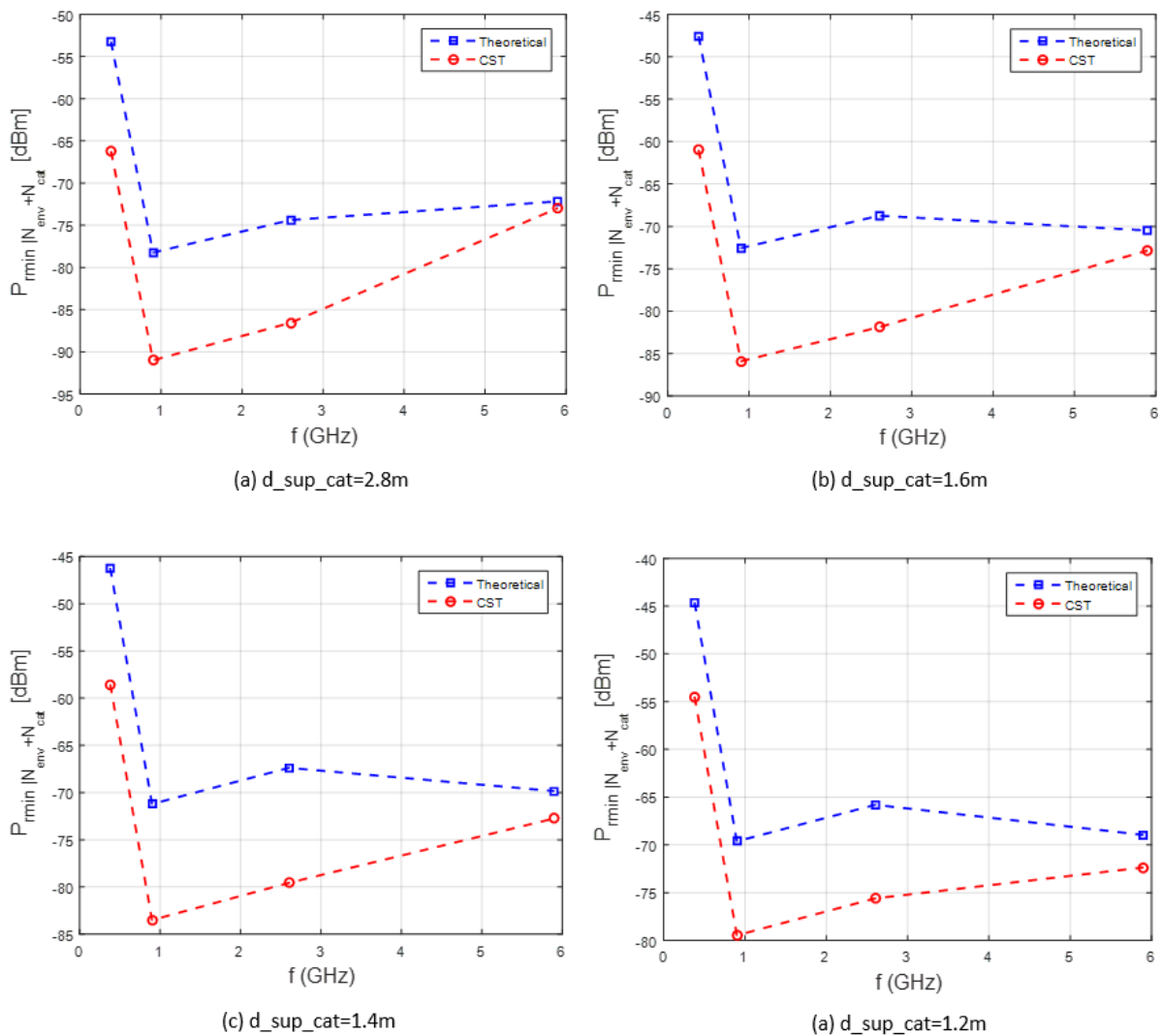(b) d_sup_cat=1.6m

(c) d_sup_cat=1.4m

(a) d_sup_cat=1.2m

Figure 4.17 Minimum Receiving Signal Power.

One observes that when the catenary is closer to the train's rooftop, SNIR increases. This is expected since the electric field has a larger magnitude when closer to the catenary, which means that N_{cat} is

highest. One also observed that the values of the $P_{min|Ncat+Nenv}$ are significantly higher than the sensitivity for each system, so the noise from the harmonics is high. This is expected, since the signal in the catenary is in the order of kV, so the resulting electric field is also high. Only the BBRS system has a value close to the sensitivity (-73 dBm) The values for the intermediate steps and the values for these parameters are available in Annex C. This means that the catenary presents a significant factor in railway communications, which may lead to low QoS or even failures in railway operations. One also must consider that these values are valid for the assumptions made in Chapter 3, where the amplitude of the harmonics decreases with a 1/*n* factor, where *n* corresponds to the harmonic order, which may not correspond to reality. The values for the intermediate parameters are given in Annex B.2.

One also analysed the difference in the minimum Receiving Signal power for two sensitivity values in BBRS, according to the correspondent data rate. The results are presented in Table 4.5. One observes that for higher data rates, meaning lower sensitivity, the minimum $P_{min|Ncat+Nenv}$ is also lower. For a data rate of 6 Mbps, the $P_{min|Ncat+Nenv}$ is rounding -86 dBm to -90 dBm, whereas for 54 Mbps it is between -69 dBm and -73 dBm. For a distance between the train rooftop and the catenary of 1.6 m or 2.8 m, the minimum Receiving Signal Power is equal to the sensitivity, so the noise from the catenary is not high enough in this case.

Table 4.5 Minimum Receiving Signal Power for BBRS system.

Data rate [Mbps]	$P_{min\ [dBm]}$		d_sup_cat [m]			
			2.8	1.6	1.4	1.2
6	-90	Theoretical	-89	-87	-87	-86
		CST	-90	-90	-89	-89
54	-73	Theoretical	-72	-70	-70	-69
		CST	-73	-73	-72	-72

.

Chapter 5

Conclusions

This chapter summarises the work developed in this thesis and presents the main conclusions, as well as suggestions for future work.

The main goal of this thesis was to assess the influence of the pantograph and the catenary in the performance of the antennas for railway communication systems, as well as the impact of the harmonics prevenient from the catenary. To achieve these objectives, a model that representes this scenario was developed and implemented using CST for EM simulations, were several simulations where ran. Also, the MATLAB tool was used for all the numerical analysis. The results obtained from these simulations allowed to perform a thorough analysis of the effect of both catenary and pantograph.

This thesis starts in Chapter 1, where an overview is given of mobile communications in railway scenarios and their evolution until recent times, as well as an explanation of the demand in terms of services. This is followed by a brief description of the railway market, as well as its future perspectives. The motivation for this work is also presented in this section, and it also concludes with a description of the chapters of this thesis.

Regarding Chapter 2, a description of relevant theoretical aspects is provided. An overview of the railway communication systems (TETRA, GSM-R, LTE-R, and BBRS) is presented, focusing on the network architecture, radio interference and the services they can provide. Also, a comparison between GSM-R and LTE-R is made, as well as possible future railway services. Then, the requirements and the scenarios for railway communications are also presented. Afterward, the relevant antenna's parameters necessary for antenna assessment are described, as well as the different types of antenna technologies. It also contains a brief description of the software that was used for modelling and simulating – CST Microwave Studio. Finally, this chapter is completed with state of the art, where an analysis of the most relevant works regarding the topic of this thesis is presented.

In Chapter 3, one presents the model overview, which describes the inputs and output parameters considered in the model to obtain the final results. To implement these parameters, one used an antenna that had already been developed by André Ribeiro [Ribe18], and used CST tool to ran the simulations, and then MATLAB, to obtain the parameters necessary to assess the antenna's behaviour: radiation pattern, α_{3dB}, reflection coefficient, electrical field and the power of the harmonics plus the SNIR. This is followed by a description of the theoretical approach. One starts with a section regarding the antennas' analysis, presenting the image theory and the implications of using vertical dipoles. Then the EMI theoretical approach is presented, where one explains how the catenary is considered a conductor above a flat plan perfect conductor, followed by the expressions that are used in MATLAB. An explanation regarding the CST tool is also offered, mentioning the main features to be informed about. Afterwards, one presents the antennas performance, for the four types of systems, providing the physical dimensions for each antenna and presenting the results obtained in CST. A brief description of the model is offered next. To conclude this chapter, one shows a section where the assessment of the developed model is made.

Chapter 4 starts with a thorough scenario description for both studies, the antenna analysis, and the EMI analysis. Regarding the first study, one presents de dimensions of the train rooftop/pantograph/catenary system, along with the values for these physical dimensions, and also the

distances between the antenna and the pantograph that were considered. Afterward, a brief description of the standard BSs placement, followed by some critical perspectives to understand the antenna's behaviours in this scenario. The four scenarios used in this first study are then presented, along with the essential angles of azimuth that one analysed to understand the pantograph and catenary's influence on the antenna. The dimensions for the train rooftop are not the same for the different technologies due to the issues regarding simulation time. Since higher frequencies mean a lower wavelength, there are more variations, which leads to more calculations in CST, taking more time to simulate. So, one has decided that the train rooftop length varies with the technology, being lower for higher frequencies. In total, CST was run 48 times, and each simulation took from 30 minutes to 36 hours. Regarding the second study, one presents the corresponding values for the physical parameters, along with the values for the noise figure, carrier bandwidth and sensitivity for each technology. Four simulations were run, taking less than 30 s each.

In the second section, one presents the results for the first study, the antenna analysis. For each technology, three distances between the antenna and the pantograph were chosen. Two of them are inside the 20λ radius from the antenna, and the other one is immediately outside. This is so that it can be possible to analyse how the behaviour of the antenna varies with the distance to the pantograph, using the theoretical limit of influence (20λ). This study can be divided into two parts, the analysis of the results for a determine distance to the pantograph inside of the 20λ radius, and the analysis of the results for the R+C+P scenario with the variation of the distance to the pantograph. The first part aims to analyse the three azimuth perspectives, the lateral view ($\varphi=0°$), the front view ($\varphi=90°$), and the back view ($\varphi=270°$). One has chosen these because of the symmetry of the scenario and the presence of the pantograph. In the second part, eight azimuth angles are analysed: for the front part of the train $\varphi = 45°$, $\varphi = 60°$, $\varphi = 75°$, $\varphi = 90°$, and for the back part of the train $\varphi = 270°$, $\varphi = 285°$, $\varphi = 300°$ and $\varphi = 315$. These perspectives allow us to assess the potential problems in the link when the train is moving away or getting closer to a BS.

For TETRA, one ran 12 simulations, changing both the distance to the pantograph (16 m, 10 m, and 5 m) and the scenario (R, R+C, R+P, R+C+P). In the first part of the antenna analysis, one has chosen to present the results of when the antenna is 10 m from the pantograph. For each azimuth view, four parameters were analysed: the maximum gain, its direction (θ) and the half-power beamwidth. For $\varphi = 0°$, one observes that the behaviour of the antenna is very similar in all four scenarios, having a slight increase in the gain and α_{3dB}. The direction of maximum decreases 8-11° relatively to the reference scenario. However, these changes may not constitute a problem, since this view implies that the BS is right beside the train, where its power is very high, so there are no issues in the communication. For $\varphi = 90°$, the opposite direction from the pantograph, one observes an improvement in the antenna's performance, so the EM wave is being directed in this direction, which increases the gain. However, this increase is accompanied by the decrease of α_{3dB}, so the antenna loses the omnidirectional behaviour, which can lead to communication problems, particularly in irregular terrain. Finally, for $\varphi = 270°$, one observes that, in the R+C+P scenario, the directivity of the antenna increases, and in the R+P scenario, the gain is below the reference. This means that the majority of the EM waves are being reflected in

another direction, which could bring communication problems with a BS that is behind the train.

So, generally, one can say that the behaviour of the antenna is affected negatively by the pantograph and catenary's structures, since there is a significant loss of the omnidirectional behaviour and a decrease in the antenna's performance in the more critical angles.

For the second part of the antenna analysis, one observes that when the antenna is 5 m and 10 m from the pantograph, there is an improvement in the generalised gain for φ=75° and φ=90°, along with a high standard deviation, so the pantograph reflects the EM waves in the direction of the front part of the car, so the antenna no longer performs as an omnidirectional antenna. When the antenna is outside of the 20λ limit, the generalised gain decreases significantly, so the antenna no longer is under the effect of the pantograph.

For GSM-R, one ran the simulations for d_pant equals to 7 m, 4 m, and 1 m. For the first part of this study, the results for a distance between the antenna and the pantograph of 4 m were chosen. For φ=0°, one observes that the maximum gain increases 7 dB to 9 dB compared to the reference, so the presence of the structures improves significantly the antenna performance, which could lead to interference issues. Also, for the scenarios with a catenary, α_{3dB} is lower than the reference, so this structure is responsible for the increase of the antenna's directivity. For φ=90°, one observes that in the R+P scenario, the maximum gain decreases, so the pantograph increases the dispersion of the EM waves. For the scenarios with catenary, it improves, so the catenary has a more significant influence in the antenna's behaviour than the pantograph. For φ=270°, the back view, one observes that in the R+P scenario, the maximum gain is equal to the reference, so this structure is reflecting the EM waves to the sides, which brings problems in the communication when the train is between BSs. For the second part of this study, once again one observes that for φ=75° and φ=90° within 20λ boundary, the generalised gain increases compared with the reference, and it remains above the reference for φ=90° when the antenna is outside the limit radius. So, the pantograph is reflecting in the direction of the train movement.

For LTE-R, the results presented are the ones where the distance d_pant is 2 m. One found that for this system, in the φ=0° perspective, the gain increases about 2 dB, and α_{3dB} was lower, so the pantograph and the catenary reflect the EM wave in such a way that the antenna has a more directive behaviour, which could lead to interference issues. One also observed that for both φ=90° and φ=270°, the gain is below the reference for all scenarios, so one concludes that the antenna is too close to the pantograph, almost under it, which results in the EM waves being reflected the sides. This results in severe communication problems for situations when the train is between BSs, where these perspectives have an important role, since the BSs are either behind the train or in front of the train. Also, there may be interference issues regarding the sides of the train. However, the proximity to the antenna is not realistic in terms of the antenna's deployment, so these issues would not occur. Regarding the second part of this study, the variation of the generalised gain, one observes for the perspectives at the front of the train, the generalised gain is for the most part below the reference for all distances (even outside the 20λ radius), so the catenary is damaging the antenna's performance. For the back part of the train, one observes that when the antenna is closer to the pantograph, the generalised gain for φ=270° and

φ=285°, it is below the reference, so the antenna is too close to the pantograph, and the EM waves are being reflected to the sides, affecting the communication when the train is moving away from the BS.

The final antenna that one tested was the BBRS antenna, and one has chosen to present the results for d_pant equals to 1 m. For φ=0°, one observes a significant improvement in the antenna's performance, so the pantograph and catenary are reflecting the EM waves for the sides of the train, which can result in interference issues. For φ=90°, the gain is very close to the reference, which means that the antenna is practically below the pantograph, and it does not have an effect on the antenna's performance. For φ=270°, one observes that the gain increases and α_{3dB} decreases, so the antenna's directivity increases in this direction, which may or not be beneficial, depending on the terrain and placement of the BSs. Regarding the variation of the generalised gain, one observes that the results for d_pant=0.5 m and d_pant=1.25 m are similar, so when the antenna is too close to the pantograph or outside the 20λ radius, the antenna behaves in the same way, as if the pantograph was not there. For φ=75° and φ=90°, the generalised gain is between 5 dB to 6 dB below the reference, so one concludes that the catenary is responsible for damaging the antenna's performance. As explained before, this could bring communication problems when the train is between BSs. For d_pant=1 m, almost 20λ from the antenna, one observes that the gain tends to the reference. In the back part of the train, one observes that for d_pant=0.5 m and d_pant=1.25 m, in all the azimuth angles, apart from φ=315°, the generalised gain is at or below the reference, so the catenary affect the antenna. When d_pant=1 m, the generalised gain improves, so the antenna is being affects by the pantograph, presenting a more directive behaviour. Once again, this scenario is not very realistic since the antenna is too close to the pantograph.

One ends this section presenting the results for the second study, the EMI analysis. One observes that as the catenary is closer to the train rooftop, the power prevenient from it is higher, which results in a higher minimum Signal-to-Noise-plus-Interference-ratio, where one considers both the environmental noise as well as the interference from the catenary, or noise because nothing is being transmitted. The values obtained are significantly above the sensitivity for TETRA, GSM-R and LTE-R systems, so the noise from the catenary is significant. For BBRS, one observes that for higher data rates, therefore higher sensitivity, the minimum SNIR is also lower. For certain distances between the antenna and the catenary, 1.6 m, and 2.8 m, SNIR is equal to the sensitivity, so the noise from the catenary is not substantial compared with the noise from the environment.

Regarding future work, this thesis can be complemented with the assessment of more precisely the effect that the pantograph and the catenary have on the antenna's performance and in railway communications. First, the model used in CST is much simplified compared with the real scenario, so there may be problems that are not being considered. Also, it is common that the contact between the pantograph and the catenary is not constant, resulting in energy peaks that may momentarily affect railway communications. This issue is aggravated in Northern Europe, where the presence of ice in the catenary makes the occurrence of these energy peaks more common, affecting operations and decreasing the quality of service. Finally, this study could be accompanied with real measurements to compare.

Annex A

Theoretical Performance

In this annex, one presents the parameters of each technology, as well as the mesh cells view in CST, the S_{11}, and the 2D and 3D gain pattern for each system (TETRA, GSM-R, LTE-R and BBRS).

A.1 Antenna Parameters

Table A.1 Systems and services parameters (adapted from [AAAl09], [FrFC17], [HAWG16], [Thal17]).

Parameter	TETRA	GSM-R	LTE-R	BBRS
Frequency	UL: 380-390, 410-420, 450-460 MHz DL: 390-400, 420-430, 460-470 MHz	UL: 876-880 MHz DL: 921-925 MHz	450 MHz, 800 MHz, 1.4 GHz, 1.8 GHz, 2.6 GHz	2.4 GHz, 5.1-5.9 GHz
Channel bandwidth	25 kHz	200 kHz	1.4-20 MHz	20 MHz or 40 MHz
Modulation	DQPSK	GMSK	QPSK, 16-QAM and 64-QAM	BPSK, QPSK, 16-QAM and 64-QAM
Multiple Access	TDMA	TDMA	OFDMA, SCFDMA	OFDM
Peak data rate	28.8 kbps	172 kbps	DL: 50 Mbps, UL: 10 Mbps	65 Mbps - 135 Mbps
Peak spectral efficiency	-	0.33 bps/Hz	2.55 bps/Hz	-
Cell range	-	8 km	4-12 km	1 km
Cell configuration	-	Single sector	Single sector	-
Data transmission	-	Requires voice call connection	Packet switching, UDP data	-
MIMO	No	No	2×2	2×2
All-IP in native mode	-	Not standalone	Yes	-
Mobility	Max. 200 km/h	Max. 500 km/h	Max. 500 km/h	Max. 250 km/h
Handover success rate	≥ 99.5%	≥ 99.5%	≥ 99.9%	--
Handover procedure	-	Hard	Soft: no data loss	-
Maturity	Mature	Mature	Emerging	-
Market Support	Standardised	Until 2025-2030	Building standards	-

A.1.1 TETRA
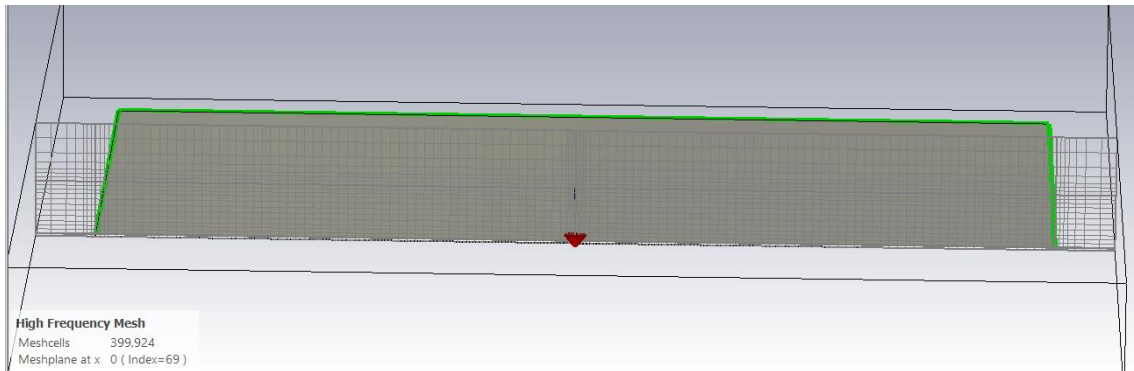
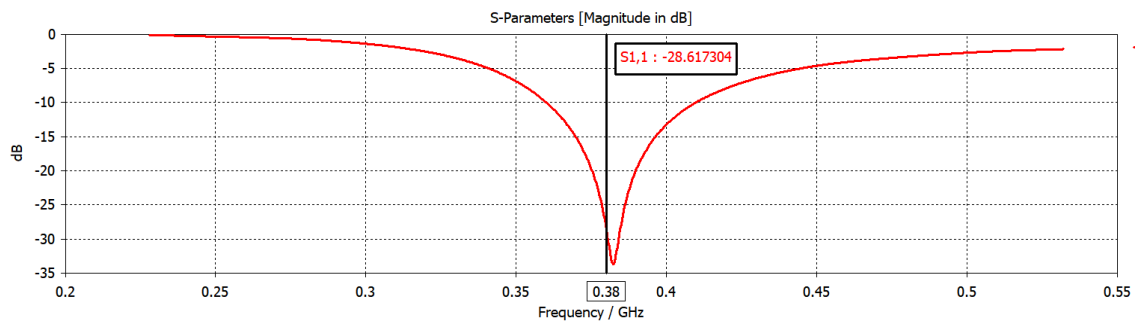Figure A.1 Mesh view of a $\lambda/4$ monopole operating at 380 MHz

Figure A.2 S$_{11}$ parameter of the $\lambda/4$ monopole operating at 380 MHz
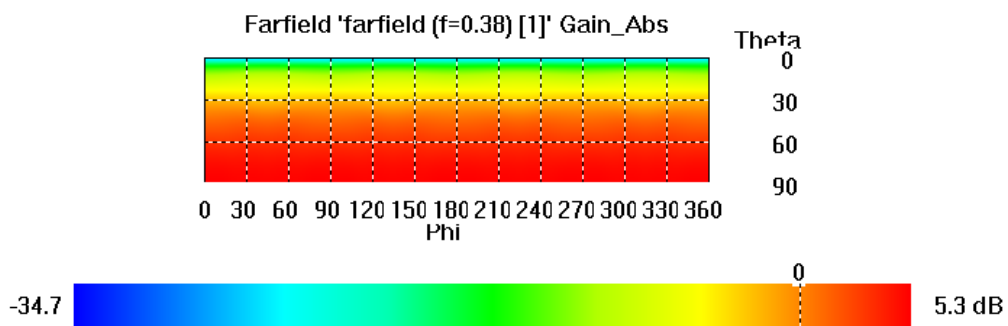

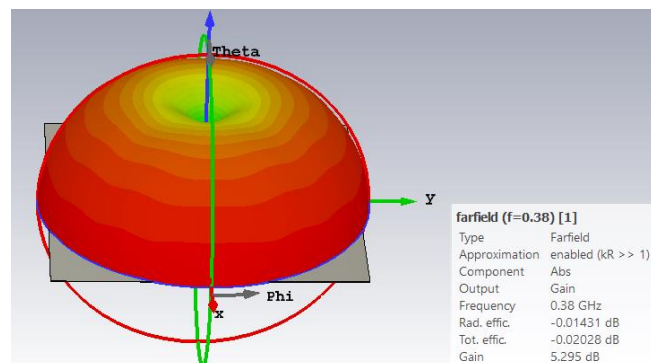Figure A.3 Theoretical 2D performance for the $\lambda/4$ monopole operating at 380 MHz

Figure A.4 Theoretical 3D performance for the $\lambda/4$ monopole operating at 380 MHz
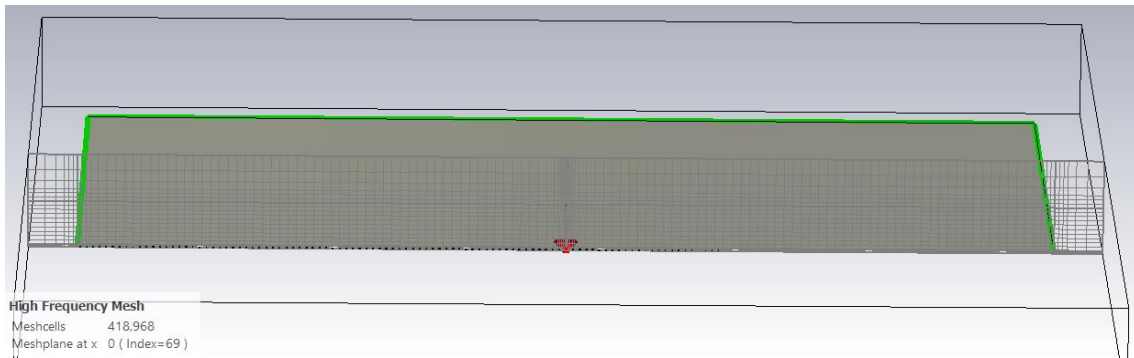
A.1.2 GSM-R

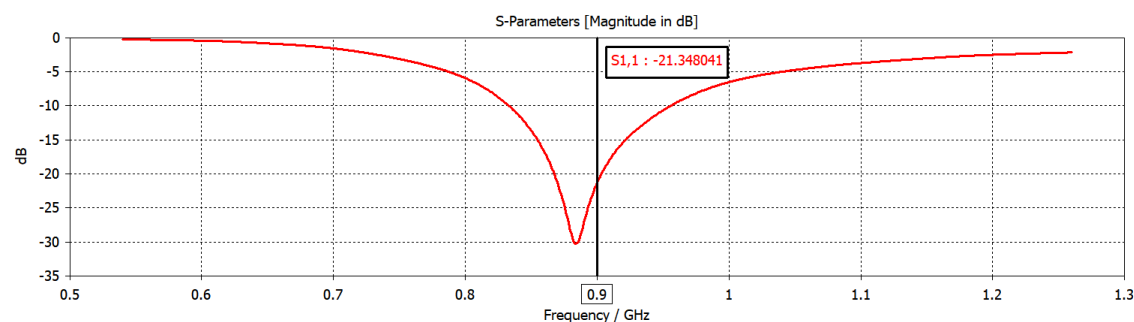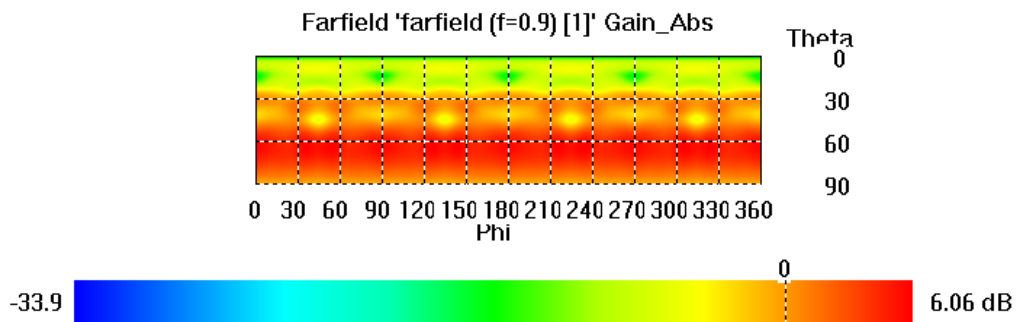Figure A.5 Mesh view of a $\lambda/4$ monopole operating at 900 MHz

Figure A.6 S_{11} parameter of the $\lambda/4$ monopole operating at 900 MHz

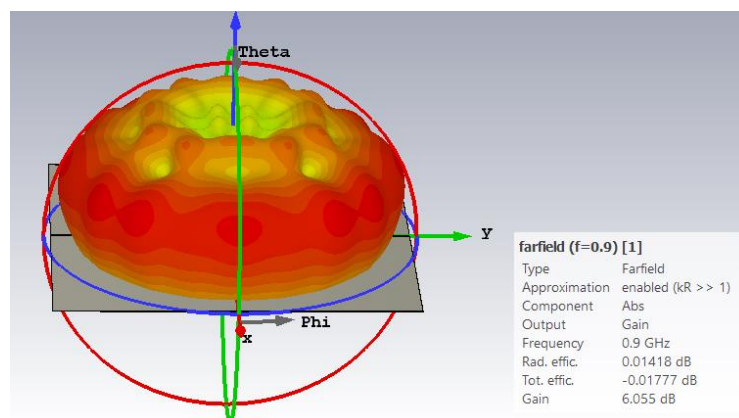Figure A.7 Theoretical 2D performance for the $\lambda/4$ monopole operating at 900 MHz

Figure A.8 Theoretical 3D performance for the $\lambda/4$ monopole operating at 900 MHz
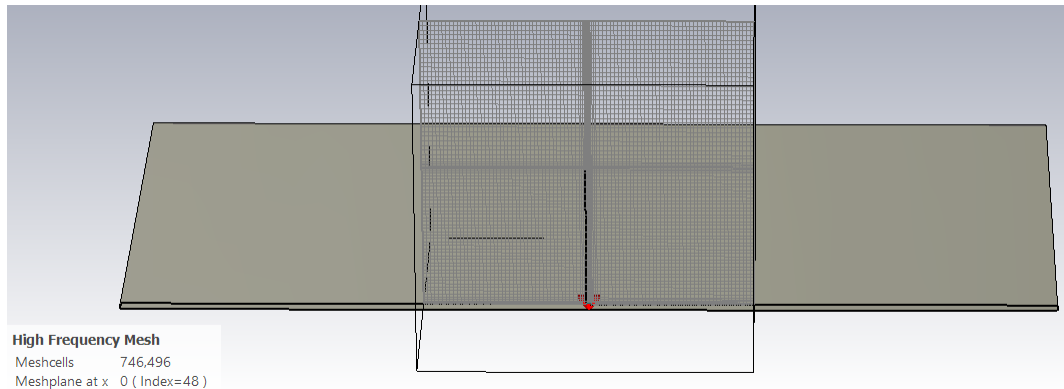
A.1.3 LTE-R

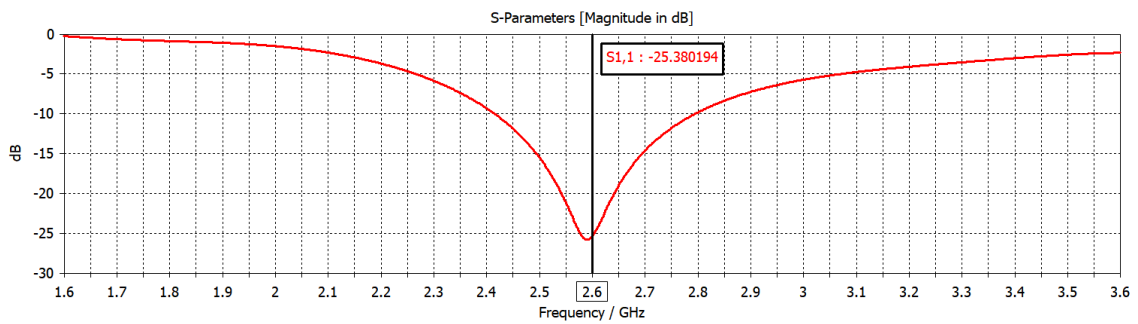Figure A.9 Mesh view of a $\lambda/4$ monopole operating at 2.6 GHz

Figure A.10 S$_{11}$ parameter of the $\lambda/4$ monopole operating at 2.6 GHz
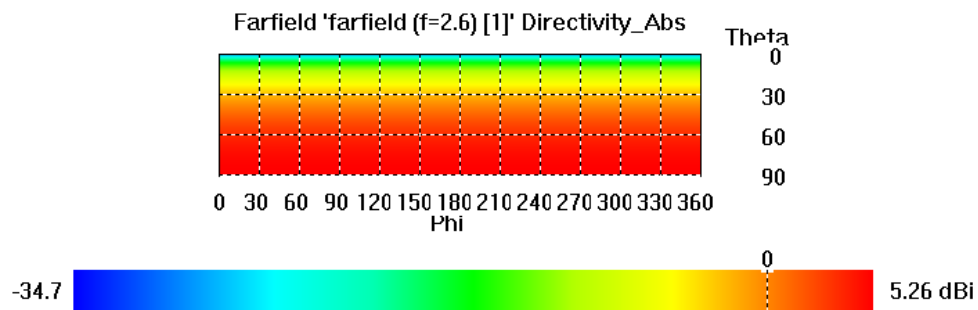

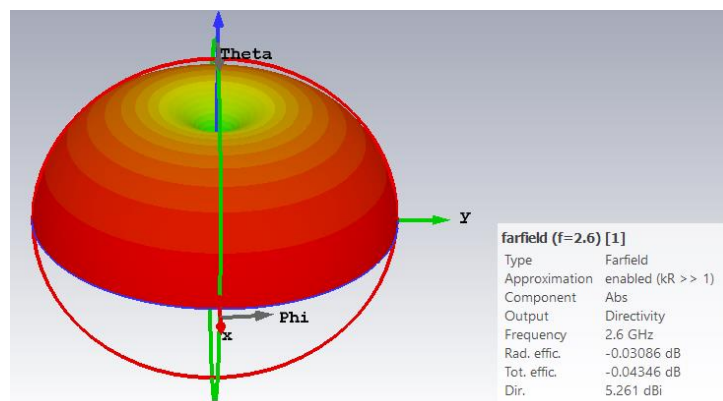Figure A.11 Theoretical 2D performance for the $\lambda/4$ monopole operating at 2.6 GHz

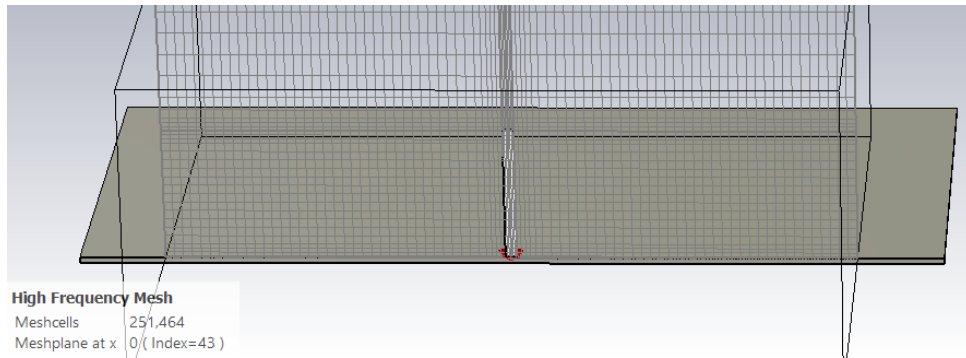Figure A.12 Theoretical 3D performance for the $\lambda/4$ monopole operating at 2.6 GHz

A.1.4 BBRS

Figure A.13 Mesh view of a λ/4 monopole operating at 5.9 GHz

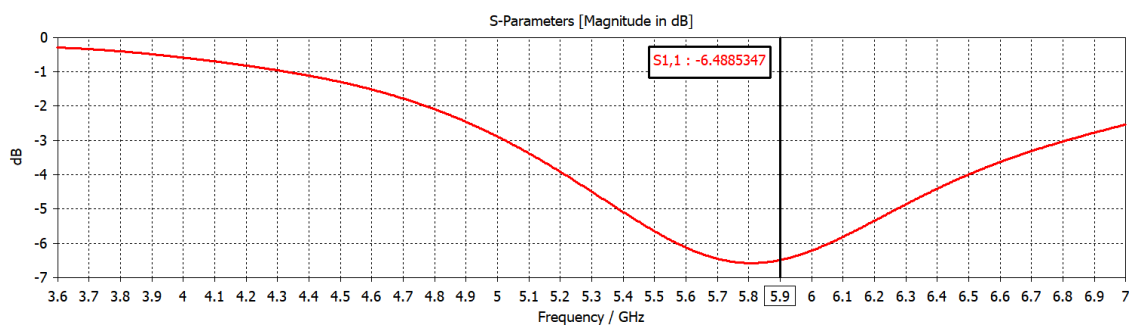

Figure A.14 S₁₁ parameter of the λ/4 monopole operating at 5.9 GHz
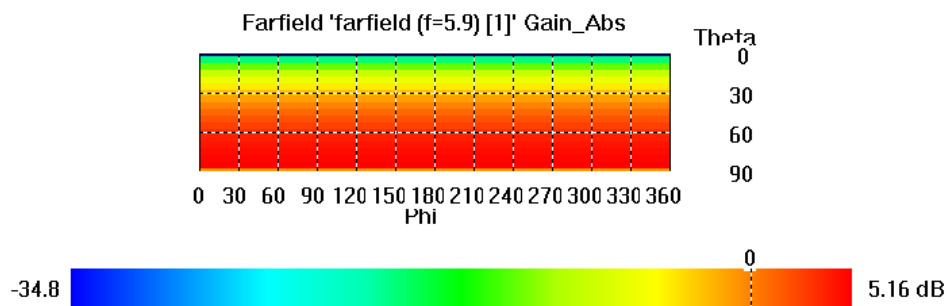
Figure A.15 Theoretical 2D performance for the λ/4 monopole operating at 5.9 GHz
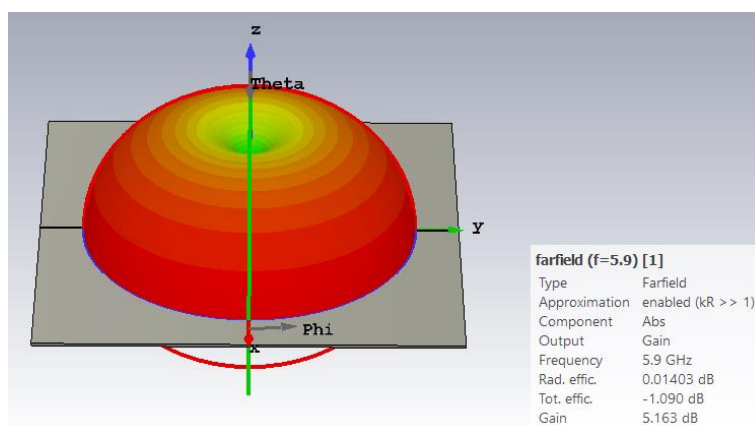

Figure A.16 Theoretical 3D performance for the λ/4 monopole operating at 5.9 GHz

Annex B

Pantograph/Catenary Performance

This annex presents the results regarding the antenna analysis, where the 2D gain pattern, as well as the values for the direction of maximum gain, direction, HPBW and L_{SSL} values for each technology, in the four scenarios.

B.1   Antenna Analysis

B.1.1 TETRA

Figure B.17 2D far-field view of a $\lambda/4$ monopole operating at 380 MHz with d_pant = 16m

Table B.1 Comparison between scenarios for d_pant = 16m

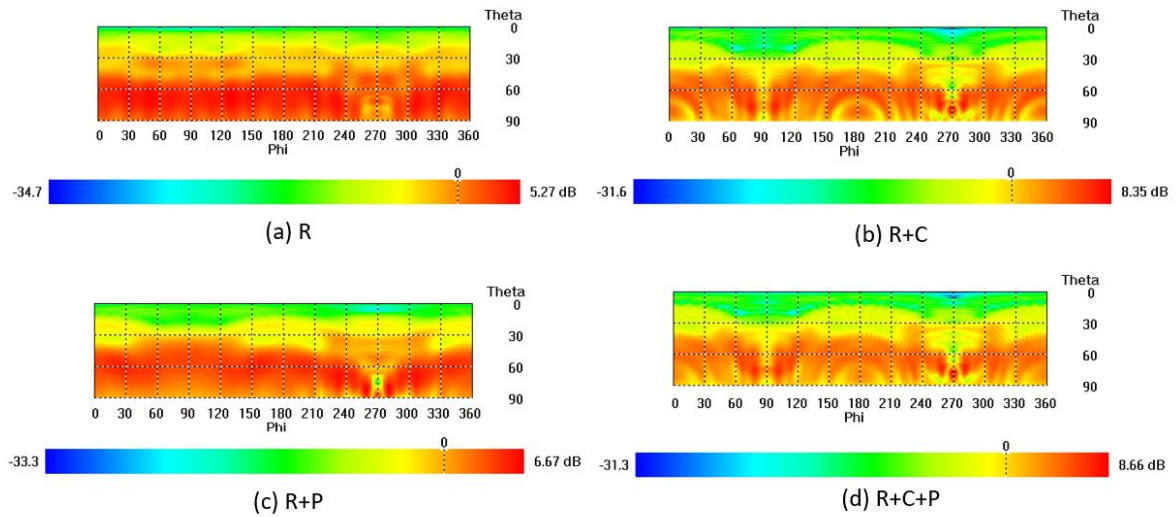| Scenario		Gain [dBi]	Direction (θ[°]).	α_{3dB} [°]	L_{SLL} [dB]
R	φ=0°	3.89	69	43.4	-6.6
	φ=90°	4.21	71	39.4	-5.7
	φ=270°	2.77	72	31.9	-2.2
R+C	φ=0°	5.35	61	23.2	-1.0
	φ=90°	1.91	73	25.9	-3.7
	φ=270°	8.35	78	8.5	-5.2
R+P	φ=0°	4.33	58	42	-7.3
	φ=90°	4.4	55	41.2	-10.0
	φ=270°	4.93	89	10.6	-2.8
R+C+P	φ=0°	4.78	61	42.1	-7.2
	φ=90°	3.99	75	11.5	-3.7
	φ=270°	8.66	78	10.3	-7.9

Figure B.2 2D far-field view of a $\lambda/4$ monopole operating at 380 MHz with d_pant = 10m

TableB.2 Comparison between scenarios for d_pant = 10m

Scenario		Gain [dBi]	Direction (θ[°]).	α_{3dB} [°]	L_{SLL} [dB]
R	φ=0°	3.93	69	43.4	-6.7
	φ=90°	4.53	74	13.7	-2.4
	φ=270°	3.42	70	9.5	-0.9
R+C	φ=0°	5.19	61	39.4	-10.1
	φ=90°	10	83	10.9	-9.5
	φ=270°	4.5	79	26.1	-3.9
R+P	φ=0°	4.39	58	43.3	-7.6
	φ=90°	9.23	88	15.3	-6.5
	φ=270°	2.75	52	24.0	-1.1
R+C+P	φ=0°	4.24	61	48.6	-7.1
	φ=90°	9.71	83	10.7	-8.4
	φ=270°	8.56	83	12.8	-8.6

B.1.2 GSM-R

(a) R

(b) R+C

(c) R+P

(d) R+C+P
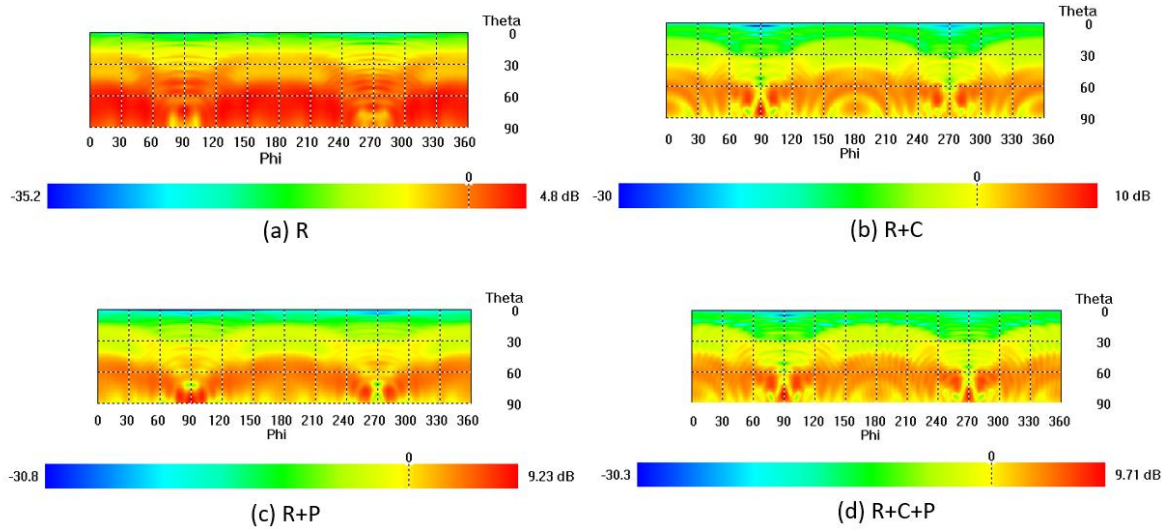
Figure B.3 2D far-field view of a $\lambda/4$ monopole operating at 900 MHz with d_pant = 7m

Table B.3 Comparison between scenarios for d_pant = 7m

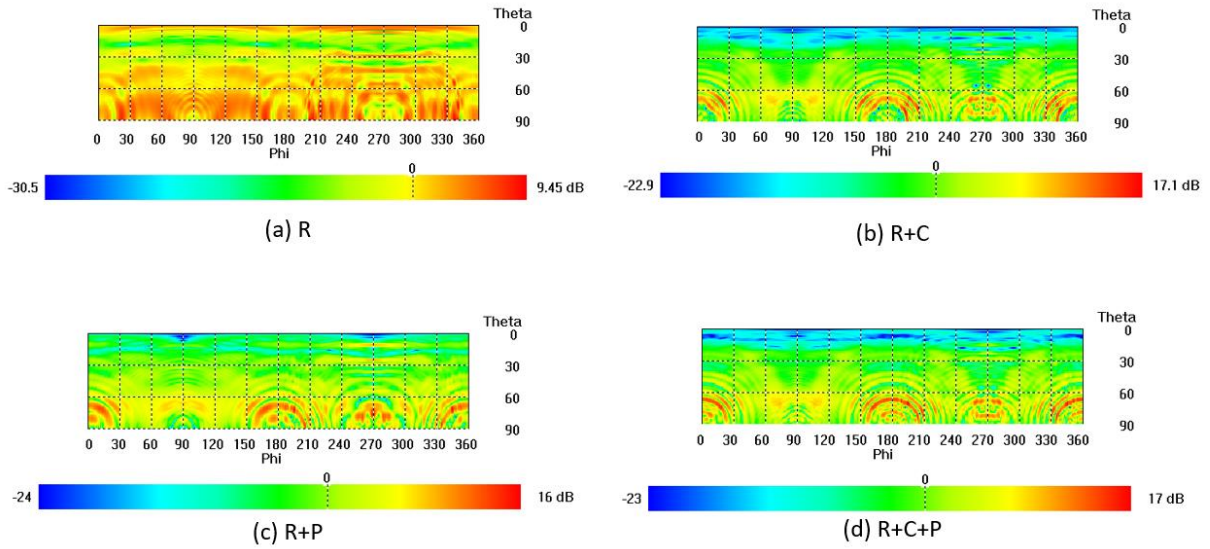| Scenario		Gain [dBi]	Direction (θ[°]).	α_{3dB} [°]	L_{SLL} [dB]
R	φ=0°	3.72	85	18.2	-1.2
	φ=90°	5.54	70	5.1	-0.6
	φ=270°	6.29	4	4.9	-1.2
R+C	φ=0°	11.9	69	5.1	-5.2
	φ=90°	8.36	68	3.5	-0.6
	φ=270°	11	77	7.4	-0.8
R+P	φ=0°	10.9	68	6.2	-2.4
	φ=90°	8.33	66	8.1	-0.9
	φ=270°	14.7	77	7.8	-5.6
R+C+P	φ=0°	13.1	66	3.5	-1.9
	φ=90°	10	85	3.1	-0.9
	φ=270°	12.5	83	5.1	-2.3

Figure B.4 2D far-field view of a $\lambda/4$ monopole operating at 900 MHz with d_pant = 4m

Table B.4 Comparison between scenarios for d_pant = 4m

Scenario		Gain [dBi]	Direction (θ[°]).	α_{3dB} [°]	L_{SLL} [dB]
R	φ=0°	4.3	4	6.1	-0.5
	φ=90°	7.36	3	3.8	-0.9
	φ=270°	9.09	4	3.1	-0.9
R+C	φ=0°	11.7	68	5.0	-5.9
	φ=90°	14.1	77	3.5	-5.6
	φ=270°	11.9	76	3.1	-3.7
R+P	φ=0°	12.1	69	6.3	-2.4
	φ=90°	9.95	79	6.0	-2.0
	φ=270°	9.01	74	10.1	-1.0
R+C+P	φ=0°	13.1	66	3.6	-2.4
	φ=90°	16.2	78	3.3	-6.5
	φ=270°	12.8	87	4.2	-3.7

B.1.3 LTE-R

(a) R

(b) R+C

(c) R+P

(d) R+C+P

Figure B.5 2D far-field view of a $\lambda/4$ monopole operating at 2.6 GHz with d_pant = 3m

Table B.5 Comparison between scenarios for d_pant = 3m

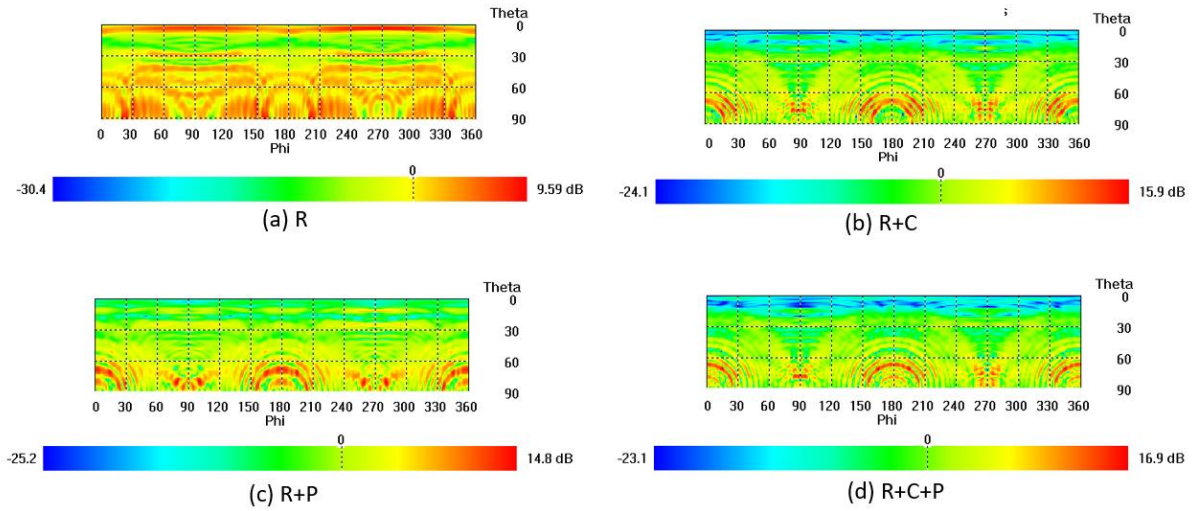| Scenario		Gain [dBi]	Direction (θ[°]).	α_{3dB} [°]	L_{SLL} [dB]
R	φ=0°	9.14	44	12.6	-3.0
	φ=90°	8.89	48	16.1	-0.5
	φ=270°	13.8	43	1.6	-1.2
R+C	φ=0°	13.7	61	1.4	-2.2
	φ=90°	8.45	62	4.7	-1.4
	φ=270°	11.2	28	1.5	-1.1
R+P	φ=0°	11.2	49	9.4	-2.2
	φ=90°	7.1	45	1.4	-0.5
	φ=270°	13.5	28	1.3	-2.3
R+C+P	φ=0°	13.4	60	1.5	-1.3
	φ=90°	8.61	62	4.8	-1.4
	φ=270°	10.3	48	1.3	-1.3

Figure B.6 2D far-field view of a $\lambda/4$ monopole operating at 2.6 GHz with d_pant = 2m

Table B.6 Comparison between scenarios for d_pant = 2m

Scenario		Gain [dBi]	Direction (θ[°]).	α_{3dB} [°]	L_{SLL} [dB]
R	φ=0°	9.14	44	15.8	-2.6
	φ=90°	10.9	49	3.3	-0.7
	φ=270°	12.6	48	2.4	-0.7
R+C	φ=0°	13.4	61	1.3	-1.9
	φ=90°	8.19	62	4.6	-1.3
	φ=270°	11.5	28	1.5	-1.3
R+P	φ=0°	11	49	7.3	-0.9
	φ=90°	9.5	29	0.7	-2.5
	φ=270°	12.5	28	1.6	-1.8
R+C+P	φ=0°	13.3	60	1.5	-0.7
	φ=90°	10.7	62	3.3	-0.8
	φ=270°	8.7	59	0.5	-0.6

B.1.4 BBRS

(a) R

(b) R+C

(c) R+P

(d) R+C+P
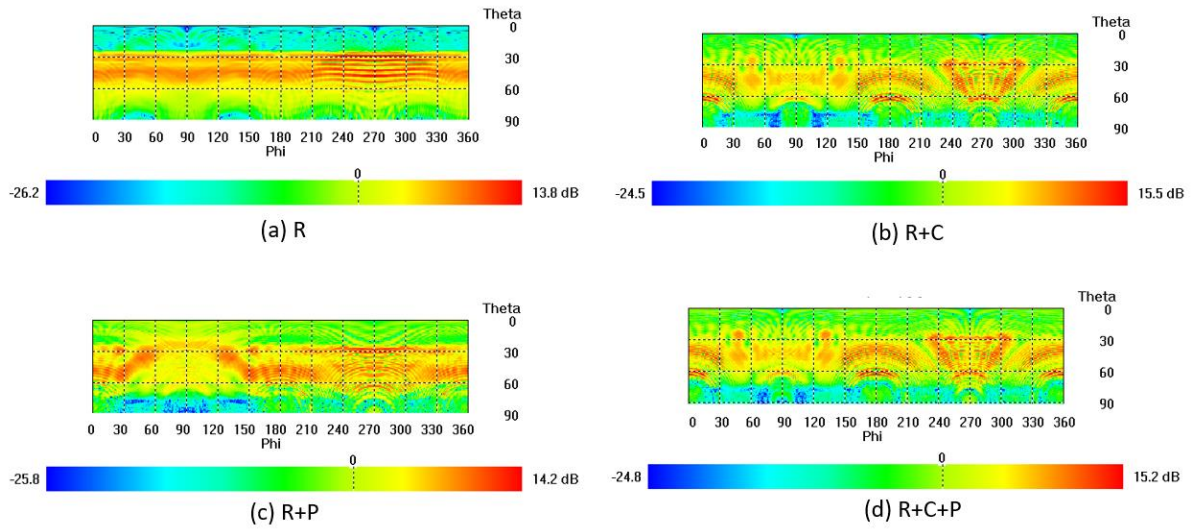
Figure B.7 2D far-field view of a $\lambda/4$ monopole operating at 5.9 GHz with d_pant = 1.25m

Table B.7 Comparison between scenarios for d_pant = 1.25m

Scenario		Gain [dBi]	Direction ($\theta[°]$).	α_{3dB} [°]	L_{SLL} [dB]
R	φ=0°	8.7	50	11.1	-4.3
	φ=90°	8.18	52	13.5	-3.8
	φ=270°	8.79	51	10.3	-4.3
R+C	φ=0°	10.6	9	1.8	-2.2
	φ=90°	8.71	69	1.1	-0.9
	φ=270°	10.5	13	2.5	-2.5
R+P	φ=0°	13.8	26	7.3	-6.5
	φ=90°	7.6	69	1.4	-1.5
	φ=270°	12.6	17	0.6	-3.3
R+C+P	φ=0°	9.24	47	0.7	-1.0
	φ=90°	8.86	25	1.3	-0.8
	φ=270°	10.2	48	2.4	-2.2

(a) R

(b) R+C

(c) R+P

(d) R+C+P

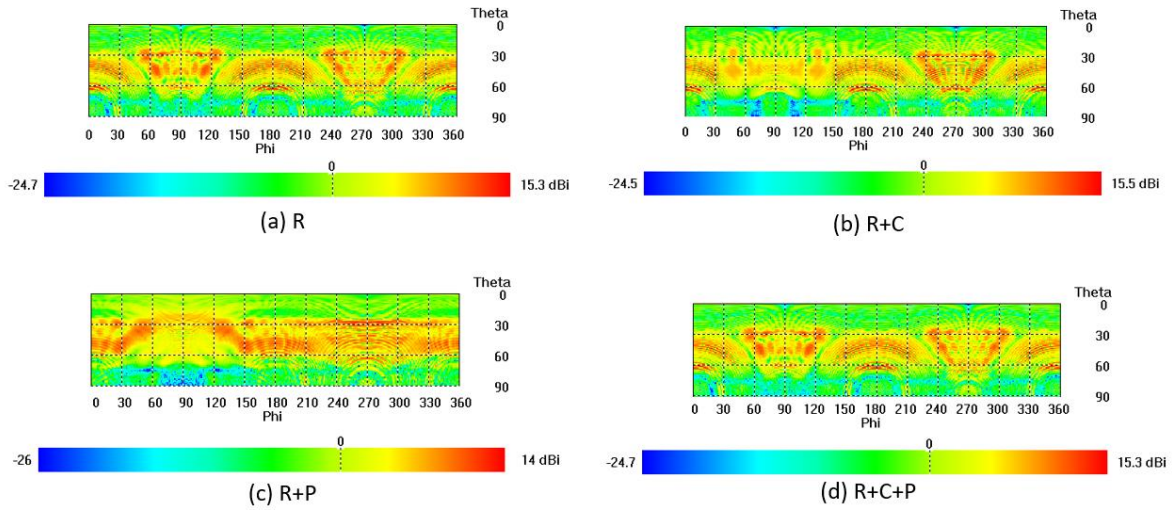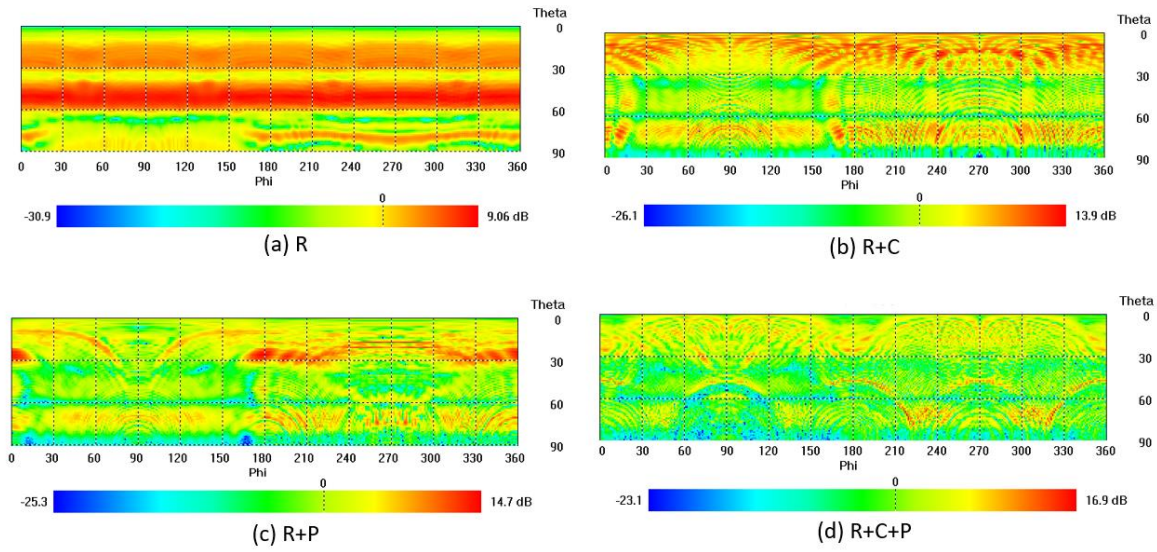Figure B.8 2D far-field view of a λ/4 monopole operating at 5.9 GHz with d_pant = 1m

Table B.8 Comparison between scenarios for d_pant = 1m

Scenario		Gain [dBi]	Direction (θ[°]).	α_{3dB} [°]	L_{SLL} [dB]
R	φ=0°	8.75	50	10.9	-4.2
	φ=90°	8.43	52	12.0	-3.8
	φ=270°	8.84	50	10.8	-4.2
R+C	φ=0°	10.6	8	2.4	-1.1
	φ=90°	7.68	68	1.9	-1.1
	φ=270°	9.49	17	4.8	-2.1
R+P	φ=0°	13	27	6.9	-5.1
	φ=90°	8.91	16	3.7	-0.5
	φ=270°	10.1	13	0.5	-0.6
R+C+P	φ=0°	10.8	71	1.3	-0.6
	φ=90°	8.57	8	3.5	-1.7
	φ=270°	11.5	30	4.8	-1.3

B.2 EMI Analysis

Table B.9 Fourier coefficients and noise power

Parameters	Harmonic frequency [GHz]			
	0.38	0.90	2.6	5.9
c_k [$\times 10^{-3}$]	1.645	0.694	0.240	0.106
N_{env} [dBm]	-122	-112	-125	-113

Table B.10 Parameters' values for the fundamental frequency

Parameters		d_sup_cat [m]			
		2.8	1.6	1.4	1.2
C [nF]		8.78	9.63	9.86	10.0
|E| [dBuV/m]	Theoretical	189.0	194.7	196.0	197.6
	CST	176	181	184	188

Annex C

Antennas' Specifications

This annex includes the specifications of the antennas that are used in railway communication systems, presenting specific characteristics for each technology (TETRA, GSM-R, LTE-R, BBRS).

C.1 TETRA Antenna

Figure C.1 TRNBG antenna (extracted from [PANO17]).

Table C.1 Antenna specifications (extracted from [PANO17]).

Frequency band [MHz]	380-430
Polarisation	Vertical
Characteristic impedance [Ω]	50
VSWR (on a metallic plane 60/60 cm)	<1.6:1
Gain (over λ/4 monopole) [dBi]	5
Dimensions (Height x Width x Depth) [mm]	100x100x240
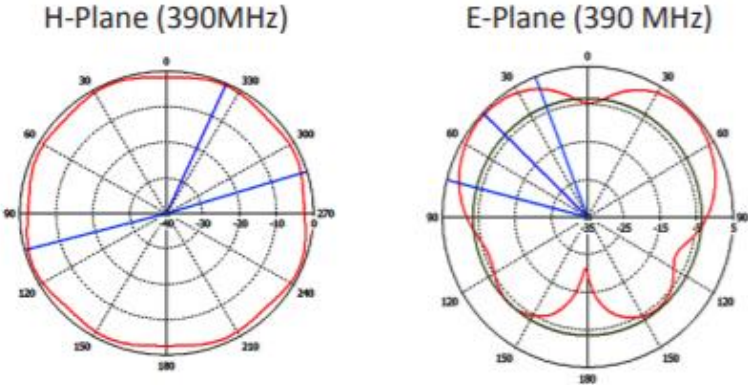
Figure C.2 Radiation patterns at 390 MHz (extracted from [PANO17]).

C.2 GSM-R Antenna

Figure C.3 BGLI antenna (extracted from [Polo16]).

Table C.2 Antenna specifications (extracted from [Polo16]).

Frequency band [MHz]	876-960
Polarisation	Vertical
Characteristic impedance [Ω]	50
VSWR (on a metallic plane 60/60 cm)	<1.7:1
Gain (over λ/4 monopole) [dBi]	0
Dimensions (Height x Width x Depth) [mm]	98 x 80 x 145

(a) Horizontal plane.   (b) Vertical plane.
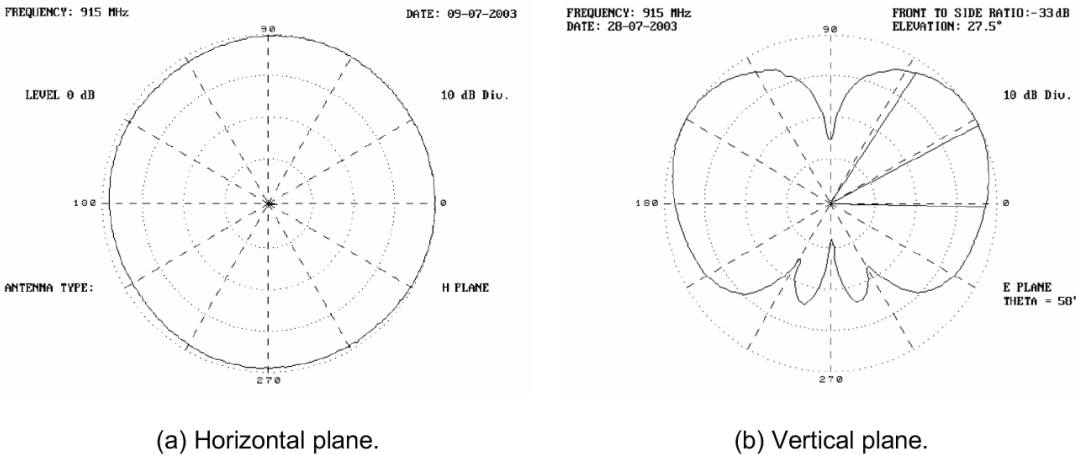
Figure C.4 Radiation patterns at 915 MHz (extracted from [BGLI10]).

C.3 LTE-R Antenna

Figure C.5 Sencity Rail Antenna (extracted from [Hube17]).

Table C.3 Antenna specifications (extracted from [Hube17]).

Frequency band [MHz]	2700-3300
Polarisation	Vertical
Characteristic impedance [Ω]	50
VSWR	1.5
Gain [dBi]	6.5
Dimensions (Height x Width x Depth) [mm]	154 x 100 x 256
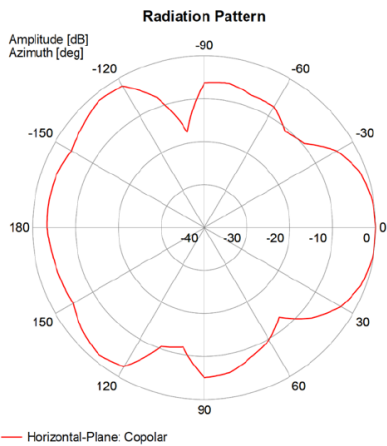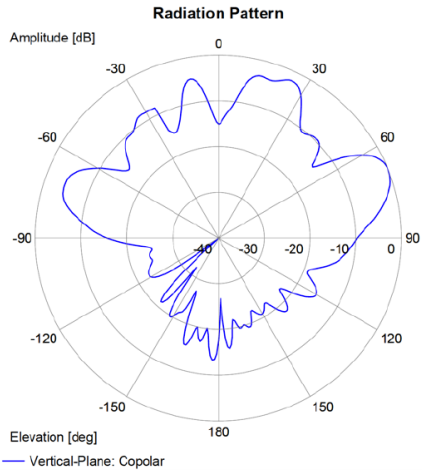
(a) Horizontal plane.   (b) Vertical plane.

Figure C.6 Radiation pattern at 2.6 GHz (extracted from [Hube17]).

C.4 BBRS Antenna

Figure C.7 Sencity Spot- S WiFi Antenna (extracted from [Hube09b]).

Table C.4 Antenna specifications (extracted from [Hube09b]).

Frequency band [MHz]	5150-5970
Polarisation	Vertical
Nominal impedance [Ω]	50
VSWR	1.5
3 dB beamwidth (h) [°]	40
3 dB beamwidth (v) [°]	35
Gain [dBi]	14
Dimensions (Height x Width x Depth) [mm]	101 x 80 x 35
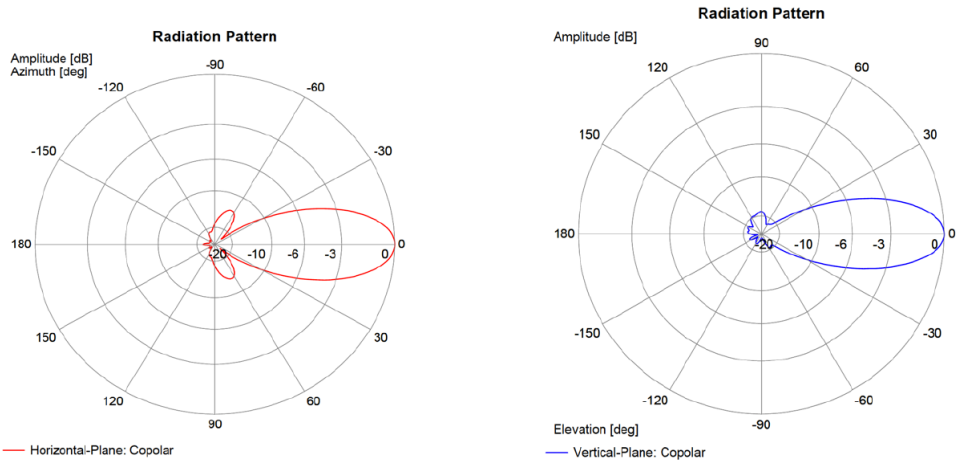
(a) Horizontal plane.

(b) Vertical plane.

Figure C.8 Radiation pattern at 5.9 GHz (extracted from [Hube09b]).

References

[3GPP19]   3GPP - A Global Initiative, The Mobile Broadband Standard, Mar 2019. [Online] Available in: (http://www.3gpp.org/) [Accessed in Sep. 2018].

[3GPP17]   3GPP, *Evolved Universal Terrestrial Radio Access (E-UTRA); User Equipment (UE) radio transmission and reception*, Report ETSI TS 36.101, V14.3.0, Release 14, Apr. 2017. [Online] Available in:(http://www.etsi.org/deliver/etsi_ts/136100_136199/136101/14.03.00_60/ts_136101v140300p.pdf) [Accessed in Sep. 2018].

[ACKZ14]   B. Ai, X. Cheng, T. Kurner, Z. Zhong, K. Guan, R. He, L. Xiong, D. W. Matolak, D. G. Michelson and C. Briso-Rodriguez, *Challenges Toward Wireless Communications for High-Speed Railways*, IEEE Transactions on Intelligent Transportation Systems, Vol.15, No.5, Oct. 2014. [Online] Available in: (http://ieeexplore.ieee.org/document/6808529/) [Accessed in Sep. 2018].

[AGRK15]   B. Ai, K. Guan, M. Rupp, T. Kurner, X. Cheng, X. Yin, Q. Wang, G. Ma, Y. Li, L. Xiong and J. Ding, *Future Railway Services-Oriented Mobile Communication Network*, IEEE Communications Magazine, Vol.53, No. 10, Oct. 2015. [Online] Available in: (http://ieeexplore.ieee.org/document/7295467/) [Accessed in Sep. 2018].

[Bala05]   C. A. Balanis, *Antenna Theory: Analysis and Design*, Fourth Edition, John Wiley & Sons, Hoboken, New Jersey, USA, 2005.

[BBRS17]   Broad Band Radio System (BBRS), Thales Portugal, June 2017.

[BFML10]   G. Baldini, I.N. Fovino, M. Masera, M. Luise, V. Pellegrini, E. Bagagli, G. Rubino, R. Malangone, M. Stefano and F. Senesi, *An early warning system for detecting GSM-R wireless interference in the high-speed railway* infrastructure, International Journal of Critical Infrastructure Protection, Vol.3, No.3, Dec. 2010. [Online] Available in: (https://www.sciencedirect.com/science/article/pii/S1874548210000430) [Accessed in Sep. 2018].

[BGLI10]   *DualBand Antenna Technical document BGLI*, $\lambda_{\epsilon\alpha}$ LEANTENNE, Technical department, DSF-07 Rev. 1, Valeggio sul Mincio, Verona, Italy, 2010.

[Bran08]   J. A. Brandão Faria, *Electromagnetic Foundations of Electrical Engineering, Electrotecnia Teórica*, John Wiley & Sons, Hoboken, New Jersey, USA, 2009.

[Cisc16]   Cisco, "Mobility Management Entity Overview", in MME Administration Guide, StarOS Release 21, Oct. 2016. [Online] Available in: (https://www.cisco.com/c/en/us/td/docs/wireless/asr_5000/21/MME/b_21_MME_Admin.pdf?dtid=osscdc000283). [Accessed in

Dec. 2018].

[CMAF13]   J. Calle-Sanchez, M. Molina-Garcia, J. I. Alonso, and A. Fernandez-Duran, *Long Term Evolution in High Speed Railway Environments: Feasibility and Challenges*, Bell Labs Technical Journal, Vol.18, No.2, Sep. 2013, pp.237-253. [Online] Available in: (http://ieeexplore.ieee.org/document/6772145/) [Accessed in Sep. 2018].

[Corr17]   L. M. Correia, *Mobile Communication Systems*, Lecture Notes, Instituto Superior Tecnico, Lisbon, Portugal, 2017.

[CST18]   CST – Computer Simulation Technology. [Online] Available in: (https://www.cst.com/). [Accessed in Dec. 2018]

[CSTH18]   CST STUDIO SUITE® Electromagnetic and Multiphysics Simulation Software 2018 Help, Help documentation 2018.

[Dan08]   M. Dan, *GSM-R SIAFI 2008*, Infrastructure Dept., UIC, Paris, France, Apr. 2008. [Online] Available in: (https://uic.org/cdrom/2008/05_SIAFI08_source/docs/april/3_mercredi/6_GSM-R.pdf) [Accessed in Sep. 2018].

[DFHR13]   v. Deniau, H. Fridhi, Heddebaut, J. Rioult, I. Adin. and J. Rodriguez, *Analysis and modelling of the EM interference produced above a train associated to the contact between the catenary and the pantograph*, Belgium, Sep. 2013. [Online] Available in: (https://hal.archives-ouvertes.fr/hal-00911695/document) [Accessed in Sep. 2018].

[DDSA12]   Stephen Dudower, Virginie Deniau, M. Nedim Ben Slimen, Ricardo Adriano, *Infrastructures Design, Signalling and Security in Railway*, *Susceptibility of the GSM-R Transmissions to the Railway Electromagnetic Environment*, 2012. [Online] Available in: (https://www.researchgate.net/publication/224829696_Susceptibility_of_the_GSM-R_Transmissions_to_the_Railway_Electromagnetic_Environment) [Accessed in Sep. 2018].

[Duar18]   Tomás Ferreira Duarte, *TETRA-based Railway Communications Network*, Dec 2018.

[Fari08]   J. A. Brandão Faria, *Electromagnetic Foundations of Electrical Engineering*, John Wiley & Sons, 2008.

[FDGH13]   H. Fridhi, V. Deniau, J.P. Ghys, M. Heddebaut, J. Rodriguez and I. Adin, *Analysis of the coupling path between transient EM interferences produced by the catenary-pantograph contact and on-board railway communication antennas,* Univ. Lille Nord de France, IFSTTAR, Villeneuve d'Ascq, France, CAF, Beasain (Guipuzcoa), Spain, CEIT and University of Navarra, Donostia - San Sebastián, Spain, Sep. 2013. [Online] Available in: (https://ieeexplore.ieee.org/document/6632310) [Accessed in Sep. 2018].

[FrFC17]   P. Fraga-Lamas, T.M. Fernandez-Carames and L. Castedo, "Towards the Internet of Smart Trains: A Review on Industrial IoT-Connected Railways", *Sensors*, Vol.17, No.6, June. 2017. [Online] Available in: (http://www.mdpi.com/1424-8220/17/6/1457/pdf) [Accessed in Sep. 2018].

[FRGC15]   P. Fraga-Lamas, J. Rodriguez-Pineiro, J. A. Garcia-Naya and L. Castedo, "Unleashing the Potential of LTE for Next Generation Railway Communications", in *Proc. of 8th International Workshop on Communication Technologies for Vehicles (Nets4Cars/Nets4Trains/ Nets4Aircraft)*, vol.9066, pp. 153-164, Sousse, Tunisia, May 2015. [Online] Available in: (https://link.springer.com/chapter/10.1007%2F978-3-319-17765-6_14) [Accessed in Sep. 2018].

[GeRK12]   C. Gessner, A. Roessler, and M. Kottkamp, UMTS Long Term Evolution (LTE) – Technology Introduction, Rohde & Schwarz, Note 1MA111, July 2012 [Online]. Available in:(https://cdn.rohde-schwarz.com/pws/dl_downloads/dl_application/application_notes/ 1ma111/1MA111_4E_LTE_technology_introduction.pdf) [Accessed in Sep. 2018].

[Gonç13]   J. Gonçalves, *Detailed Design Plan – BMRC Project,* 2STDM-THAL-GEN-COM-DOC-0020-A03, Thales Portugal, Lisbon, Apr. 2013.

[GMT01]   R. Giannetti, M. Macucci, B. Tellini B. Tellini, *Remarks on models for prediction of radiated fields in electrical discharge events,* Electronics Letters, Volume 37, Issue 13, Jun. 2001. [Online] Available in: (https://ieeexplore.ieee.org/abstract/document/933396) [Accessed in Dec 2018].

[GSMR15a] GSM-R Operations Group, EIRENE – System Requirements Specification Version 16.0.0, UIC, Paris, France, 2015. [Online] Available in: (https://uic.org/IMG/pdf/srs-16.0.0_uic_951-0.0.2_final.pdf) [Accessed in Sep. 2018].

[GSMR15b] GSM-R Operations Group, EIRENE – Functional Requirements Specification Version 8.0.0, UIC, Paris, France, 2015. [Online] Available in: (https://uic.org/IMG/pdf/frs-8.0.0_uic_950_0.0.2_final.pdf) [Accessed in Sep. 2018].

[HAWG16]   R. He, B. Ai, G. Wang, K. Guan, Z. Zhong, A. F. Molisch, C. Briso-Rodriguez and C. P. Oestges, "High-speed railways communications: From GSM-R to LTE-R", *IEEE Vehicular Technology Magazine,* Vol. 11, No. 3, Sep.2016, pp.49-58. [Online] Available in: (http://ieeexplore.ieee.org/document/7553613/) [Accessed in Sep. 2018].

[HoTo11]   H. Holma and A. Toskala, LTE for UMTS: Evolution to LTE Advanced (2nd edition), John Wiley & Sons Ltd, Chichester, UK, 2011.

[Hube09b]   Huber+Suhner, *Sencity Spot- S WiFi Antenna*, 1356.17.0077, SPA 5600/40/14/0/V 2, June 2009 [Online]. Available in: (https://ecatalog.hubersuhner.com/?fcode=m_cs_ catdeta114il&m_cs_gv_itmguid=051MaWqK7jUmaeRPR4RBV0&m_cs_gv_with_navi=X) [Accessed in Oct. 2019].

[Hube17]   Huber+Suhner, *Sencity Rail Antenna*, 1399.17.0094, SWA 0459/360/4/25/V, Feb. 2017. [Online]. Available in: (https://ecatalog.hubersuhner.com/product/ecatalog/Radio-frequency/Antennas-Accessories/Antennas/1399-17-0094) [Accessed in Oct. 2019].

[IRSt17]   International Railway Statistics, *High Speed Traffic in the world*, Internal Report, UIC, Nov. 2017 [Online]. Available in: (https://uic.org/IMG/pdf/high_speed_passengerkm_

20171130_.pdf) [Accessed in Sep. 2018].

[Kunz17]   A. Kunze, *It is not just self-driving cars. Trains could soon be autonomous too*, World Economic Forum, June 2017. [Online]. Available in: (https://www.weforum.org/agenda/2017/06/digitization-can-mean-a-bright-future-for-railtravel-heres-how/) [Accessed Dec. 2018].

[LLLW11]   Weiping Liu, Yanwen Liu, Ru Li, Pai Wang, *Research and Development of Communication Between PC and Mobile Base on Embedded System and GPRS*, College of Computer Science, Inner Mongolia University, Aug. 2011. [Online]. Available in: (https://ieeexplore.ieee.org/stamp/stamp.jsp?tp=&arnumber=6010034&tag=1) [Accessed in Oct. 2018].

[Maso13]   S. H. Masood, *Performance comparison of IEEE 802.11g and IEEE 02.11n in the presence of interference from 802.15.4 networks,* Department of Electrical Engineering, McGill University, Montreal, Quebec, Canada, Aug. 2013. [Online] Available in: (https://arxiv.org/ftp/arxiv/papers/1308/1308.0678.pdf) [Accessed in Oct. 2018].

[MBST09]   Surajit Midya, Dierk Bormann, Ziya Mazloom, Thorsten Schutte, Tajeev Thottappillil, *Conducted and radiated emission from pantograph arcing in AC traction syste*m, 2009 IEEE Power & Energy Society General Meeting, Sweden, Jul 2009. [Online] Available in: (https://ieeexplore.ieee.org/document/5275833/authors) [Accessed in Oct. 2018].

[Mend10]   L. Mendonça, *Detail Design Plan – Technical Specification Broad Band Radio System,* MMMP-SL-THA-MSN-GEN-DSP-D-00437-A05, Thales, Mar. 2010.

[MTBL08]   Surajit Mydya, Dierk Bormann, Ziya Mazloomm, Thorsten Schutte, Rajeev Thottappillil, *Conducted and radiated emission from pantograph arcing in AC traction system*, 2009 IEEE Power & Energy Society General Meeting, Oct 2009. [Online] Available in: (https://ieeexplore.ieee.org/document/5275833/authors) [Accessed in Oct. 2018].

[MUMi07]   M.Mandic, I. Uglesic, V. Milardic, *Study of Electromagnetic Fields from AC 25Kv/50Hz Contact Line Systems*, International Review of Electrical Engineering (I.R.E.E.), vol. xx, nº x, 2007. [Online] Available in: (https://www.researchgate.net/publication/290261770_A_study_of_electromagnetic_fields_from_AC_25_kV50_Hz_contact_line_systems) [Accessed in Oct. 2018].

[Over18]   *Overview of TETRA*. [Online] Available in: (http://shu.bg/tadmin/upload/storage/877.pdf) [Accessed in Oct. 2018].

[Pals13]   V. A. F. Pals, *Analysis of influence on antenna radiation patterns by conducting environments for the development of vehicle antennas*, MS.c Thesis, Technische Universitat Munchen, Munchen, Germany, 2013. [Online]. Available in: (https://riunet.upv.es/bitstream/handle/10251/33007/FuertesPals_VicenteAlejandro_MasterERASMUS.pdf;jsessionid=CDA7DC7555FEB6FBD7F6578E6C4454CF?sequence=1) [Accessed in Oct. 2018].

[PANO17] PANORAMA ANTENNAS, *Product Data Sheet, Train Antenna*, 2017. [Online]. Available in: (http://tetraforum.pl/produkty-tetra/Panorama-Antennas/Panorama-Train-Antenna-trnbg-tet-kolejowa-antena-TETRA-GPS.pdf) [Accessed in Oct. 2018].

[Palu13] M. Palumbo, "Railway Signalling since the birth to ERTMS", *railway signalling.eu*, Italy, Nov. 2013. [Online] Available in: (http://www.railwaysignalling.eu/wp-content/uploads/2014/06/Railway_Signalling_since_birth_to_ERTMS.pdf) [Accessed in Oct. 2018].

[Polo16] Polomarconi, *Dual Band GSM-R – GPS Antenna,* Ver. 04, June 2016. [Online] Available in: (https://www.polomarconi.it/wp-content/uploads/datasheet/BGLI.pdf) [Accessed in Sep. 2018].

[PuTa09] L. Pushparatnam, T. Taylor, "Overview of GSM-R", in UIC, *GSM-R Implementation and Procurement Guide*, UIC, Paris, France, 2009. [Online] Available in: (https://uic.org/IMG/pdf/2009gsm-r_guide.pdf) [Accessed in Oct. 2018].

[Reed18] Marc Reed, *Licensed vs. Unlicensed Spectrum for Utility Communications* [Online]. Available in: (http://www.utilityproducts.com/articles/print/volume-7/issue-7/productfocus/amr_ami/licensed-vs__unlicensed.html) [Accessed in Oct. 2018].

[REFE15] REFER, *Instrução Técnica, GR.IT.GER.002 Retorno da Corrente de Tração, Terras e Proteções, Parte 2: Funcionamento do Sistema de 25 Kv*, May, 2015.

[Ribe18] André Gonçalves Ribeiro, *Analysis of Antennas' Locations on Trains for Mobile Communications,* MSc. Thesis, Instituto Superior Técnico, Universidade de Lisboa, Lisboa, Portugal, Jul. 2018.

[RGXK17] César Briso-Rodríguez, Ke Guan, Yin Xuefeng, Thomas Kurner, "Wireless Communications in Smart Rail Transportation Systems", Hindawi, Wireless Communications and Mobile Computing, Volume 2017, 2017. [Online] Available in: (https://www.hindawi.com/journals/wcmc/2017/6802027/) [Accessed in Sep. 2018].

[SAUH14] M. K. Sarkar, G.M. F. Ahmed, A.T.M. J. Uddin, M.H. Hena, M. A. Rahman and R. Kabiraj, *Wireless cellular network for high speed (up to 500 km/h) vehicles*, *IOSR Journal of Electronics and Communication Engineering*, Vol.9, Issue 1, Jan. 2014, pp.1-9. [Online] Available in: (https://pdfs.semanticscholar.org/8ffd/77a407197382f074b3b1af95fde221f45c4b.pdf) [Accessed in Sep. 2018].

[SCIV17] SCI Verkehr, Rail Transport Markets – Global Markets Trends 2016-2025, MultiClient Study, Hamburg, Germany, Mar. 2017. [Online] Available in:(https://www.sci.de/fileadmin/user_upload/Flyer_Rail_Transport_Markets_eng.pdf) [Accessed in Sep. 2018].

[Stat19] Statista Inc., *Annual average accessible railway market from 2013 to 2021, by segment (in billion euros)*, Hamburg, Germany, May 2017. [Online] Available in : (https://www.statista.com/statistics/201760/worldwide-market-share-of-leading-global-rail-

equipmentmanufacturers/) [Accessed in Mar. 2019].

[Thal17]   Thales Group – A French company dedicated in services for aerospace, space, ground transportation, defence and security. [Online] Available in:(https://www.thalesgroup.com/en/european-train-control-system-etcs), [Accessed in Dez. 2018].

[THAL09]   THALES Security Solutions & Services, S.A., REFER EPE, *Sistema de Controlo – Comando e Sinalização da Linha de Cascais e Respetiva Manutenção, Memória Descritiva e Justificativa do Sistema RCT+TP (Retorno da Corrente de Tração, Terras e Proteções)*, 2009.

[TMGA01a]   B. Tellini; M. Macucci; R. Giannetti; G.A. Antonacci, *Line-pantograph EMI in railway systems,* Pisa University, Italy, Dec. 2001. [Online] Available in: (https://ieeexplore.ieee.org/document/975459) [Accessed in Oct. 2018].

[TMGA01b]   B. Tellini; M. Macucci; R. Giannetti; G.A. Antonacci, *Conducted and Radiated Interference Measurements in the Line-Pantograph System,* IEEE TRANSACTIONS ON INSTRUMENTATION AND MEASUREMENT, Volume 50, Nº 6, Dec. 2001. [Online] Available in: (https://ieeexplore.ieee.org/document/982964/figures#figures) [Accessed in Oct. 2018].

[Trai19]   TL - Train Logistic. [Online] Available in: (https://www.trainlogistic.com/pt/Comboios/Gabinete/fich_atm4000.htm) [Accessed in May 2019].

[WaZG12]   J. Wang, H. Zhu and N.J. Gomes, *Distributed Antennas Systems for Mobile Communications in High Speed Trains*, *IEEE Journal on Selected Areas in Communications*, Vol.30, No. 4, May 2012. [Online] Available in: (http://ieeexplore.ieee.org/document/6180090/) [Accessed in Oct. 2018].

[XZAZ16]   S. Xu, G. Zhu, B. Ai and Z. Zhong, A Survey on High-Speed Railway Communications: A Radio Resource Management Perspective, State Key Laboratory of Rail Traffic Control *and safety*, Beijing, China, Mar. 2016. [Online] Available in: (https://arxiv.org/pdf/1603.05368.pdf) [Accessed in Oct. 2018].